NAVAL POSTGRADUATE SCHOOL

MONTEREY, CALIFORNIA

THESIS

JOINT SENSING/SAMPLING OPTIMIZATION FOR SURFACE DRIFTING MINE DETECTION WITH HIGH-RESOLUTION DRIFT MODEL

by

Kristie M. Colpo

September 2012

Thesis Advisor:	Peter Chu
Second Readers:	Thomas A. Wettergren
	Ronald E. Betsch

Approved for public release; distribution is unlimited

THIS PAGE INTENTIONALLY LEFT BLANK

REPORT DOCUMENTATION PAGE			Form Approved OMB No. 0704-0188
Public reporting burden for this collection of information is estimated to average 1 hour per response, including the time for reviewing instruction, searching existing data sources, gathering and maintaining the data needed, and completing and reviewing the collection of information. Send comments regarding this burden estimate or any other aspect of this collection of information, including suggestions for reducing this burden, to Washington headquarters Services, Directorate for Information Operations and Reports, 1215 Jefferson Davis Highway, Suite 1204, Arlington, VA 22202-4302, and to the Office of Management and Budget, Paperwork Reduction Project (0704-0188) Washington DC 20503.			
1. AGENCY USE ONLY *(Leave blank)*	**2. REPORT DATE** September 2012	**3. REPORT TYPE AND DATES COVERED** Master's Thesis	
4. TITLE AND SUBTITLE Joint Sensing/Sampling Optimization for Surface Drifting Mine Detection with High-Resolution Drift Model		**5. FUNDING NUMBERS** **N6230611PO00123** **N0001412WX20510**	
6. AUTHOR(S) Kristie M. Colpo			
7. PERFORMING ORGANIZATION NAME(S) AND ADDRESS(ES) Naval Postgraduate School Monterey, CA 93943-5000		**8. PERFORMING ORGANIZATION REPORT NUMBER**	
9. SPONSORING /MONITORING AGENCY NAME(S) AND ADDRESS(ES) Ronald E. Betsch, Naval Oceanographic Office 1002 Balch Blvd Stennis Space Center, MS 39529		**10. SPONSORING/MONITORING AGENCY REPORT NUMBER**	
11. SUPPLEMENTARY NOTES The views expressed in this thesis are those of the author and do not reflect the official policy or position of the Department of Defense or the U.S. Government. IRB Protocol number _____N/A_____.			
12a. DISTRIBUTION / AVAILABILITY STATEMENT Approved for public release; distribution is unlimited		**12b. DISTRIBUTION CODE**	

13. ABSTRACT (maximum 200 words)

Every mine countermeasures (MCM) operation is a balance of time versus risk. In attempting to reduce time and risk, it is in the interest of the MCM community to use unmanned, stationary sensors to detect and monitor drifting mines through harbor inlets and straits. A network of stationary sensors positioned along an area of interest could be critical in such a process by removing the MCM warfighter from a threat area and reducing the time required to detect a moving target.

Although many studies have been conducted to optimize sensors and sensor networks for moving target detection, few of them considered the effects of the environment. In a drifting mine scenario, an oceanographic drift model could offer an estimation of surrounding environmental effects and therefore provide time critical estimations of target movement. These approximations can be used to further optimize sensor network components and locations through a defined methodology using estimated detection probabilities. The goal of this research is to provide such a methodology by modeling idealized stationary sensors and surface drift for the Hampton Roads Inlet.

14. SUBJECT TERMS DELFT3D, Drift Model, Mine Countermeasures, Monte Carlo Simulation, Optimization, Sensor Networks			**15. NUMBER OF PAGES** 101
			16. PRICE CODE
17. SECURITY CLASSIFICATION OF REPORT Unclassified	**18. SECURITY CLASSIFICATION OF THIS PAGE** Unclassified	**19. SECURITY CLASSIFICATION OF ABSTRACT** Unclassified	**20. LIMITATION OF ABSTRACT** UU

NSN 7540-01-280-5500

Standard Form 298 (Rev. 2-89)
Prescribed by ANSI Std. 239-18

THIS PAGE INTENTIONALLY LEFT BLANK

Approved for public release; distribution is unlimited

JOINT SENSING/SAMPLING OPTIMIZATION FOR SURFACE DRIFTING MINE DETECTION WITH HIGH-RESOLUTION DRIFT MODEL

Kristie M. Colpo
Lieutenant, United States Navy
B.S., United States Naval Academy, 2004

Submitted in partial fulfillment of the
requirements for the degree of

MASTER OF SCIENCE IN METEOROLOGY AND PHYSICAL OCEANOGRAPHY

from the

NAVAL POSTGRADUATE SCHOOL
September 2012

Author: Kristie M. Colpo

Approved by: Peter C. Chu
Thesis Advisor

Thomas A. Wettergren
Thesis Co-Advisor

Ronald E. Betsch
Thesis Co-Advisor

Mary L. Batteen
Chair, Department of Oceanography

THIS PAGE INTENTIONALLY LEFT BLANK

ABSTRACT

Every mine countermeasures (MCM) operation is a balance of time versus risk. In attempting to reduce time and risk, it is in the interest of the MCM community to use unmanned, stationary sensors to detect and monitor drifting mines through harbor inlets and straits. A network of stationary sensors positioned along an area of interest could be critical in such a process by removing the MCM warfighter from a threat area and reducing the time required to detect a moving target.

Although many studies have been conducted to optimize sensors and sensor networks for moving target detection, few of them considered the effects of the environment. In a drifting mine scenario, an oceanographic drift model could offer an estimation of surrounding environmental effects and therefore provide time critical estimations of target movement. These approximations can be used to further optimize sensor network components and locations through a defined methodology using estimated detection probabilities. The goal of this research is to provide such a methodology by modeling idealized stationary sensors and surface drift for the Hampton Roads Inlet.

THIS PAGE INTENTIONALLY LEFT BLANK

TABLE OF CONTENTS

LIST OF FIGURES

LIST OF TABLES

THIS PAGE INTENTIONALLY LEFT BLANK

LIST OF ACRONYMS AND ABBREVIATIONS

ADCP	Acoustic Doppler Current Profiler
AMCM	Air Mine Countermeasures
BSP	Battle Space Profiler
CTD	Conductivity Temperature Depth
EOD	Explosive Ordnance Disposal
MCM	Mine Countermeasures
MEDAL	Mine Warfare Environmental Decisions Aid Library
MMS	Marine Mammal Systems
SMCM	Surface Mine Countermeasures
UMCM	Underwater Mine Countermeasures
UUV	Unmanned Undersea Vehicles

THIS PAGE INTENTIONALLY LEFT BLANK

ACKNOWLEDGMENTS

First and foremost, I would like to thank Professor Chu. Professor, thank you for your dedication. It is clear that you make your thesis students a top priority and I cannot thank you enough. I have learned a lot from you and will miss our mine warfare discussions.

Mr. Fan, you are a Matlab genius. Thank you for always being there to answer my questions and help me with Matlab. Your patience and guidance truly helped me through the thesis process and made it a worthwhile experience. I will always be grateful of your help.

I would also like to thank Tom Wettergren and Russell Costa at the Naval Undersea Warfare Center, Division Newport. Tom, thank you for encouraging me through the thesis process and letting me bounce ideas off of you. You helped me to think of things that I would not have thought of otherwise. Russell, thanks for taking time out of your busy day to discuss my thesis ideas over the phone. I learned a lot from you both. Thank you so very much.

To Dennis Krynen and his team at the Naval Oceanographic Office (NAVO), thank you for helping me find DELFT3D data and answering all of my questions related to oceanographic models. Having worked at NAVO, I know how busy it can be which makes me even more appreciative of your time and support. Thank you.

To Bill Teague at the Naval Research Laboratory, thank you for sending me DELFT3D data and allowing me to read your report on its performance. I could not have started my research without it.

To my mom, JoAnn, and my step-father, Jack, it is difficult to know where to start. Thank you for always supporting and loving me. I would not be where I am today, if you had not been there every step of the way. I could only hope to be as good a parent one day as you are to me. From the bottom of my heart, thank you. I love you so much.

Dedicated to JoAnn and Jack Cassidy

THIS PAGE INTENTIONALLY LEFT BLANK

I. INTRODUCTION

A. MINE WARFARE OVERVIEW

Mine warfare is defined as the strategic and tactical employment and countering of sea mines. The employment of sea mines, or "mining," is primarily used to gain sea control. This can be done by laying mines using ships, aircraft, or submarines, or simply by the threat to do so. Mining can be offensive in nature for the purposes of denying enemy forces access to a strategic location, in which case, it is referred to as "offensive denial." Mining can also be used to protect territorial and international waters against enemy invasion and this is known as "defensive protection." Actions taken to counter mines laid for either offensive or defensive purposes are known as "mine countermeasures." Mine countermeasures include any actions actively or passively employed to deter a mine's ability to damage or sink an allied or neutral vessel. As will be discussed, it is essential to have knowledge of both mining and mine countermeasures to fully understand the complexity of mine warfare of the past, present, and future.

1. Mine Threat

Whether mining or conducting mine countermeasures, mines are classified by the same three categories: position in the water column, the method by which they are delivered to the battlespace, and their activation mechanism. The first category, position in the water column, is divided into three subcategories: bottom, moored, and drifting. Mines can be placed almost anywhere in the water column from 0 to 500 m. Bottom mines are generally placed in shallow water to target ships and submarines. Moored mines, also known as tethered or buoyant mines, are also used to target ships and submarines but can be placed at virtually any depth in the water column. Lastly, drifting, or floating, mines usually move with ocean currents and are built to float at or near the sea surface. Due to the indiscriminate nature of the drifting mine, it was banned by the Hague Convention in 1907 but it is still used by many rogue nations. One or all three of these water column positions can be used to make an effective minefield (National Research Council, 2000).

The second category by which mines are classified, method of delivery, can also be divided into three subcategories: aircraft, surface, and submarine. Mines are generally dropped by aircraft in offensive actions where delivery time is limited. These mines are generally subject to the greatest amount of impact burial, depending on the ocean floor composition and the height from which they were dropped; this may make them more difficult to detect than mines deployed by surface or submarine assets. Mines can also be laid by a variety of ships and boats, some of which are disguised as tankers or other merchant vessels allowing for mines to be laid in secret. Mines laid by submarines are designed to be fired out of torpedo tubes and therefore will often have the shape of torpedoes. Each method of delivery offers advantages and disadvantages to the mine layer depending on the weighing factors of time, risk to mining assets, and necessity for covert operations.

The third category by which mines are classified is arguably the most important to mining and mine countermeasures operations: the actuation mechanism. There are three subcategories of actuation mechanisms: contact, influence, or controlled. Contact mines are the oldest type of mines and they require physical contact with the hull of a vessel to detonate. They are typically designed with chemical horns that protrude from the top of the mine so as to cause detonation upon contact. Influence mines are the most common and have detectors to sense variations in pressure or acoustic, magnetic, and electrical fields. They can be built to sense different types of vessels, have time delays before detonating, or both. Controlled mines are usually fired from shore sites using hidden lines or cables. They are typically used as a defensive tactic and are most effective in preventing passage into confined areas. Given that mines can be classified by three different mine categories, their respective subcategories, and various combinations thereof, the design possibilities for a minefield can easily range from straight-forward to extremely complex (National Research Council, 2000).

2. Mine Countermeasures

Mine countermeasures can be classified as passive or active. Passive mine countermeasures usually involve reducing the signature of a vessel in an effort to avoid

detonating a mine. Passive mine countermeasures may involve one or a combination of the following: mine watching, mine avoidance, deperming, degaussing, noise reduction, and ship-protection devices such as mine-catching nets attached to vessels used in the Civil War. Deperming is the process of demagnetizing a ship's hull by electrical current which, through periodic application, reduces the ship's magnetic signature. Degaussing involves installing a permanent coil system onboard to neutralize the ship's magnetic signature. Noise reduction is a technique used to avoid acoustic actuating mines and it includes, but is not limited to, installing features and procedures during shipbuilding that reduce noise. Although all of these passive techniques act to reduce effective risk to transiting vessels, they are defensive in nature and therefore do not act to diminish or eliminate the presence of a minefield (Melia, 1991).

Active mine countermeasures, on the other hand, are offensive in nature and involve locating and neutralizing mines or mine-like contacts. Active mine countermeasures include sweeping, hunting, and neutralization. All three forms of active mine countermeasures require a thorough examination of time to render the minefield passable versus risk to allied assets. The general guideline is "hunt when you can, sweep when you must" and neutralize whenever possible.

Minesweeping, which is typically used when time is the most important operational factor, can use both mechanical and influence methods to combat a minefield. Mechanical minesweeping is the process of physically cutting moored mine cables to enable mines to float to the surface and become more visible for rapid disposal. This can be accomplished with various modifications of floating 'otters' and cutters towed behind a mine countermeasures ship or helicopter. Influence sweeping uses acoustic, magnetic, and pressure signals generated from a towed body to detonate mines with actuating mechanisms susceptible to the emitted signals. In order to maximize sweeping effectiveness, both types of minesweeping require timely intelligence of the minefield dimensions, types of mine actuating systems involved, and current environmental conditions.

Minehunting is literally the search for mines using optical and acoustic means. This can be accomplished in many ways but it is typically done using side-scan sonar,

hull-mounted sonar, underwater cameras, or simply the naked eye. Minehunting is particularly necessary when there is no intelligence available about the types of mines that have been laid because minesweeping requires this information to be most effective. Furthermore, minehunting is often considered the safest way of dealing with mines; it is not used to intentionally actuate the mine while assets are in the water and it does not cut moored cables, allowing an active contact mine to drift freely through the water (National Research Council, 2000).

The last of the active mine countermeasures is neutralization. Neutralization refers to the disposal of mines after or during the time they are located. It can be accomplished using several methods including gunfire and sympathetic explosions, but the most common methods require divers, Marine Mammal Systems, or remotely operated vehicles. These three assets can be used to identify and attach an explosive charge to a bottom, moored, or drifting mine which is inherently a high risk activity. This process, although high risk, is almost always essential to render a minefield passable; hunting does not remove mines from the water and mechanical sweeping may cause active moored mines to rise and drift on or near the surface.

To accomplish active mine countermeasures, the United States employs what is known as the Mine Countermeasures (MCM) Triad. The MCM Triad includes three branches: air mine countermeasures (AMCM), surface mine countermeasures (SMCM), and underwater mine countermeasures (UMCM). The primary U.S. AMCM asset is the MH-53E Sea Dragon helicopter. It can be configured for mechanical or influence sweeping or minehunting. The U.S. SMCM asset is the Avenger (MCM-1) class minesweeper and it is equipped to conduct mechanical and influence sweeping, minehunting, and mine neutralization. For the purpose of avoiding influence mine detonation, the Avenger class minesweeper is outfitted with several types of passive mine countermeasures including a wood hull covered in fiberglass to reduce acoustic and magnetic signatures. Lastly, the U.S. UMCM branch is comprised of Explosive Ordnance Disposal (EOD) divers, Unmanned Undersea Vehicles (UUVs), and Marine Mammal Systems (MMS). UMCM brings a unique capability to MCM efforts because they are primarily designated as identification and neutralization assets; they are able to

identify and neutralize mines as the AMCM and SMCM assets continue to hunt and sweep. The goal of the MCM Triad is to work seamlessly to actively reduce the mine threat while maintaining an acceptable timeline and risk level (National Research Council, 2000).

B. IMPORTANCE OF CONTINUOUSLY UPDATING METHODS OF MINE COUNTERMEASURES

Mine countermeasures is one of the most necessary aspects of naval combat. It is necessary in the sense that the potential for sea mines has, can, and will continue to threaten freedom of movement throughout the world's oceans as long as the mine continues to be one of the most cost-effective and clandestine weapons in naval arsenals (National Research Council, 2000). The need for mine countermeasures is particularly necessary when conducting naval operations in and near constricted waterways and littoral combat zones where mines are generally most effective. Transporting necessary supplies or conducting offensive maneuvers in these areas require unobstructed sea lanes for strategic, operational, and tactical mobility (National Research Council, 2000). These operations can be stalled or even aborted due to the simple threat of a minefield. Moreover, the inexpensive nature of mines allows countries with a mining capability, particularly countries of limited military means, the potential to bring a large, more capable navy to a standstill. Therefore, mining is a powerful weapon for defensive and offensive actions and mine countermeasures is a necessary combat skill.

1. Historical Examples of Repercussions Associated with Advanced Mining and Obsolete Countermeasures

The importance of mine warfare, particularly mine countermeasures, has been learned and relearned throughout U.S. history. Since the first successful sea mine, built by David Bushnell in 1776 "the history of MCM has been a history of progress, decline, and resurgence" (Melia, 1991). This cyclical process is caused by the lag of mine countermeasures behind the constantly growing number and evolving complexities of underwater mines. The simple statistical growth in the number of mine-producing countries should be enough to warrant world-wide concern; there has been a 75%

increase from 1988 to 2000. By the year 2000, more than 50 countries had mining capabilities with over 300 mine types to use (National Research Council, 2000). However, mine countermeasures continue to lag as the current surface MCM assets in use by the United States were acquired almost three decades ago and there is still no dedicated pipeline for mine warfare officers within the U.S. Navy. This disparity is shown throughout history and only truly comes to light when there is a known minefield or catastrophic mine strike invoking the hasty development of a series of "quick-fix" solutions (Melia, 1991). Given the scope of this thesis, only a few historical examples of this disparity will be discussed but there are many more that also emphasize the necessity for mine countermeasures technological developments. Examining these and other historical examples is one of the best ways to describe the importance of mine warfare and what needs to be done in the United States to avoid repeating history.

a. Civil War

A notable example of the importance of mine warfare and how mine countermeasures has been known to lag behind mining technology is the Civil War. As the Confederacy did not have a substantial navy at the time of the war, it turned to funding mine warfare as a way to combat the more traditional naval tactics of the Union. In fact, it funded a specialized Torpedo Bureau in October 1862. Conversely, the Union left mine countermeasures to the individual captain of each ship; if any devices were used, they were designed and applied at the captain's discretion. However, by the end of the war, fifty ships, four-fifths of which were Union vessels, were crippled or sunk by sea mines (Melia, 1991).

This is not to say that the Union as a whole failed to conduct mine countermeasures. While many Union officers simply avoided mined waters unless given a direct order, there were some that understood the mine threat and the processes required to gain a tactical advantage. One of the most memorable statements in naval history was given by Rear Admiral David Glasgow Farragut in 1864: "Damn the torpedoes! Full speed ahead, Drayton" (Melia, 1991). Using "torpedoes" as another word for mines, Farragut did not simply ignore the mines at Mobile Bay and charge into enemy waters; he

ordered several minehunting missions prior to his advance. Farragut sent his flag lieutenant and personal friend, Lieutenant John Crittenden Watson, and a special boat crew to search for the Confederate laid mines between Forts Morgan and Gaines. During this reconnaissance, Watson and his crew found that many of the mines were inactive due to long immersion. Watson's crew also worked to sink or disable the remaining active mines or mark their location for avoidance purposes. In light of this, Farragut was able to order his fleet to remain 'eastward of the easternmost buoy' and took the lead through the Bay entrance. However successful or unsuccessful Union mine countermeasures, the high-echelons of the Navy did not disseminate mine warfare lessons learned or establish an operational minesweeping department and thus the burden of mine countermeasures continued to reside on the shoulders of the individual naval officer (Melia, 1991).

b. Hague Conference of 1907

The Hague Conference convened in 1907 after mining events during the Russo-Japanese War caused international concern. Live contact mines that had broken free of their mooring cables threatened the Western Pacific, neutral and warships alike. Therefore, the conference convened to establish international guidelines for mining to include: the automatic sterilization of moored mines if separated from their cables, the responsibility of mining nations to clear the mines they laid in international waters following wartime hostilities, the use of drifting mines only if they self-sterilized in one hour or less, and the banning of unlimited minelaying. Given these restrictions, many nations chose to forgo their mine warfare research and focus on other areas of warfare (Melia, 1991).

c. World War I

The lack of continuous mine warfare research in the United States from 1907 until the start of WWI became evident as the Navy raced to prepare its fleet for a growing mine warfare problem. The U.S. Navy did not develop its first mine sweeping fleet organization, the Atlantic Fleet Mining and Mine Sweeping Division, until 1915, approximately only two years before the United States entered the war (Melia, 1991). Furthermore, it was not until 7 months after the war began that the United States led its

first large-scale mine warfare exercise (Melia, 1991). As for ship protection, the United States borrowed a British paravane design that was only put into operation as of May 1917 (Melia, 1991). Given the infancy of the U.S. mine warfare program, mine warfare personnel lacked experience and therefore thought mine warfare to be easy (Melia, 1991). Moreover, minesweeping was not a high priority and other duties began to take precedence: patrols, search and rescue, and anti-submarine missions (Melia, 1991).

Meanwhile, the Germans developed delayed-rising mines that allowed for a minefield to remain lively even after sweeping operations had declared the area clear. On the Allied front, the United States developed the Mark 6 antenna mine which was particularly effective against German U-boats and the British developed the first magnetic influence mine (Melia, 1991). In addition to mining advances, mine counter-countermeasures became more sophisticated to include sprocket wheels on mooring cables to avoid cutting and explosives on mooring cables to destroy sweeping gear (Melia, 1991). Mine countermeasures, however, continued to fall behind the technological advances of mining. All of these factors combined created a very complex mine warfare problem for both the Allies and Central Powers, particularly in the North Sea where mines were laid by both parties.

Despite the difficult race to mine countermeasures adequacy, little was done following the war to continue such efforts in the United States. While the British learned a valuable lesson from their mining and mine countermeasures efforts leading to the opening of an active mine warfare school, development of active and reserve minesweeping fleets, and enhanced promotion opportunities for MCM officers, the United States continued to struggle. It considered the quick American ingenuity in mining and mine countermeasures to be successful, particularly in the North Sea, and therefore much of American interest in mine warfare was lost (Melia, 1991). In the area of mining, the United States used its newly developed antenna mines to form a complete antisubmarine barrier, known as the North Sea Mine Barrage, which sank at least three German U-boats, and damaged three or for more (Melia, 1991). As for mine countermeasures, in the post-war mine sweeping operations, the United States declared the sweep successful even though the minesweepers could only account for 40 percent of

the mines laid and declared the rest to have self-destructed; mines not swept were found for many years after the sweeping operations ended (Melia, 1991). The widely accepted successes of the mine warfare front, combined with limited promotion opportunities of U.S. mine warfare officers, led to yet another stagnation of mine warfare development during peacetime.

d. World War II

Due to the continued lack of mine warfare professional interest in the years leading up to WWII, the United States did not capitalize on some of the opportunities for advanced mine warfare studies. While there were annual Navy exercises conducted from 1923 to 1941, mine warfare rarely played a role in them (Melia, 1991). In addition, the Naval Ordnance Laboratory, an independent research agency funded by the Bureau of Ordnance, conducted only limited research in the mine warfare area, roughly 20 percent of its total mission; mine countermeasures research comprised the smallest portion of that 20 percent effort (Melia, 1991). Meanwhile, the British continued to improve their magnetic mines, and associated countermeasures to include degaussing and deperming. Germans also continued their research by improving ship counters on mine activation devices, developing acoustic influence mines, and creating magnetic-acoustic combination mines (Melia, 1991). As tensions began to build in Europe, the British recalled their well-trained MCM naval reserve force to counter the German mine threat. The U.S. Navy department, however, did not start restructuring its mine warfare program until 1939 (Melia, 1991).

Germany employed its capabilities in mine warfare as soon as the war began. In 1939, Germany mined the coast of England as it had done before the start of WWI. By 1942, Germany carried its mining efforts to the coast of the United States and, using U-boats, laid over three hundred influence mines off of the Delaware Bay, Chesapeake Bay, Jacksonville, and Charleston (Melia, 1991). Although the U.S. military pulled 125 fishing trawlers for the minesweeping effort and strung large steel nets across some harbor entrances, it simply was not enough to combat the threat (Melia, 1991). As a result, some American ports were closed for over a month. The restrictions and

hardships placed on the U.S. fleet at home show that continued mine warfare effort and vigilance is extremely necessary during peacetime and war. Yet, once again, due to a lack of professional interest, many of the experienced mine warfare personnel left the community after the war and many of the necessary lessons and springboards for MIW development were lost (Melia, 1991).

e. Iran-Iraq War

During and leading up to the Persian Gulf War, there were three catastrophic mine strikes. First, on April 14, 1988, while participating in Operation Earnest Will, the Samuel B. Roberts (FFG-58) struck a submerged M-08 mine. The M-08 mine, laid by Iranian forces, blew a 20 ft hole in the ship's hull, broke the keel, blew the engines off their mounts, and caused significant flooding (Melia, 1991). The $96 million dollars of damage inflicted on the USS Samuel B. Roberts was caused by a mine that only cost $1,500 (Khan, 2010). Later, the USS Tripoli (LPH-10) struck a moored mine on February 18, 1991, and was left with a large hole in the side of her hull that was approximately 16 by 25ft (Melia, 1991). Lastly, the USS Princeton (CG-59) detonated one or more influence mines which lifted her out of the water and caused significant damage to her hull and propeller (Melia, 1991). Two of these three mine strikes occurred in waters that were believed to be clear of mines (Melia, 1991). This assumption, in addition to the catastrophic damage incurred by three Navy vessels, caused the United States to re-evaluate its mine warfare capabilities once again. Just before the Tripoli and Princeton mine strikes, the bulk of the U.S. Navy surface MCM force was comprised of only 20 Korean War-era MSOs (Minesweeper, Ocean) (Melia, 1991). Some explained the lack of adequate capability was due to a reliance on NATO allies for minesweeping assistance, but the Secretary of the Navy in 1991, H. Lawrence Garrett III, showed his awareness by stating that the Navy "spent more than 25 years not developing or buying new minesweepers or minehunters" (Melia, 1991).

C. A MODERN UNCONVENTIONAL MINE THREAT AND FORWARD-THINKING COUNTERMEASURES

1. The Drifting Mine Threat

Today, the United States and the international community at large, is faced with an unconventional mine threat: the drifting mine. During recent Libyan conflicts in May 2011, three drifting mines were laid off the coast of Misrata by forces loyal to the late Libyan leader, Muammar Gaddafi (Reuters Africa, 2011). These mine-laying operations were intended to threaten to flow of humanitarian aid into Libya, and they did (Zeitungzeid, 2011). Desperately needed aid was blocked and the evacuation of foreigners and wounded Libyans ceased (Reuters Africa, 2011). Italian Navy Vice Admiral Rinaldo Veri, Commander of the Maritime Headquarters in Naples (NATO) commented, "The mining of a civilian port by pro-Qadhafi forces is clearly designed to disrupt the lawful flow of humanitarian aid to the innocent civilian people of Libya and is another deliberate violation of United Nations Security Council Resolution 1973" (Zeitungzeid, 2011). Facing adversaries with little or no concern for the loss of civilian lives is a harsh but true reality of modern-day warfare.

Pushing even closer in time towards the present date, Iran threatened to close the Strait of Hormuz in December 2011 (Blair, 2012). This threat surfaced from a senior member of Iran's parliament after European Union nations set an oil embargo against Iran to deter its nuclear program (Blair, 2012). The Strait of Hormuz, measuring 280km long and 45km wide at its narrowest point, connects the Sea of Oman to the Arabian Gulf (Khan, 2010). Any successful attempt to close the strait would have international consequences; 17 million barrels of oil move through the waterway every day and they account for 35% of the world's seaborne crude oil shipments (Blair, 2012). While attempts to close the strait may or may not include the laying of mines, "many experts agree that closing the strait largely rests on the ability of Iranian forces to rapidly lay a web of naval mines in its narrow passages without early interception" (Khan, 2010). Therefore, it is prudent to consider the easiest of all mines, and arguably the most rapid, to deploy: the drifting mine (Khan, 2010). Although closing the strait using drifting mines could exercise Iranian power and drastically increase the price of crude oil

worldwide, it is important to note that approximately 87% of Iranian imports and 90% of its exports travel by sea (Khan, 2010). Therefore, it is logical to assume that economic interests could be the only deterring factor to Iranian mining operations (Khan, 2010).

By examining the aforementioned examples in recent history, a disconcerting yet reasonable question arises: what if a nation or terrorist group is able to deploy a drifting mine in an area that will not harm its own interests but can deliver potentially devastating consequences to its adversary? This is a question that will hopefully never be answered by the United States or its Allies. However, it must be considered to stay ahead of mine threat tactics and avoid repeating the past.

2. Forward-Thinking Countermeasures

The countermeasure for drifting mines has stayed relatively the same throughout history. For example, during the Persian Gulf War, intelligence reports showed that Iraqi forces may have intentionally deployed drifting mines to deter Coalition naval operations (Desert Shield/ Desert Storm, 2010). As always, the standard procedure to counter drifting objects was to set shipboard mine watches and deploy helicopters to search the area. This, however, is time consuming and detracts from other necessary missions required of operational aircraft carriers and supporting ships. If a drifting mine, which can easily be deployed from a small boat, was set free in a U.S. port, it can be assumed that the same search and destroy procedure would apply.

II. OCEANOGRAPHIC DESCRIPTION OF THE CHESAPEAKE BAY AND HAMPTON ROADS INLET

A. HAMPTON ROADS INLET SELECTION

The Hampton Roads Inlet, as shown in Figure 1, is located at the mouth of the James River, between the northern end of the Hampton Roads Bridge Tunnel and Fort Wool. This area, measuring slightly less than one nautical mile across, was chosen for two main reasons. First, it is located within three nautical miles of Naval Station Norfolk, the largest U.S. naval station in the world. Second, Hampton Roads is the world's leading bulk cargo harbor (PAWSA Report, n.d). In fact, commercial barges carry approximately 150,000 to 500,000 barrels of petroleum in and around Hampton Roads biweekly (PAWSA Report, n.d). Furthermore, six military tankers, each with a 7.5 million gallon capacity, are homeported in Norfolk (PAWSA Report, n.d).

Given that U.S. naval movements roughly equal the commercial traffic in this area, Hampton Roads is an appealing target for terrorist activity (PAWSA Report, n.d). To further this point and provide a real-life example of the shipping traffic near Norfolk, AIS data for the modeling period used for this study was collected and is displayed in Figure 2. Due to the high traffic density and military importance, an attack, or threat of attack, on this area using drifting mines could have immediate impacts on economic stability and national security (PAWSA Report, n.d).

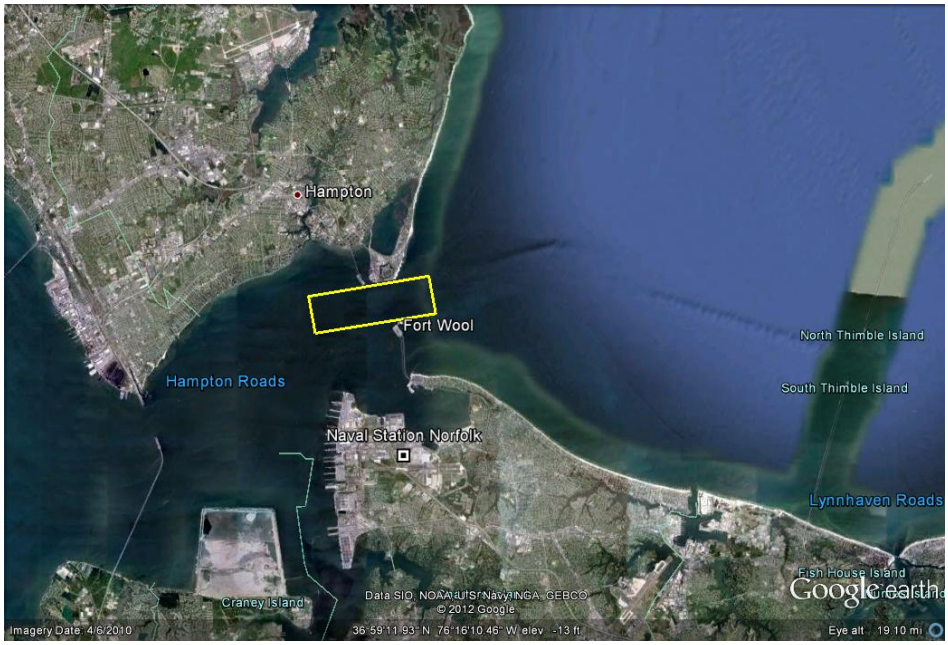

Figure1. Hampton Roads Inlet area at the mouth of the James River

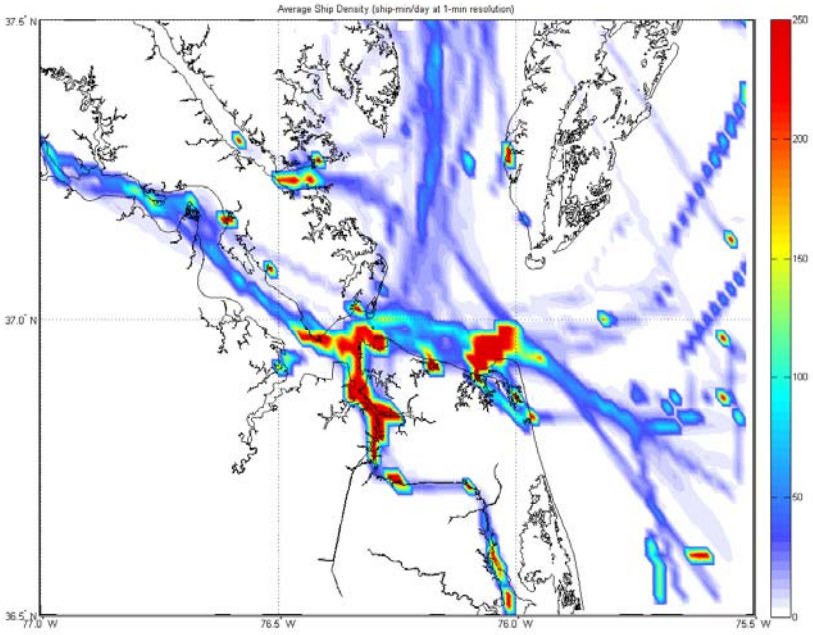

Figure 2. Average ship density in the southern Chesapeake Bay (Courtesy of C.W. Miller and J.E. Joseph, NPS Ocean Acoustics Lab)

B. HAMPTON ROADS INLET FLOW DYNAMICS

The flow dynamics in the lower part of the bay, near Norfolk, are mostly affected by bathymetry, wind, buoyancy and tidal forcing (Teague, 2011).

1. Bathymetry

Serving as a connection between the Thimble Shoal Channel and the James River, the Hampton Roads Inlet ranges from approximately 5 to 30 m in depth, as shown in Figure 3. This area is relatively deep when compared to the remainder of the south Chesapeake Bay, Figure 4, and therefore is sufficient for several ship traffic channels, Figure 5 and 6. The portion of the Thimble Shoal Channel that reaches into the Hampton Roads Inlet is bounded to the north by the Thimble Shoal, Old Point Comfort, and the Hampton Bar, and to the south by Willoughby Bank, Fort Wool, and Sewells Point Spit.

Channels in the South Chesapeake Bay, such as this one, may have large influences over the total flow dynamic. In particular, bathymetric variations can influence stratification over channels and bottom front formation (Valle-Levinson & Lwiza, 1997). Any increase in stratification over channels can increase the elliptical nature of the M2 tidal constituent with depth and therefore affect the overall flow (Valle-Levinson & Lwiza, 1997). In general, the bathymetry and hydrography of the lower Chesapeake Bay have the most notable effect on the tidal flow characteristics of the area which will be discussed in a later section.

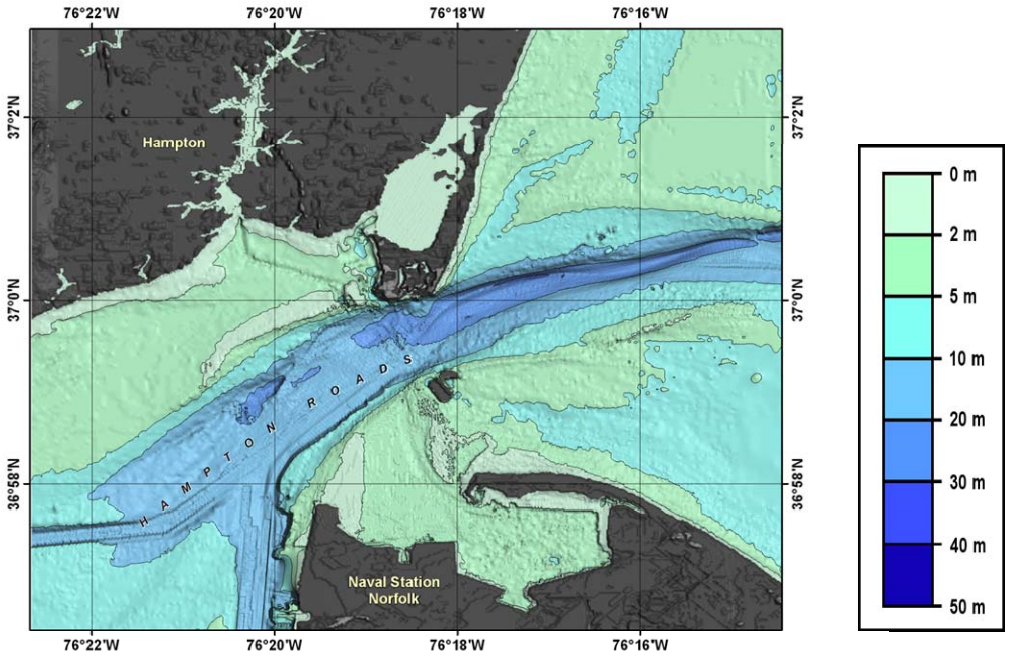

Figure 3. Bathymetry for Hampton Roads Inlet

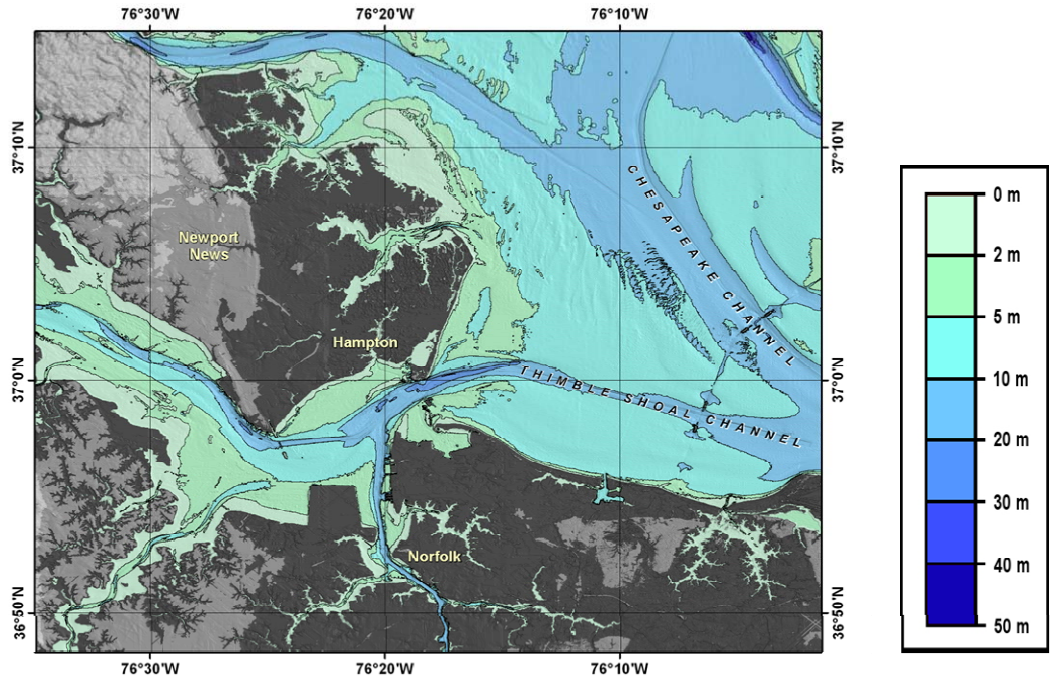

Figure 4. Bathymetry for South Chesapeake Bay

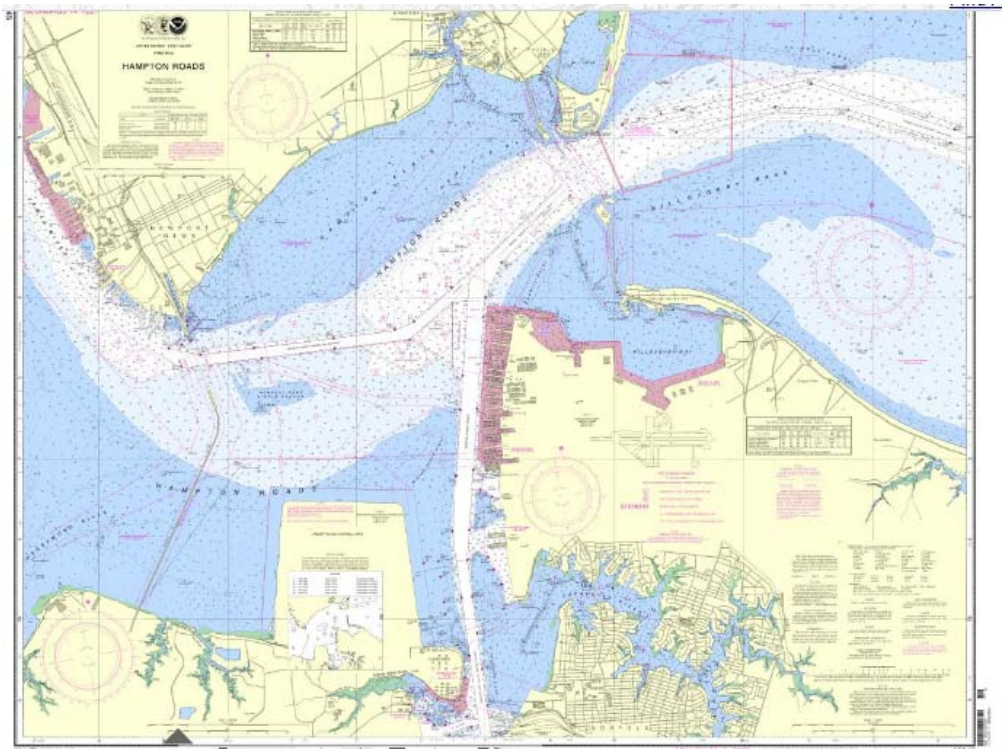

Figure 5. NOAA Nautical Chart of the Hampton Roads Inlet and surrounding area (From NOAA, 2008)

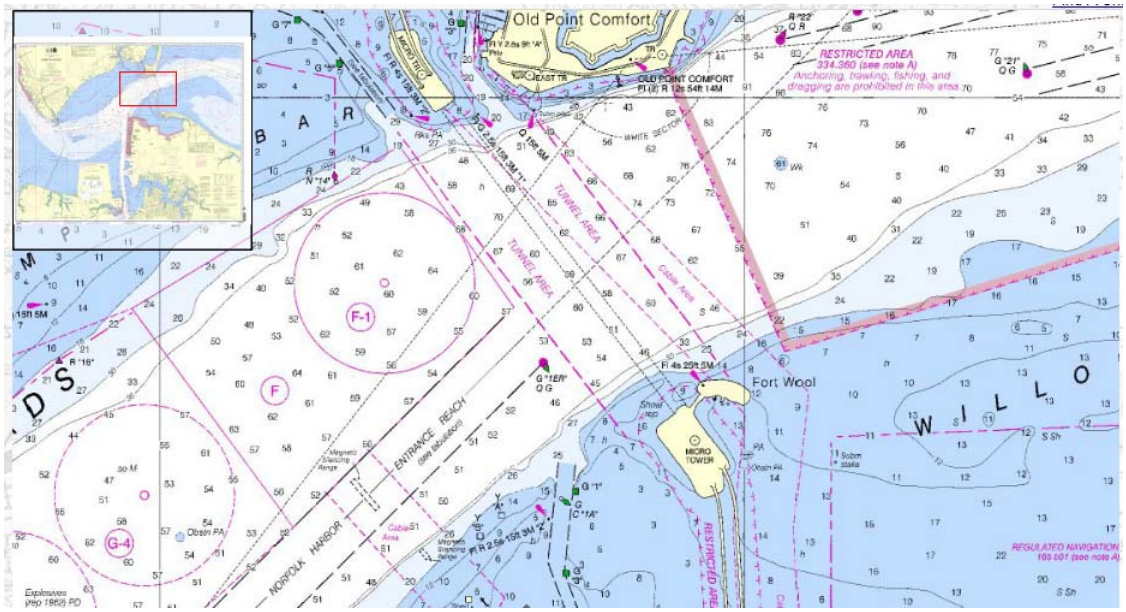

Figure 6. NOAA Nautical Chart Inset of Hampton Roads Inlet (From NOAA, 2008)

2. Atmospheric Conditions

a. Wind

Prevailing seasonal winds in the Chesapeake Bay area are typically northeasterly and southwesterly and vary between 4 and 6 m/s, except in summer when wind speeds are generally slower (Levinson, Li, Royer, & Atkinson, 1998). From late summer to early spring, northeasterly winds dominate until summer when they change to a more southwesterly direction. Observed seasonal variation in these winds showed that the highest energy wind forcing was commonly seen during late fall and winter from the northeast or northwest. Although strong wind forcing is generally seen during the late fall and winter, highly energetic winds can occur during any season and are not always from a northeast or northwest direction (Levinson, Li, Royer, & Atkinson, 1998).

Prevailing winds, combined with the orientation of the bay entrance, can cause large variations in current flow and subtidal sea-level within the Chesapeake Bay (Levinson, Li, Royer, & Atkinson, 1998). Wind can reinforce or reverse current flow throughout the bay's two-layered vertical density structure (L13). As for sea-level variations, a northeasterly wind will normally lead to an increase in subtidal sea surface elevation at the entrance of the bay caused by a net barotropic inflow. In contrast, a southwesterly wind often causes barotropic outflow which leads to a decrease in sea-level. The effects of wind, from the aforementioned directions, on sea-level and current flow in the lower bay have been observed to occur in less than 10 hours (Levinson, Li, Royer, & Atkinson, 1998).

b. River Run-off and Buoyancy

River run-off has a significant effect on density stratification, hence surface buoyancy, throughout the bay. On average, the Chesapeake Bay intakes 2500 m^3/s of freshwater run-off each year (Levinson, Li, Royer, & Atkinson, 1998). Approximately 14% of the total run-off comes from the James River and flows into the lower Chesapeake Bay (Levinson, Li, Royer, & Atkinson, 1998). River run-off maximums are typically seen in March and April whereas the minimums are during August and September. Therefore, a strongly stratified, meaning vertical differences in

salinity of order 10, environment can be expected in April and May and a virtually homogeneous, meaning vertical differences of less than 2, environment in October and November (Levinson, Li, Royer, & Atkinson, 1998).

3. Tidal Variations and Current Flow

Hampton Roads Inlet exhibits a semi-diurnal tidal flow with a mean range of 0.740 meters and a diurnal range of 0.841 meters (NOAA Tides and Currents, n.d.). The tidal variations in this region are particularly important because of their link to two important oceanographic features near the mouth of the James River that affect overall current flow. The first feature is a frontal system that develops during early flood tide under normal lunar variation (Mann, 1988). It forms mainly because of tidal current phase differences in the region and can usually be seen on the surface as a line of foam or litter (Mann, 1988). The second feature, a cyclonic gyre in the Hampton Roads region, acts to strengthen the flood current during early flood tide. It combines with the frontal system to partially retain downstream-flowing water in the James River estuary (Mann, 1988). Overall flow, in the three dimensional sense, can be affected by this retention as downstream-flowing water may be injected into deeper upstream-flowing water. Contributing to this three dimensional flow is the flooding water itself. The more saline flood water from the Bay flows into the Inlet from the Hampton Flats and dives under fresh ebbing water from the River; the downward movement of the saline water is enhanced by the steep bottom features near Newport News Point. To further explain the circulation in the area, non-tidal currents and the Hampton Roads frontal feature are shown below in Figure 7.

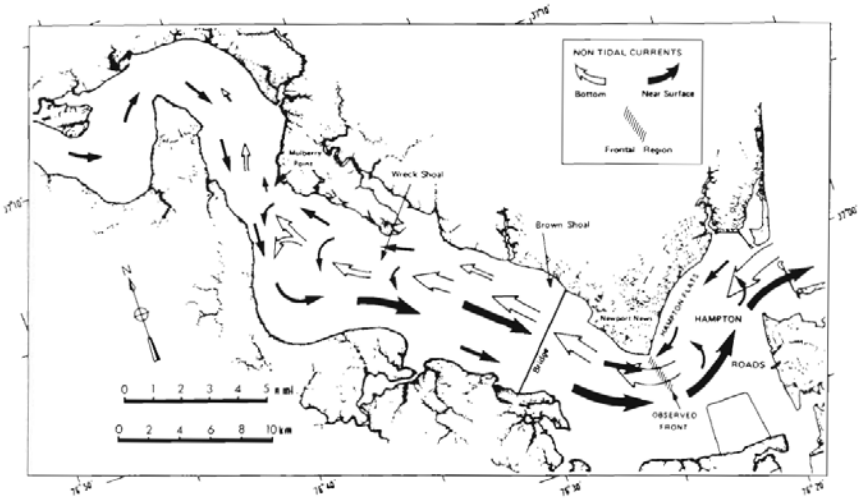

Figure 7. Current flow throughout the James River (From Mann, 1988)

As can be expected, tidal variations will play a large role in the modeling of drifters in this area due to its inner bay location and small scale.

III. MINE DRIFT MODELING

A. DELFT3D CIRCULATION MODEL

Delft3D, developed by a Dutch institute entitled Deltares, is an integrated computer software program that can provide multi-dimensional simulations of current flows, sediment transports, waves, water quality, and ecology for coastal, river, and estuarine environments (Deltares, 2011). While the Delft3D package has several modules, the primary module used for current simulations is Delft3D-FLOW (Deltares, 2011). Delft3D flow layers tidal and meteorological forcing on a rectangular or curvilinear grid to calculate non-steady flow and transport phenomena (Deltares, 2011). Delft3D applications include, but are not limited to, the aforementioned tide and wind-driven flow simulations, density driven flows, river flow simulations, fresh-water river discharge into bays, thermal stratification, and wave-driven currents (Deltares, 2011).

The Delft3D model applications were used by the Naval Oceanographic Office in Stennis Space Center, MS. to create a relatively small scale, approximately 60 meters resolution, Chesapeake Bay flow simulation (M. Toner, personal communication, April 18, 2012). This flow simulation, known as the Chesapeake Bay Delft3D model, is one of several high resolution oceanographic simulations developed for the purposes of homeland defense. Acting as a nested model, its flow is forced at the open boundaries by temperature, salinity, water level, and velocities provided by the USEAST Regional NCOM model (Teague, 2011; M. Toner, personal communication, April 17, 2012). The local wind stress input, provided by 15 km COAMPS, forces flow at the free surface (Teague, 2011; M. Toner, personal communication, April 18, 2012). Computation of flow within the model is accomplished through solving unsteady shallow water equations in three dimensions (Teague, 2011). The flow computation produces both depth averaged currents and horizontal velocity vectors for several depth layers. For the purposes of this study, only the horizontal velocity vectors, U and V, at the surface were used to develop drift simulations.

The evaluation and validation of the Delft3D current model for the Chesapeake Bay was conducted in 2011 by the Naval Research Laboratory (Teague, 2011). Real-time current observations for the purposes of model comparisons were taken from NOAA's Tides and Currents website for July 28 to August 30, 2011 (Teague, 2011). Five stations near Norfolk, each with operational acoustic current Doppler profilers (ADCPs), were used to evaluate the model: Cape Henry, York Spit Channel, Thimble Shoal, Naval Station, and Newport News Channel (Teague, 2011). The evaluation concluded that the Chesapeake Delft3D model is tidally driven (Teague, 2011). Although the comparison showed significant differences in mean model currents and mean observed currents, the tidally driven model should still be able to "provide a reasonable depiction of current fluctuations" (Teague, 2011). Furthermore, Michael Toner, from the Naval Oceanographic Office, stated that "if an operational situation arose that required drift predictions in the Chesapeake, we would definitely use the DELFT3D model because it is the most accurate we have; the 80% solution on time is much more useful than the 99% solution delivered late or not at all" (M. Toner, personal communication, April 18, 2012). Therefore, it is assumed that the high resolution Chesapeake Delft3D model is adequate to provide input for drift model calculations formulated during this research.

Chesapeake Delft3D covers a large portion of the Chesapeake Bay; a smaller region was specified to extract data for the Norfolk area (see Figure 8).

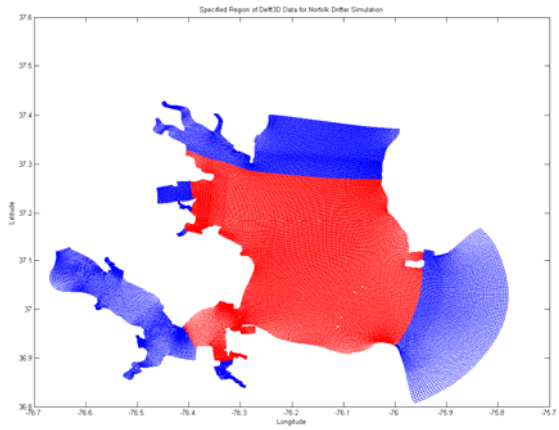

Figure 8. Subsection of Chesapeake Delft3D for the purposes of drift model research

Delft3D data, including depth, longitude, latitude, and 4-dimensional U and V current vectors, was extracted and imported into a netcdf file for the red region shown above. As previously mentioned, the U and V vectors from this data were used to force the drifter simulations. For the explanation of drifter formulation, U and V will be used to represent the Delft3D current velocity components and u and v will be used to represent drifter velocity components.

B. DRIFT FORMULATION

1. Curvilinear Grid Conversion

The grid used for the Delft3D model is a curvilinear grid that uses latitude and longitude to identify position. To simplify grid locations and follow-on calculations, the grid was converted from latitude and longitude to distance in meters. The center of the red area above was identified as the origin of the drifter grid, $(x_d, y_d) = 0$, and all other locations within the grid were converted accordingly.

2. Starting Drifter Positions and Times

To simulate a realistic scenario of drifters intended for the Hampton Roads Inlet, all of the drifters used for this research started with a randomly selected position within a 2 nautical mile by 1.6 nautical mile box located 0.75 nautical miles east of Fort Wool. The start positions within the box were randomly selected using both uniform and normal distribution formulas. Uniform and normal random positions were generated using the MATLAB function rand(n) and randn(n), respectively, which give n x n matrices of pseudorandom values taken from a standard uniform, or normal, distribution on the open interval (0,1).

The start time used for each drifter trajectory coincides with the beginning of flood time for each day (see Table 1). Using a total of 12 days of Chesapeake DELFT3D data, July 28, 2011 to August 9, 2011, the period of flood for each day lasted approximately three hours and acted to drive the most of the simulated drifters through

the length of the inlet. For each day, 10,000 drifters were randomly placed in the start box, according to uniform or normal distribution as described above, and permitted to run for three hours.

Table 1. Flood times according to Chesapeake Delft3D Model

Day (2011)	Flood Time Period
7/28	10Z – 13Z
7/29	10Z – 13Z
7/30	11Z – 14Z
8/01	12Z – 15Z
8/02	13Z – 16Z
8/03	14Z – 17Z
8/04	14Z – 17Z
8/05	15Z – 18Z
8/06	16Z – 19Z
8/07	17Z – 20Z
8/08	18Z – 21Z
8/09	19Z – 22Z

3. Drifter Movement

The drifters move via a step by step process that uses position, time, and corresponding U, V data to update each position.

To calculate the second point location in the drifter simulation, (x_{n+1}, y_{n+1}),

$$x_{n+1} = x_n + \int_0^{\Delta t} u dt$$
$$y_{n+1} = y_n + \int_0^{\Delta t} v dt \tag{1}$$

Second point location is estimated using

$$x_{n+1} = x_n + u_n \Delta t$$
$$y_{n+1} = y_n + v_n \Delta t \tag{2}$$

This position is used to interpolate (u_{n+1}, v_{n+1}) in order to correct the location

$$x_{n+1} = x_n + \frac{1}{2}(u_n + u_{n+1})\Delta t$$
$$y_{n+1} = y_n + \frac{1}{2}(v_n + v_{n+1})\Delta t \tag{3}$$

The time interpolation for (u_{n+1}, v_{n+1}) was a simple linear interpolation of Delft3D time layers. Spatial interpolation of Delft3D (U, V) for (u_{n+1}, v_{n+1}) was accomplished by the following method:

Minimum distance calculation from Delft3D grid point to the drifter location (see Figure 9)

$$dist^2 = (x_d - x)^2 + (y_d - y)^2 \tag{4}$$

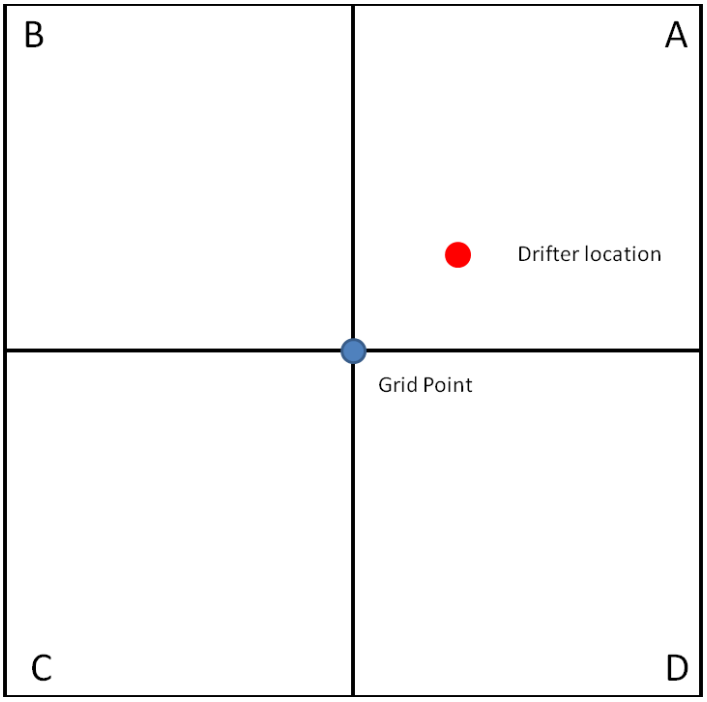

Figure 9. An example drifter location with respect to Delft3D grid point

To determine which box, A, B, C, or D above, the drifter was located (see Figure 10 and 11)

$$\theta_1 + \theta_2 + \theta_3 + \theta_4 = 2\pi \tag{5}$$

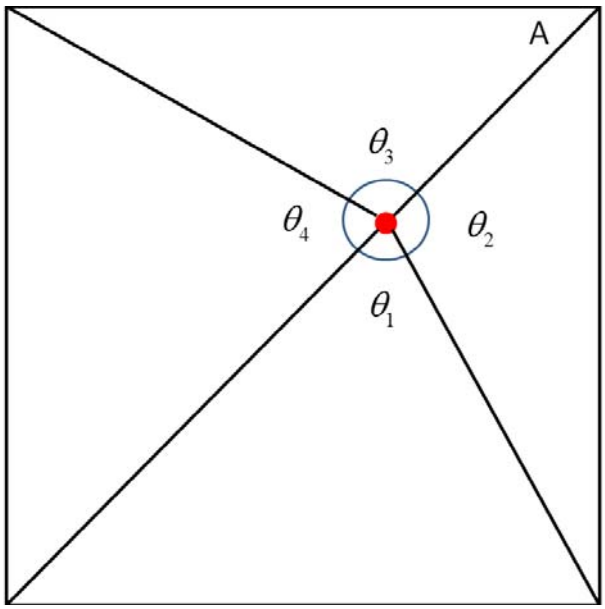

Figure 10. Diagram to show that if the drifter was located in the box, the sum of the angles is 2π

$$\theta_1 + \theta_2 + \theta_3 + \theta_4 = 0 \tag{6}$$

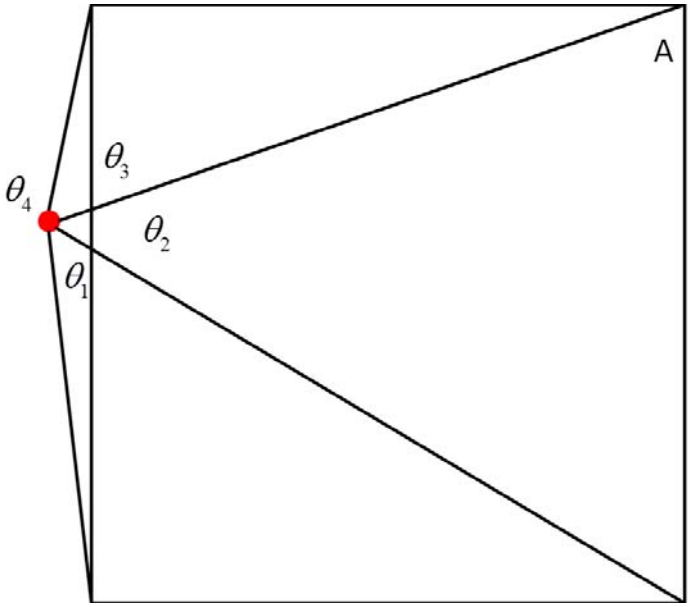

Figure 11. Diagram to show that if the drifter was located outside of the box, the sum of the angles is 0

Several box locations calculations were completed until the correct box location was found. Having found the correct box, multiple dimension linear interpolation was used the find the drifter location, point $f(x_{n+1}, y_{n+1})$ (see Figure 12). This process was repeated for the duration of the specified drift time or until the drifter collided with a boundary.

$$f(x_{n+1}, y_{n+1}) = F_1(\frac{S_{34}}{S_{12}+S_{34}})(\frac{S_{23}}{S_{23}+S_{41}}) + F_2(\frac{S_{34}}{S_{12}+S_{34}})(\frac{S_{41}}{S_{23}+S_{41}})... \quad (7)$$

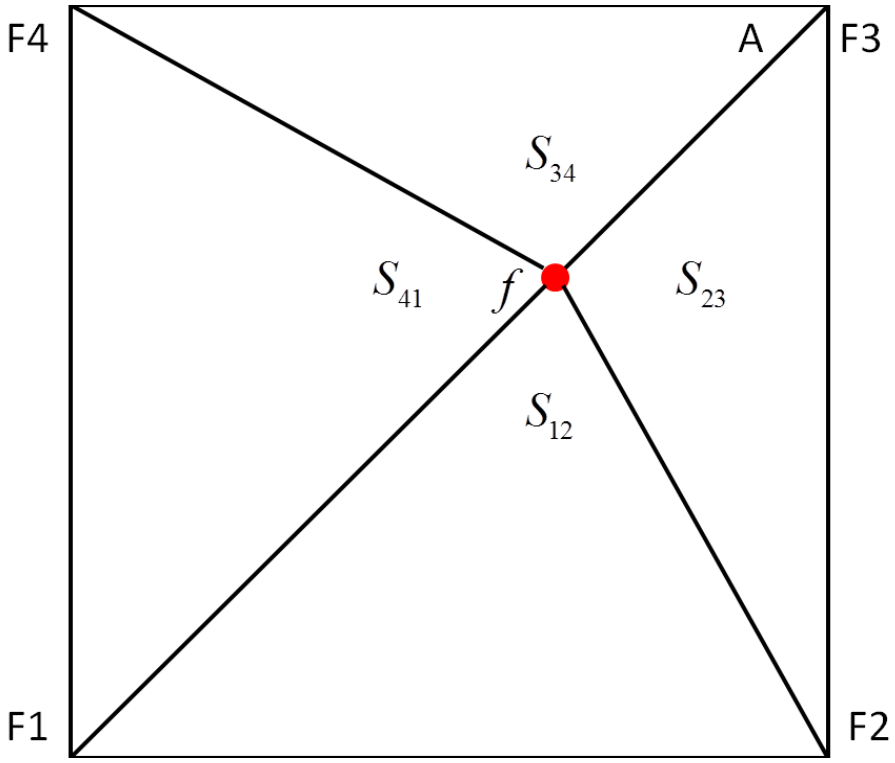

Figure 12. Weighted areas to calculate drifter location

IV. STATIONARY SENSOR GRID AND PROBABILITY OF DETECTION

A. SENSOR GRID FOR MOVING TARGET DETECTION SIMULATION

To simulate detection of drifters generated by the high-resolution current model, a hypothetical and ideal sensor grid was formulated. Each of the "sensors" in the sensor grid was modeled as an upward looking sonar system that has a circular detection footprint on the surface with a radius, R_d, of 100 meters. Forty-nine of these sensors were placed in a seven by seven grid to cover almost 100% of the Hampton Roads Inlet. The grid, each sensor with a specific index number, was placed just to the west of the drifter start box, as shown in Figure 13.

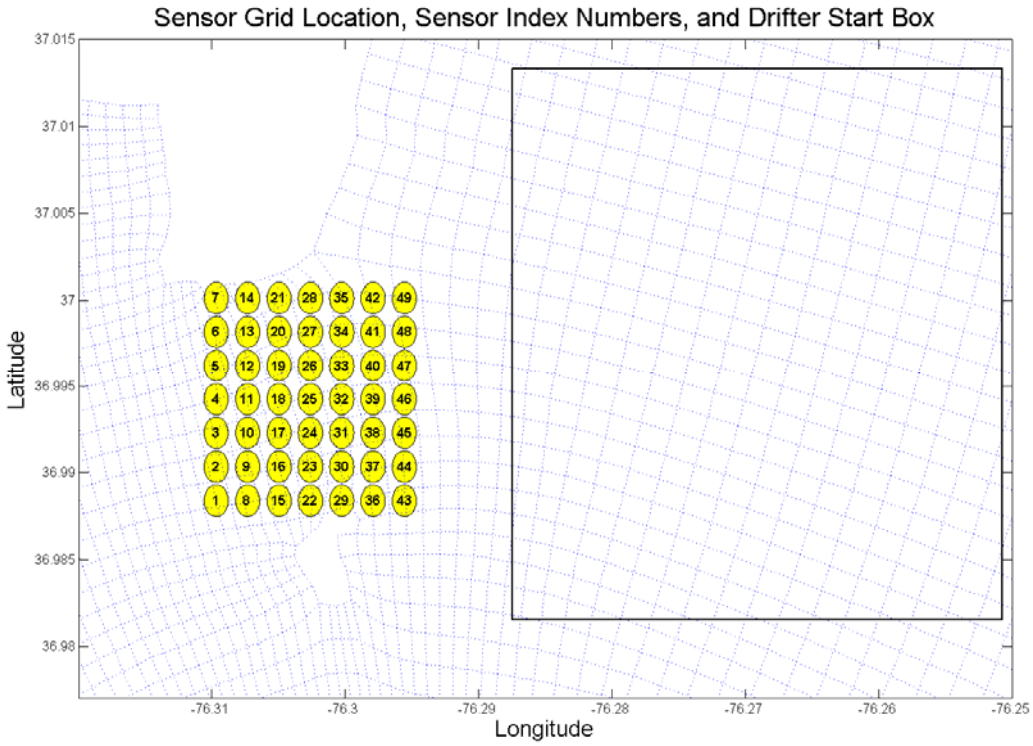

Figure 13. Sensor grid with associated index numbers and drifter start box

B. PROBABILITY OF DETECTION

1. Detection of Drifters

Each sensor was set to detect drifters that remained within its circular detection footprint for a period of five seconds or more during the three hour flood period of each day. At the conclusion of the flood period, the sensor with the most detection calls, or highest drifter density, was considered the "lead sensor" and the drifters that it called could not be considered detections by the remaining sensors. The sensor with the second highest number of detections, not including those called by the lead sensor, was marked as the "second place sensor." The sensor in third place had the highest number of detections, not including those called by the first and second sensors, and so on. In other words, the "lead sensor" is the only detector that is completely independent of the others. This ranking process continued until all of the drifters that ran through the grid were counted. Some of the drifters were directed away from or did not move fast enough to traverse the sensor grid and therefore were not included in the total count for each day. This process formed a sensor hierarchy which ranked each of the sensors with more than zero drifter detections for each day.

2. Probability of Detection

The probability of detection for each of the 49 sensors, referred to as sensor detection probability, was simply the number of drifters that each sensor called, not previously called by other sensors as described above, divided by 10000. Some of the 49 sensors were assigned a probability of zero because the drifters did not cross their surface footprints or all of the drifters they detected were previously called by other sensors.

Assuming that a detection scenario would allow more than one sensor to be used, a combined probability of detection can be calculated by adding sequential sensor detection probabilities in the hierarchy. For example, if three sensors are to be used, the sensor detection probabilities for the third, second, and first place sensors in the hierarchy

were summed together to form the combined probability of detection for three sensors. The total probability of detection, for a given day, is the combined probability associated with the number of sensors necessary for detection of the total drifter count. The total probability of detection from day to day could have large variations due to current speed and direction.

THIS PAGE INTENTIONALLY LEFT BLANK

V. OPTIMAL DEPLOYMENT OF STATIONARY SENSORS

A. IMPORTANCE OF UTILIZING DRIFT MODELS TO OPTIMIZE SENSOR NETWORKS

In past studies, networks of passive sensors have been discussed as potential tools for large area detection coverage while being moderately inexpensive (Wettergren, Performance of Search via Track-Before-Detect for Distribute Sensor Networks, 2008). Due to these features and many others, optimizing sensor networks for underwater port surveillance has been a long-standing and important area of study (Penny, 1999). Methods of optimizing sensor networks are usually discussed from two different perspectives: the point coverage approach and the target path coverage approach. Seeking to find ways to detect stationary objects within a surveillance region is known as point coverage; target path coverage seeks solutions to detect targets as they move across areas of surveillance (Wettergren & Costa, Optimal Placement of Distributed Sensors Against Moving Targets, 2009). Both of these methods have been used to specifically address sensor network optimization.

This study is related to target path coverage and is designed as an addition to previous work. It aims to use knowledge of the environment to specifically address some of the issues and conclusions stated in previous studies of moving target detection. There are several areas of sensor network research that could benefit from environmental knowledge, however, only a few are addressed in this study. First, in Wettergren (2009) it states "the increase in (sensor network) performance becomes more significant as prior knowledge of target dynamics increases" (Wettergren & Costa, Optimal Placement of Distributed Sensors Against Moving Targets, 2009). Secondly, also in Wettergren (2009), it states one of the hardships associated with undersea sensor systems is that "cost and deployment limitations lead to necessarily sparse coverage fields" (Wettergren & Costa, Optimal Placement of Distributed Sensors Against Moving Targets, 2009). Lastly, in Wettergren (2008), it concludes the following: "To minimize false search for a fixed search performance, it was shown that a smaller number of larger range sensors is desirable" (Wettergren, Performance of Search via Track-Before-Detect for Distribute

Sensor Networks, 2008). These statements highlight three specific needs to further sensor network research: high-resolution estimations of target movement, optimal sensor numbers, and optimal sensor locations. The goal of this research is to provide guidance for all three of these needs while also giving insight into how often sensor locations should be updated. The key to providing such guidance, in the example that will be presented, is a high-resolution drift model.

B. SENSOR ALLOCATIONS RESULTING FROM DRIFT MODEL INPUTS

1. Optimal Sensor Locations

For the 12-day Hampton Roads example used in this research, the drift model outputs serve as high-resolution estimations of target movement. The drift estimations were used in a greedy optimization process, as described in Chapter IV, to recommend sensor locations. The optimal sensor locations, associated with both uniform and normal Monte Carlo simulations, are presented in Appendix A, B, and C. Appendix A shows the numerical results of the greedy optimization process for each day using bar graphs. Appendix B shows sensor ranking results by displaying the appropriate ranking number inside of the sensor locations used to accomplish a total drifter count for that day. Appendix C is a detailed table of the graphic results shown in Appendix A and B. As can be observed, optimal sensor locations varied according to daily drifter tracks and the type of Monte Carlo simulation used for each flood period. Due to these variations, each flood period required a different number of sensors to achieve total probability, as shown in Appendix B and C. Therefore, it became important to optimize both sensor location and sensor number.

2. Optimal Number of Sensors

Each flood period was examined to find how many sensors were necessary to achieve a 90%, 95%, or 99% of the total probability. As shown in Table 2, this varied depending on the Monte Carlo distribution and the day. Therefore, the mean number of sensors for each percentage of the total probability was calculated and recorded. To offer the highest level of detection, the mean number of sensors associated with the highest percentage, 99%, will be the focus for the rest of this chapter. The lines representing the

99% cutoff are plotted in Figures 14 and 15. This line is plotted to show that adding more sensors than the mean number does not contribute significantly to the total probabilities for any of the days. Therefore, the optimal number of sensors, for this location and period of time, is 10 for a uniform distribution of drifters and 8 for a normal distribution of drifters. It is important to note that these numbers will change given a change in location or time period.

Table 2. Number of sensors required to achieve 90%, 95%, and 99% of the total probability

Uniform	Days												
Pd	1	2	3	4	5	6	7	8	9	10	11	12	Mean
90%	6.3960	5.7517	5.8258	5.1278	4.5709	4.4934	5.1692	5.1833	5.6069	5.4840	5.4614	6.1694	5.4367
95%	7.5973	6.6427	7.5671	5.7656	5.5691	5.2273	5.9727	5.8936	6.7911	6.5520	6.4489	8.2564	6.5237
99%	10.8560	9.9734	10.2296	9.5674	7.7432	6.2715	9.1552	10.5417	10.1171	10.6267	10.8340	11.2742	9.7658

Normal	Days												
Pd	1	2	3	4	5	6	7	8	9	10	11	12	Mean
90%	3.1350	3.7985	3.3369	3.4169	2.9500	3.2805	3.2687	3.8439	4.0632	4.0070	3.8286	4.1375	3.5889
95%	4.5772	5.2384	4.2491	4.2928	3.7010	4.0136	4.2500	4.7895	4.9115	5.0953	5.0435	5.0651	4.6022
99%	7.2518	8.7979	6.8719	6.4432	5.2712	5.5278	6.7500	7.4348	7.6643	8.0463	7.8424	8.5749	7.2064

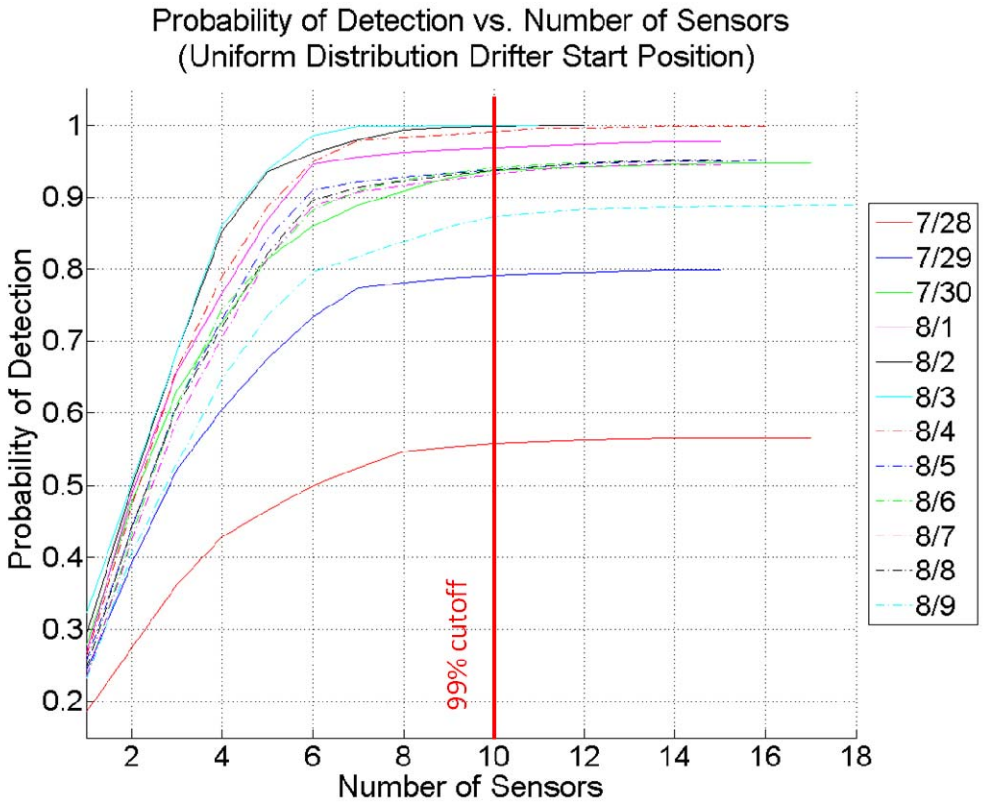

Figure 14. Total probability reached with a given number of sensors for each of the 12 days. The red line shows the number of sensors necessary to reach 99% of the total probability for the uniform Monte Carlo simulation

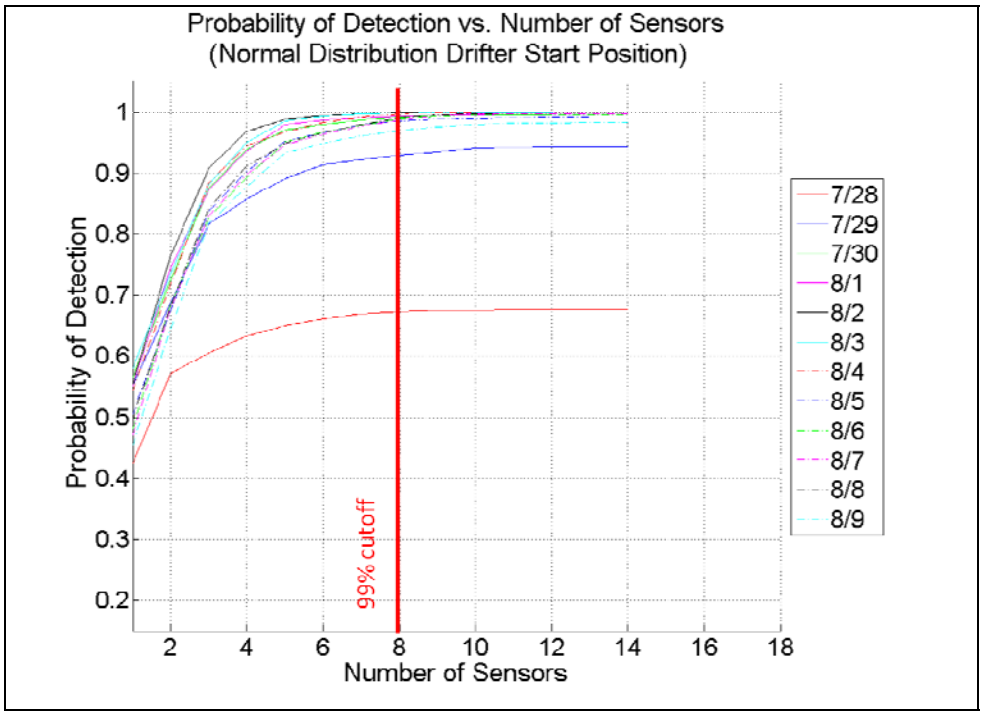

Figure 15. Total probability reached with a given number of sensors for each of the 12 days. The red line shows the number of sensors necessary to reach 99% of the total probability for the normal Monte Carlo simulation

3. Time Sensitivity of Sensor Locations

The time sensitivity of sensor locations is defined as how often a sensor position needs to be updated based on the latest model run. For this case study, it was found that when using the optimum number of sensors for 99% of the total probability, updating sensor positions based on the daily model run does not significantly increase detection probability. As shown in Figures 16 and 17, using a red line, advancing the drift model one day while maintaining the optimal sensor positions of the previous day yields a minimal change in detection probability. To further test time sensitivity, the optimal sensor positions from 2 to 6 days prior were also tested using the model run from the current day. This showed that even when using the optimal sensor positions from 6 days prior, in both the uniform and normal case, the maximum variation in detection probability was only on the order of 5%. Therefore, although updating sensor positions based on the current model run for each day leads to the highest detection probability, the benefit is minimal.

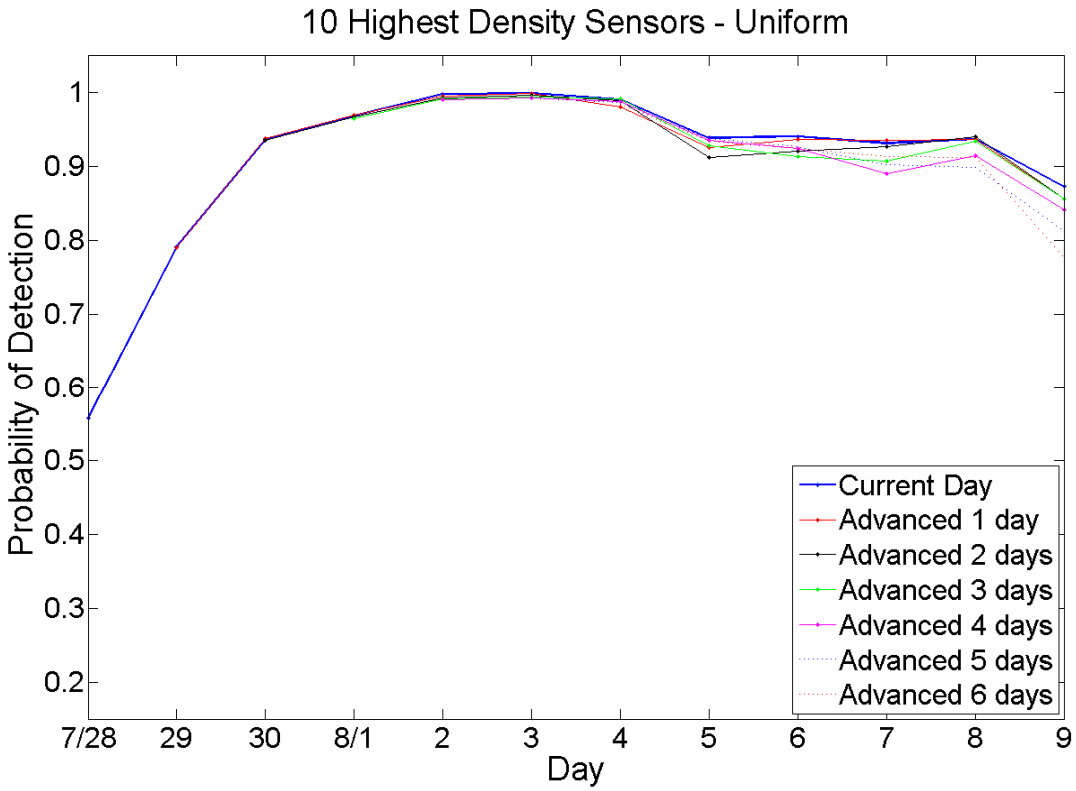

Figure 16. Time sensitivity for 99% of total detection probability of uniformly distributed drifter start positions

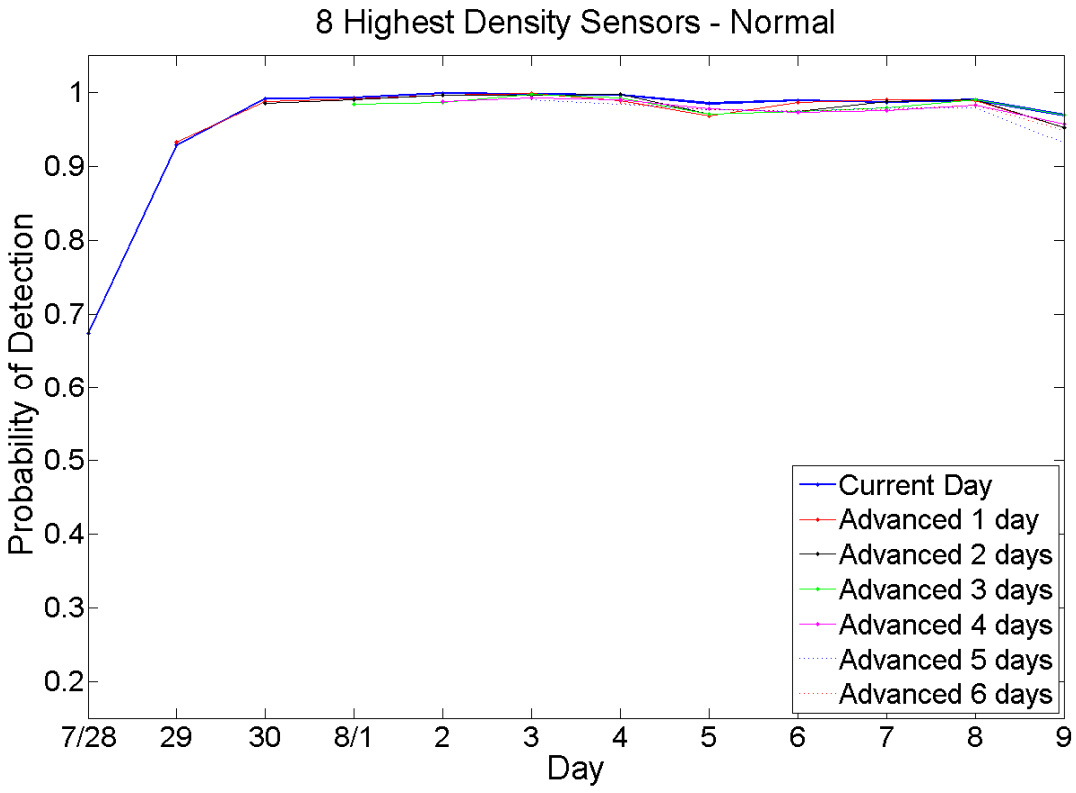

Figure 17. Time sensitivity for 99% of total detection probability of normally distributed drifter start positions

It should be noted, however, that using a number of sensors that was less than the optimum number for this case study significantly affected the time sensitivity associated with the normal and uniform model runs. If using a fewer number of sensors than the optimum number, maintaining sensor positions for more than a couple of days could significantly decrease detection probability, particularly for the uniform case. However, as the number of sensors increased towards the optimum number, the time sensitivity decreased, as shown in Figures 18 and 19. This reinforces the importance of determining and employing the optimum number of sensors based on current flow model predictions.

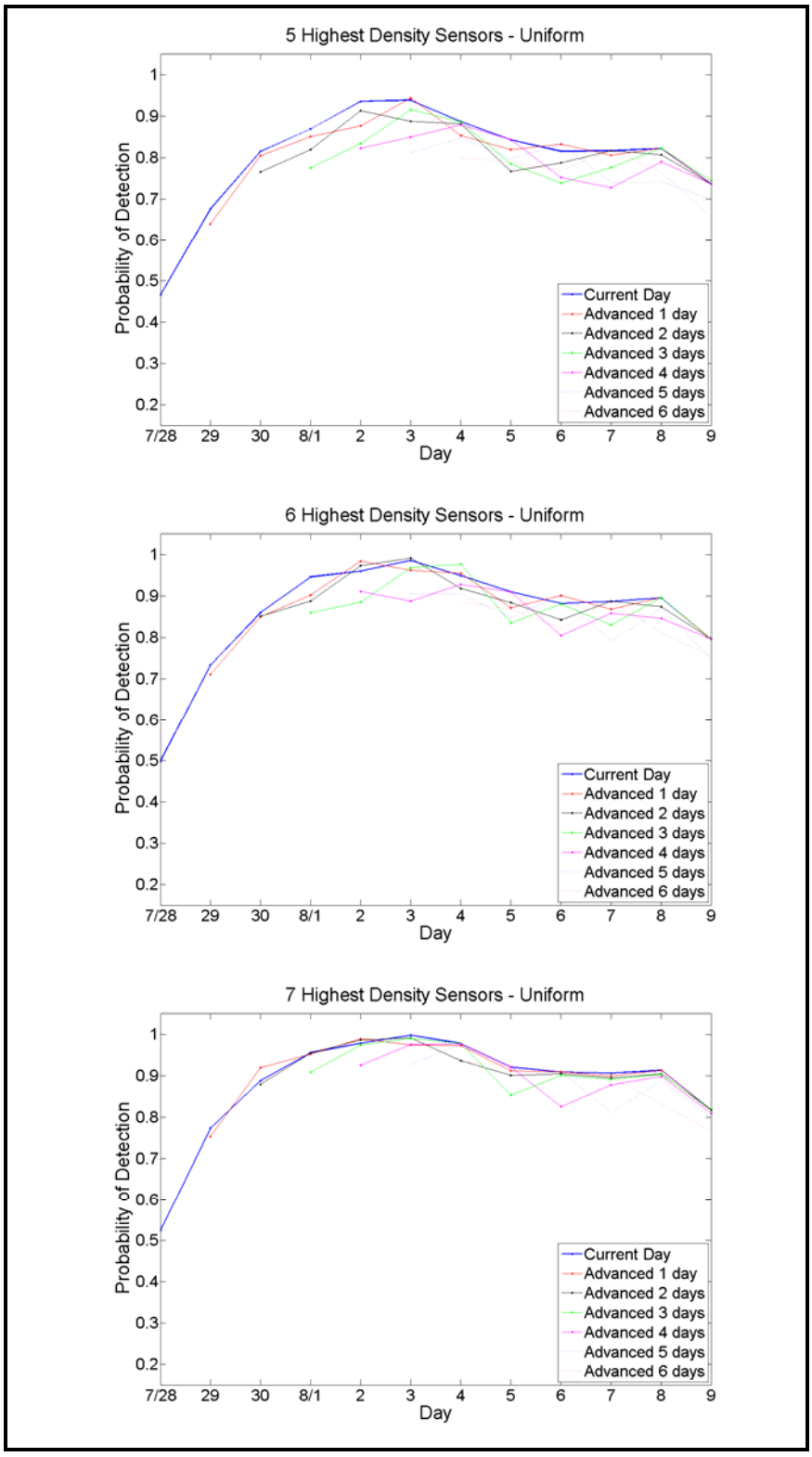
5 Highest Density Sensors - Uniform
Probability of Detection
Day
7/28
29
30
8/1
2
3
4
5
6
7
8
9
0.2
0.3
0.4
0.5
0.6
0.7
0.8
0.9
1
Current Day
Advanced 1 day
Advanced 2 days
Advanced 3 days
Advanced 4 days
Advanced 5 days
Advanced 6 days
6 Highest Density Sensors - Uniform
Probability of Detection
Day
Current Day
Advanced 1 day
Advanced 2 days
Advanced 3 days
Advanced 4 days
Advanced 5 days
Advanced 6 days
7 Highest Density Sensors - Uniform
Probability of Detection
Day
Current Day
Advanced 1 day
Advanced 2 days
Advanced 3 days
Advanced 4 days
Advanced 5 days
Advanced 6 days

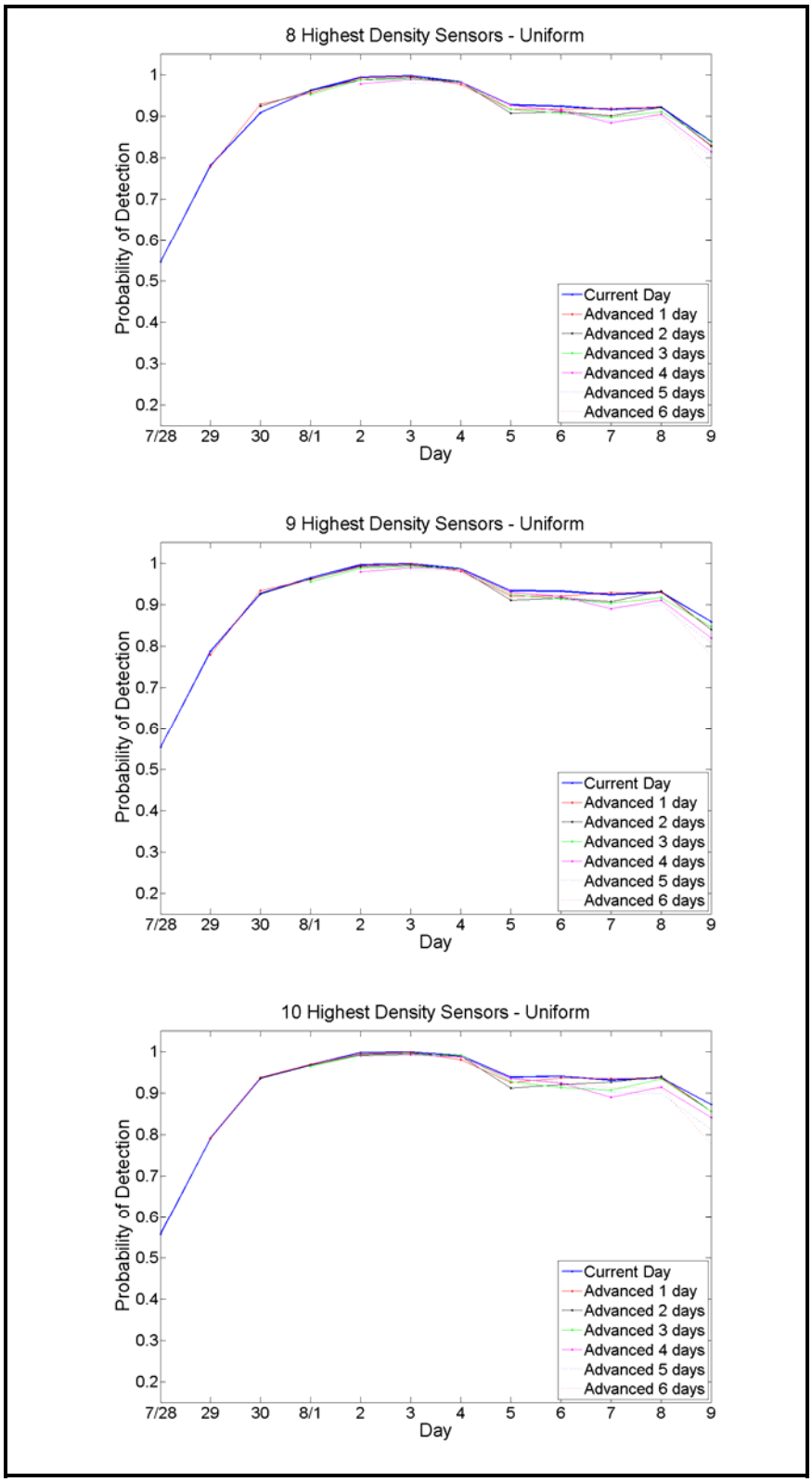

Figure 18. Time sensitivity for a varying number of sensors—uniform case.

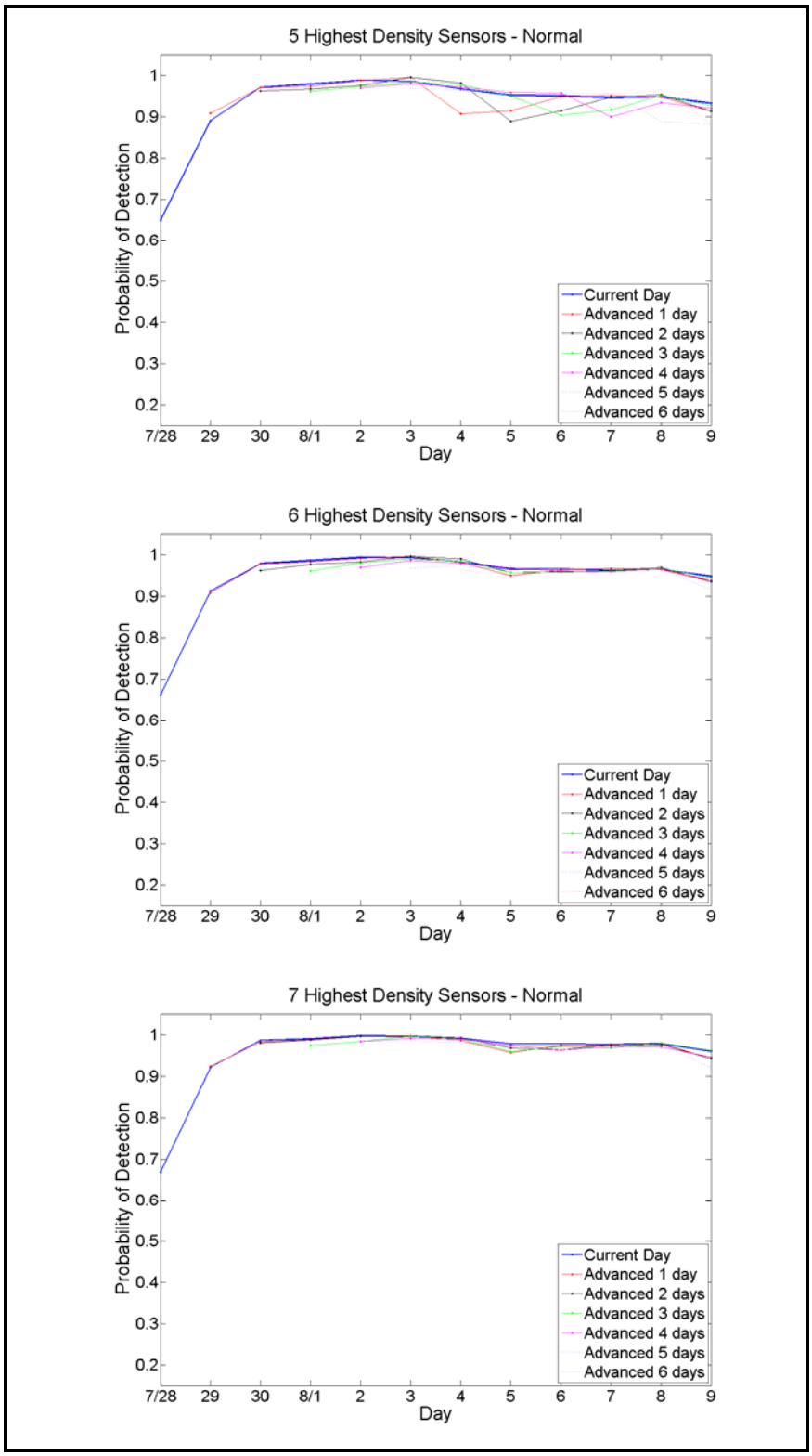
5 Highest Density Sensors - Normal
Probability of Detection
Day
7/28
29
30
8/1
2
3
4
5
6
7
8
9
0.2
0.3
0.4
0.5
0.6
0.7
0.8
0.9
1
Current Day
Advanced 1 day
Advanced 2 days
Advanced 3 days
Advanced 4 days
Advanced 5 days
Advanced 6 days
6 Highest Density Sensors - Normal
Probability of Detection
Day
Current Day
Advanced 1 day
Advanced 2 days
Advanced 3 days
Advanced 4 days
Advanced 5 days
Advanced 6 days
7 Highest Density Sensors - Normal
Probability of Detection
Day
Current Day
Advanced 1 day
Advanced 2 days
Advanced 3 days
Advanced 4 days
Advanced 5 days
Advanced 6 days

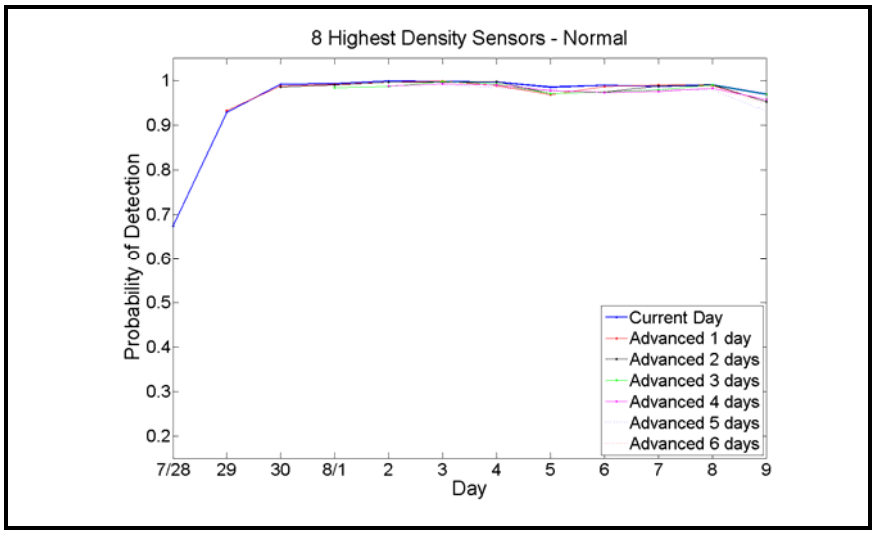

Figure 19. Time sensitivity for a varying number of sensors—normal case

C. SENSOR ALLOCATIONS WITHOUT USING DRIFT MODEL INPUTS

Some may argue that placing sensors according to drift model outputs is unnecessary and using sensors in a line formation across an inlet is just as efficient. There are several problems with choosing to use a line of sensors in this fashion. First, a line of sensors does not allow for flexibility in the number of sensors to be used. Secondly, some of the sensors in the line may be extraneous depending on the flow pattern for a particular time period. Lastly, selecting the location of such a line could dramatically affect the combined probability of detection and without environmental predictions the selection would be an educated guess at best. Therefore, to investigate the added benefit of employing the sensor optimization methodology previously described, combined probabilities resulting from the optimization process and a line of sensors were contrasted.

Using the grid as show in Figure 13, a sensor line was considered a north-south column of sensors numbered 1 through 7, west to east. The combined probability for each column was calculated as described in Chapter IV and was contrasted to the combined probability of the top seven sensors found using the optimization process for each day. The daily comparison results are shown individually in Appendix D. As seen in Figures 20 and 21, the differences in combined probabilities range from approximately

-1 to 19% for a uniform distribution and 0 to 27% for a normal distribution of drifters. This shows that, for this case study, depending on the day and the column of sensors chosen to create the detection line, the added benefit of using the sensor placement optimization process can be quite substantial.

It should be noted that some of the sensor lines yielded slightly higher combined probabilities than those of the optimized sensor formations for a particular day. These differences, however, were on the order of 1%. Furthermore, this was only true for the uniform case for three of the columns on August 8th and two of the columns on August 6th and 7th. This reinforces that column selection, for this case study, is paramount if attempting to achieve a higher detection probability than that reached using the sensor optimization process.

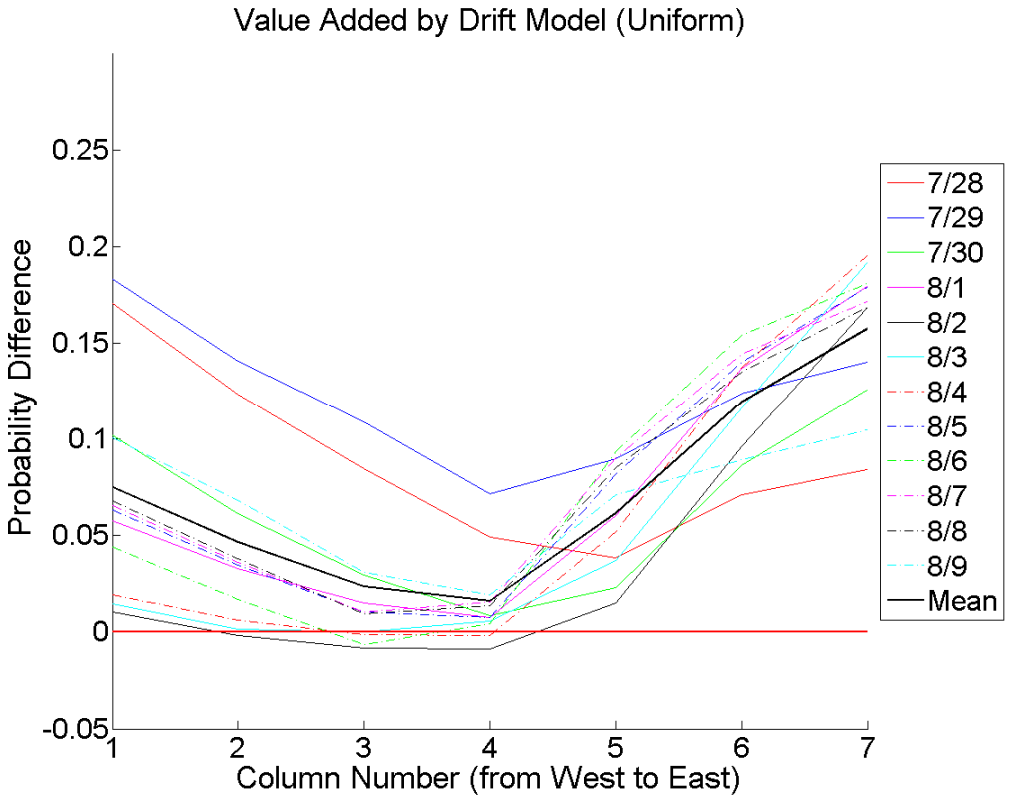

Figure 20. Combined probability differences found when contrasting optimized sensor results and sensor line results for the uniform case. Positive values indicate the value added by using drifter models to optimize sensor locations.

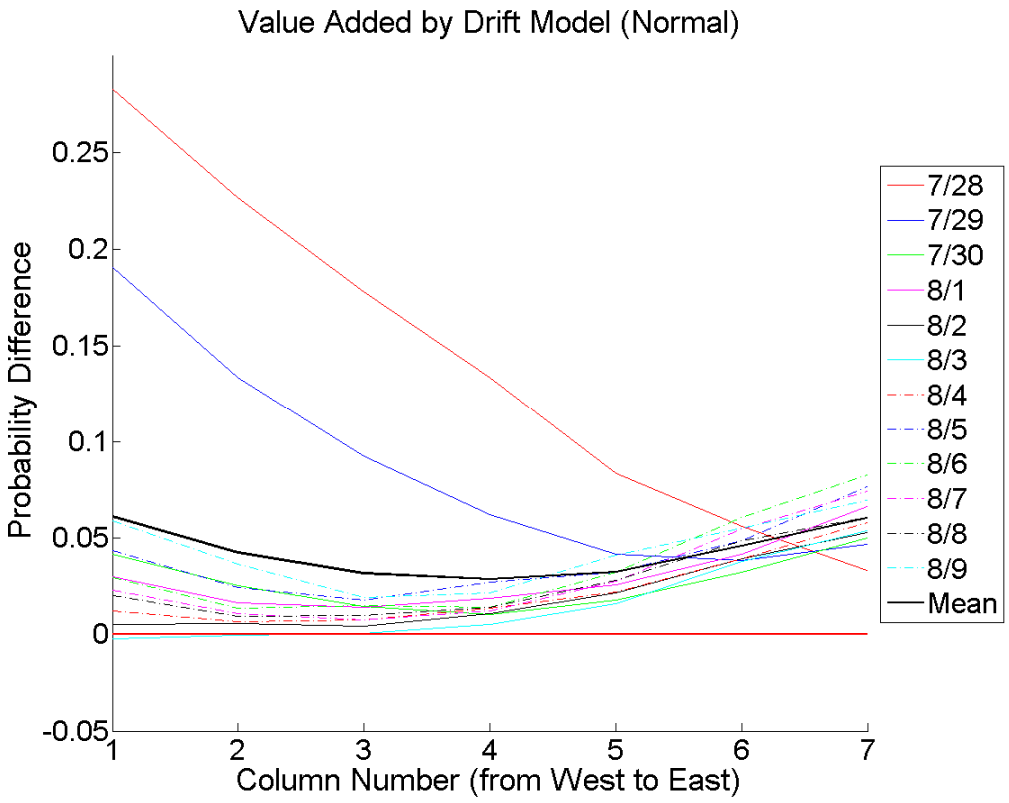

Figure 21. Combined probability differences found when contrasting optimized sensor results and sensor line results for the normal case. Positive values indicate the value added by using drifter models to optimize sensor locations.

THIS PAGE INTENTIONALLY LEFT BLANK

VI. CONCLUSIONS AND FURTHER RESEARCH

A. CONCLUSIONS

This research was intended to build upon previous sensor network studies that called for better target movement estimations. By marrying tactical oceanographic models with an optimized network, it was possible to provide improved target movement estimations and thereby build an environmentally realistic plan for detecting a floating target. The plan presented was an optimization process that used a current drift model to recommend the number of sensors needed to achieve an estimated level of detection and optimal locations for their use. Also incorporated in the plan was a time sensitivity study to show the effect of persisting sensor locations on detection probability. Lastly, to challenge the optimization plan presented, an alternative sensor arrangement, a line of sensors, was used to generate detection probabilities. Contrasting the two results showed how the optimization plan can offer higher detection probabilities than a line of sensors stretched across the width of an inlet or harbor. Thus this research was able to show the usefulness of and methodology for using ocean current models to optimize sensor networks.

It should be noted, however, that the optimization results are highly dependent on the target distribution chosen for each model run. Without prior intelligence of enemy tactics or field research, conclusions of the appropriate distribution for target simulations are circumstantial. While the uniform runs may be more applicable to a scenario involving a line of deployed drifting mines, normal runs may be more appropriate for an attack of simultaneous mine deployments from the same position. Therefore, both normal and uniform results are presented for completeness and future flexibility.

B. FURTHER RESEARCH

To further the research presented in this paper, large timescale studies should be conducted in order to determine monthly or seasonal positions for stationary sensors. While this study only focused on twelve days of data, the methodology can still apply to large timescales, provided there is archived model data for the larger timeframe to be

studied. Applying the methodology in this way could show that the cost of frequently moving sensors according to updated model data outweighs the benefit of doing so. Thus furthering the timescale of the methodology presented has the potential to offer optimized guidance for nearly continuous surveillance of U.S. inlets and ports.

Applying the optimization methodology to actual underwater sensors is another way to further the research presented. At the 3rd International Conference on Waterside Security in Singapore from May 28 to May 30 2012, several underwater systems were presented that could be used in future studies of this methodology. One of those systems is known as "Starfish," see Figure 22. Developed by Defence Research and Development Canada—Atlantic, Starfish, and the more recent model, "Starfish Cube" shown in Figure 23, are multi-influence sensor platforms used for underwater surveillance of littoral waters, choke points, and inlets. Starfish Cube contains internal processing for the detection and tracking of surface and subsurface targets. Its ARM processor is capable of performing real-time signal processing of sensor data which can be sent to a network of underwater modems and surface gateway buoys for remote satellite communications. It is designed for shallow water, typically less than 200 meters depth, and can run autonomously for more than two weeks of continuous use (Lucas, Heard, & Pelavas, 2012). If extended operation is needed, additional battery vessels can be linked to the Starfish Cube to further the operation time beyond two weeks. These features make the Starfish Cube an ideal device for harbor entrance monitoring. Therefore, in a future study, the optimization process presented in this research should be tested in a real-world setting by incorporating it into the deployment plans for a Starfish Cube network and evaluating its usefulness (Lucas, Heard, & Pelavas, 2012).

Figure 22. First generation of the Starfish sensor pods
(From Lucas, Heard, & Pelavas, 2012)

Figure 23. Second generation of the DRDC Starfish known as the Starfish Cube
(From Lucas, Heard, & Pelavas, 2012)

As a second option for field evaluation of the methodology presented in this paper it may be possible to use passive acoustic diver detection devices. Also presented at the 3rd International Conference on Waterside Security, passive acoustic diver detection devices can be used to track surface and subsurface contacts. Tested by the Netherlands Organization for Applied Scientific Research (TNO) and the Stevens Institute of Technology, the diver detection system, comprised of four hydrophones as shown in Figure 24, uses cross-correlation of acoustic signals to determine a target's Direction of Arrival (DOA). DOA triangulation is then used to detect and track targets. Given that a system can only have a certain number of sensors and may only be useful in certain locations, the usefulness of the methodology presented in this paper could also be tested when planning to use acoustic diver detection devices (Sutin et al., 2012).

Figure 24. SMID Technology (Italy) hydrophones used for diver detection system (From Sutin et al., 2012)

LIST OF REFERENCES

Barbosa, S. M., & Silva, M. E. (2009). Low-frequency sea-level change in Chesapeake Bay: Changing seasonality and long-term trends. *Estuarine, Coastal, and Shelf Science*, *83*, 30–38.

Blair, D. (2012, January 23). Iran threatens to close Strait of Hormuz over EU oil sanctions. Retrieved from *The Telegraph*: http://www.telegraph.co.uk/news/worldnews/middleeast/iran/9032948/Iran-threatens-to-close-Strait-of-Hormuz-over-EU-oil-sanctions.html

Committee for Mine Warfare Assessment. (2001). *Naval mine warfare: Operational and technical challenges for naval forces.* Washington: National Academy Press.

Deltares. (2011). *Delft3D-FLOW: Simulation of multi-dimentional hydrodynamic flows and transport phenomena, including sediments.* The Netherlands: Deltares.

Desert Shield/Desert Storm. (2010, 11 26). Retrieved from http://102msos.8m.net/desertshield_desertstorm.html

Khan, S. (2010). *INEGMA Special report no. 4: Iranian mining of the Strait of Hormuz-plausibility and key considerations.* Dubai and Beirut: Institute of Near East and Gulf Military Analysis (INEGMA).

Levinson, A. V., Li, C., Royer, T. C., & Atkinson, L. P. (1998). Flow patterns at the Chesapeake Bay entrance. *Continental Shelf Research*, *18,* 1157–1177.

Lucas, C., Heard, G., & Pelavas, N. (2012). The DRDC Starfish Underwater Multi-Influence Sensor Platorm. *3rd International Conference on Waterside Security* (pp. 1–7). Singapore: Bjorno, Leif.

Mann, R. (1988). Distribution of bivalve larve at a fronta system in the James River, Virginia. *Marine Ecology Progress Series*, *50*, 29–44.

Melia, T. M. (1991). *"Damn the torpedoes": A short history of U.S. naval mine countermeasures, 1777–1991.* Washington: Naval Historical Center.

National Research Council. (2000). *Oceanography and mine warfare.* Washington: National Academy Press.

Nihoul, J. C. (1978). *Hydrodynamics of estuaries and fjords.* Amsterdam: Elsevier Scientific Publishing Company.

NOAA Tides and Currents. (n.d.). Retrieved from Sewells Point, VA 8638610: http://tidesandcurrents.noaa.gov/geo.shtml?location=Norfolk%2C+VA

NOAA. (2008, August). Retrieved from Office of Coast Survey: http://www.charts.noaa.gov/OnLineViewer/12245.shtml

PAWSA Report Appendix A. (n.d). Retrieved from http://www.navcen.uscg.gov/pdf/pawsa/finalReport/PAWSA%20Report%20Appendix%20A.pdf

Penny, D. E. (1999). Multi-sensor management for passive target tracking in an anti-submarine warfare scenario. *Proceedings of the IEE Colloquium on Target Tracking*, *3*, 1–5.

Reuters Africa. (2011, May 2). Retrieved from NATO searches for drifting mine off Misrata: http://af.reuters.com/article/libyaNews/idAFLDE7411UU20110502?pageNumber=2&virtualBrandChannel=0&sp=true

Sutin, A., Bruno, M., Salloum, H., Dzielski, J., Sedunov, N., Sedunov, A., Tsionsky, M., et al. (2012). Passive acoustic diver detection in a Dutch harbor. *3rd International Conference on Waterside Security* (pp. 1–6). Singapore: Bjorno, Leif.

Teague, W. (2011). *Homeland defense coastal modeling validation and verification: Evaluation of Delft3D model current prediction for Chesapeake Bay.* Stennis Space Center: Naval Research Laboratory.

Titley, R. A. (2010, January). Naval oceanography and information dominance. *Sea Technology Magazine*, *51*, 1, 11–12.

Valle-Levinson, A., & Lwiza, K. M. (1997). Bathymetric influences on the lower Chesapeake Bay hydrography. *Journal of Marine Systems*, *12*, 221–236.

Wettergren, T. A. (2008). Performance of search via track-before-detect for distributed sensor networks. *IEEE Transactions on Aerospace and Electronic Systems*, *44*(1), 314–325.

Wettergren, T. A., & Costa, R. (2009). Optimal placement of distributed sensors against moving targets. *ACM Transactions on Sensor Networks*, *5*(26), 1–25.

Zeitungzeid. (2011, April 29). *Eufor in Libya*. Retrieved from Humanitarian ship movements cancelled: http://euformisurata.wordpress.com/category/unocha/

APPENDIX A

Uniform Distribution

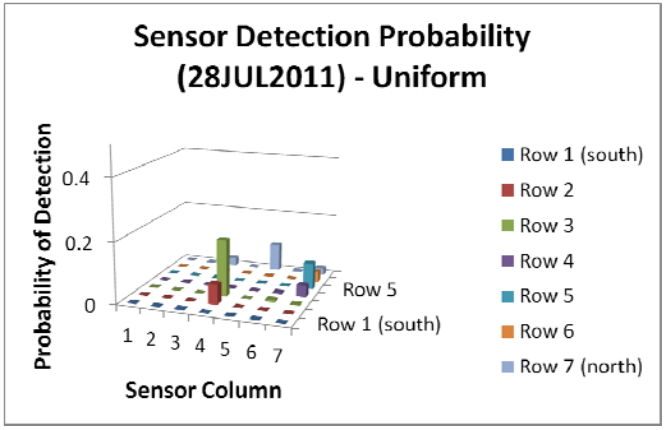

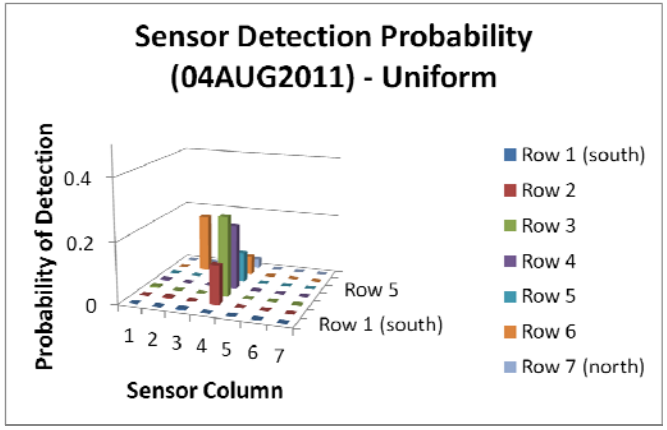

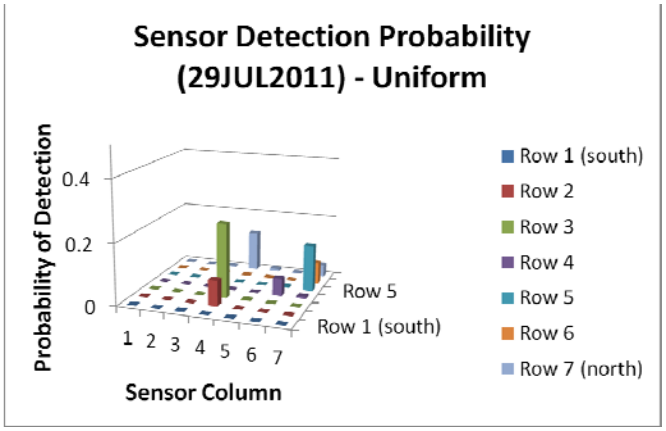

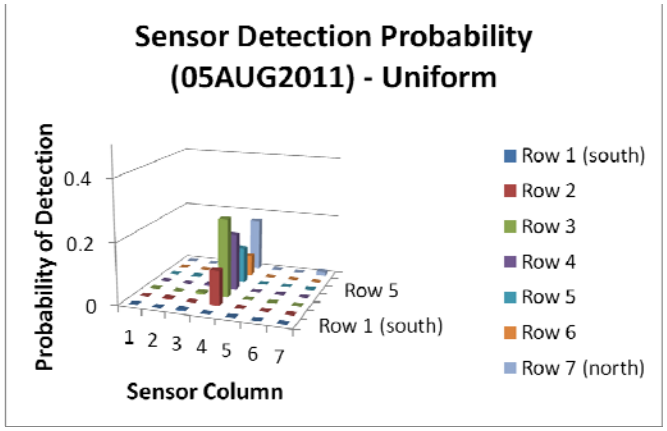

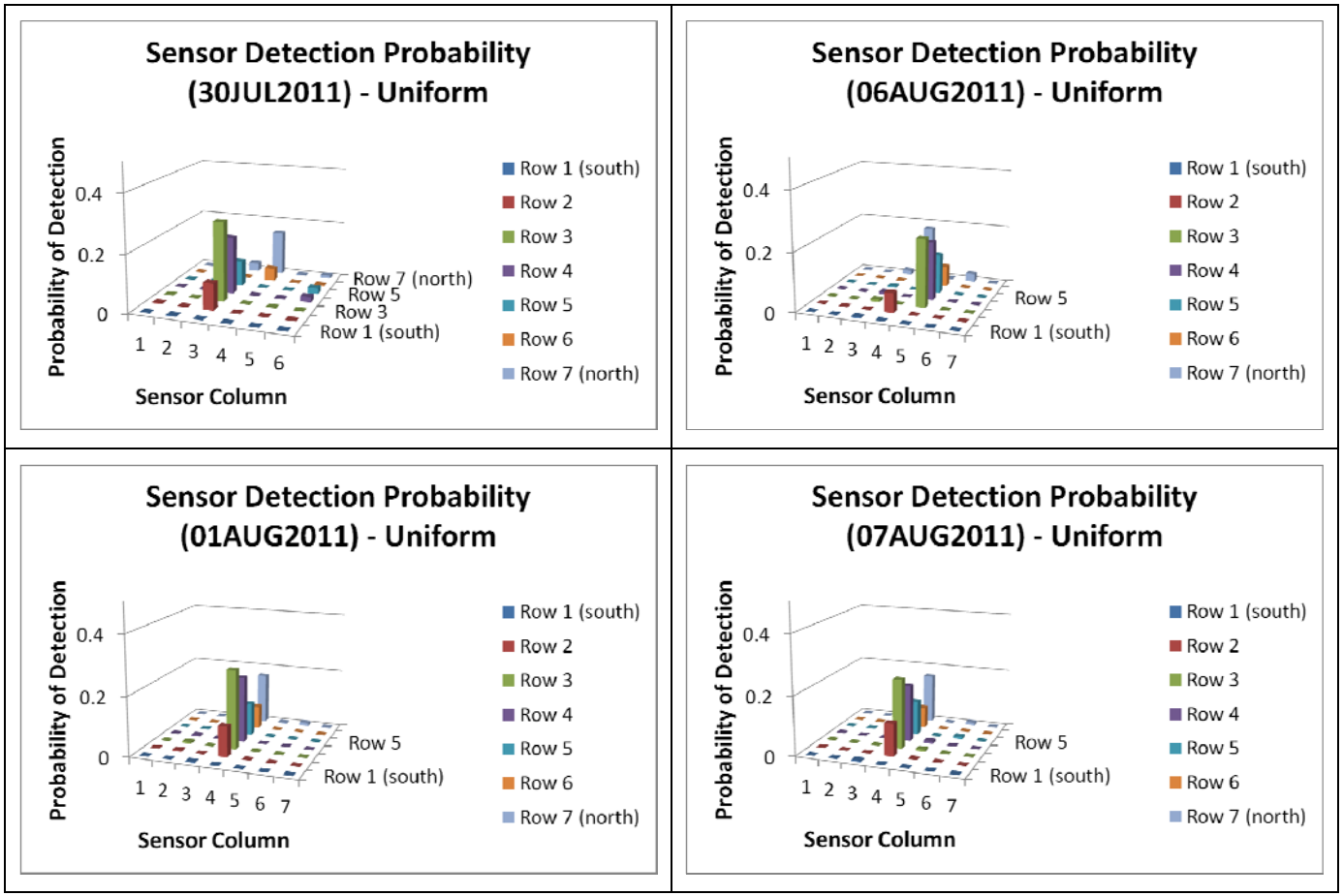
Sensor Detection Probability
(30JUL2011) - Uniform
Probability of Detection
0.4
0.2
0
1 2 3 4 5 6
Sensor Column
Row 7 (north)
Row 5
Row 3
Row 1 (south)
Row 1 (south)
Row 2
Row 3
Row 4
Row 5
Row 6
Row 7 (north)
Sensor Detection Probability
(06AUG2011) - Uniform
Probability of Detection
0.4
0.2
0
1 2 3 4 5 6 7
Sensor Column
Row 5
Row 1 (south)
Row 1 (south)
Row 2
Row 3
Row 4
Row 5
Row 6
Row 7 (north)
Sensor Detection Probability
(01AUG2011) - Uniform
Probability of Detection
0.4
0.2
0
1 2 3 4 5 6 7
Sensor Column
Row 5
Row 1 (south)
Row 1 (south)
Row 2
Row 3
Row 4
Row 5
Row 6
Row 7 (north)
Sensor Detection Probability
(07AUG2011) - Uniform
Probability of Detection
0.4
0.2
0
1 2 3 4 5 6 7
Sensor Column
Row 5
Row 1 (south)
Row 1 (south)
Row 2
Row 3
Row 4
Row 5
Row 6
Row 7 (north)

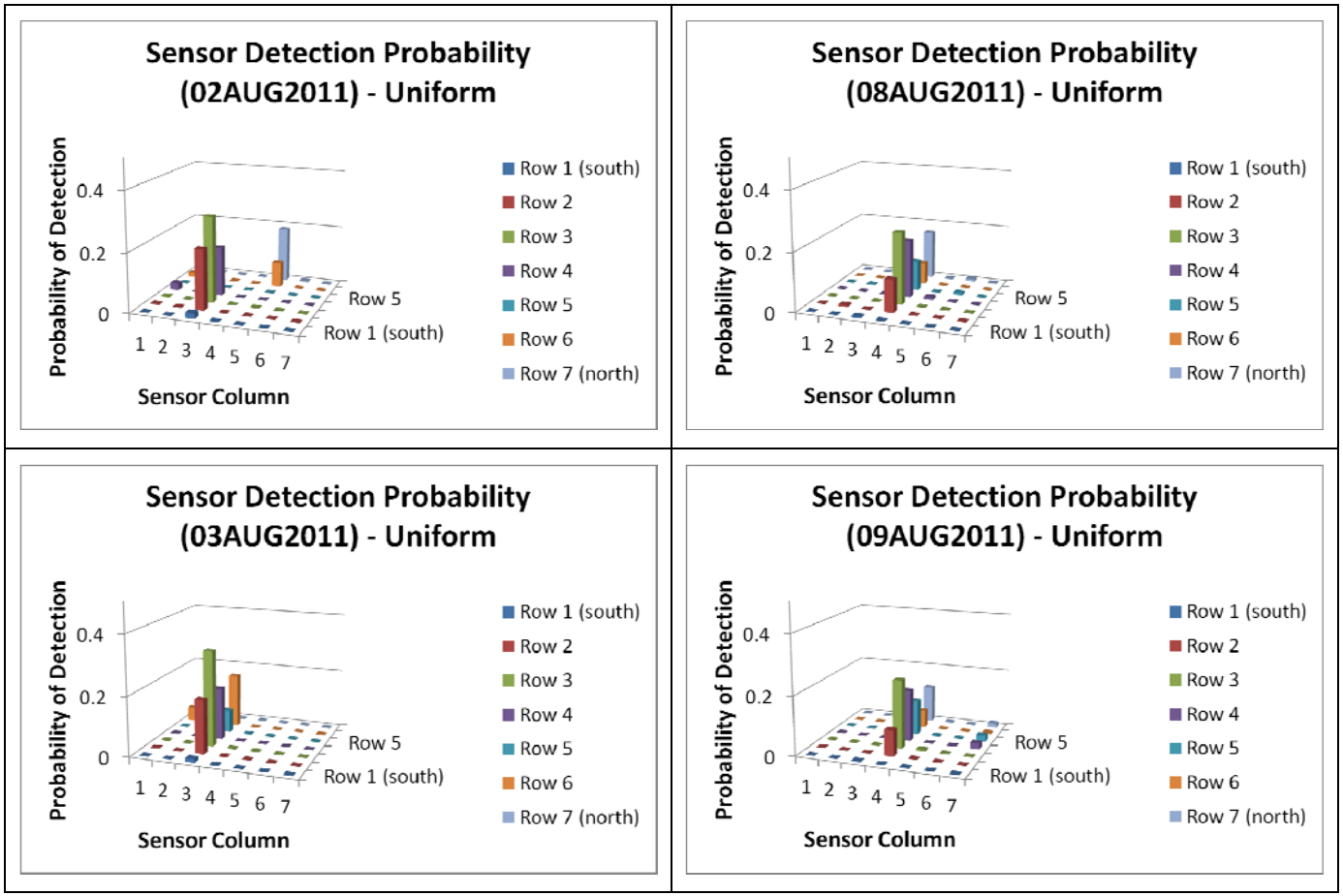
Sensor Detection Probability
(02AUG2011) - Uniform
Probability of Detection
0.4
0.2
0
1 2 3 4 5 6 7
Sensor Column
Row 5
Row 1 (south)
Row 1 (south)
Row 2
Row 3
Row 4
Row 5
Row 6
Row 7 (north)
Sensor Detection Probability
(08AUG2011) - Uniform
Probability of Detection
0.4
0.2
0
1 2 3 4 5 6 7
Sensor Column
Row 5
Row 1 (south)
Row 1 (south)
Row 2
Row 3
Row 4
Row 5
Row 6
Row 7 (north)
Sensor Detection Probability
(03AUG2011) - Uniform
Probability of Detection
0.4
0.2
0
1 2 3 4 5 6 7
Sensor Column
Row 5
Row 1 (south)
Row 1 (south)
Row 2
Row 3
Row 4
Row 5
Row 6
Row 7 (north)
Sensor Detection Probability
(09AUG2011) - Uniform
Probability of Detection
0.4
0.2
0
1 2 3 4 5 6 7
Sensor Column
Row 5
Row 1 (south)
Row 1 (south)
Row 2
Row 3
Row 4
Row 5
Row 6
Row 7 (north)

Normal Distribution

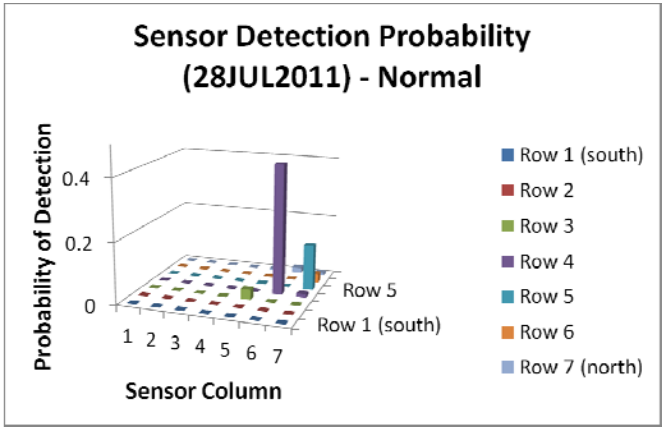

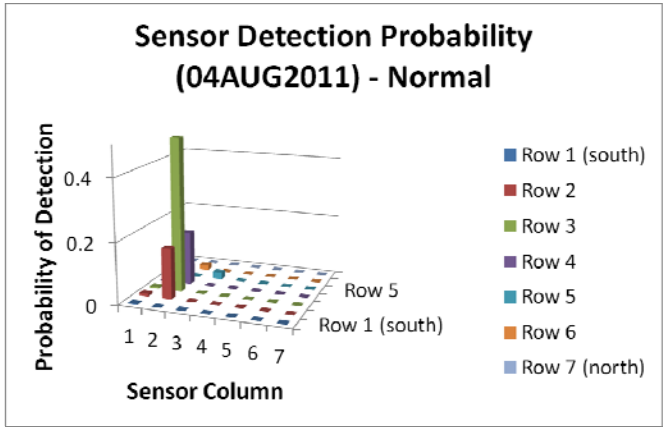

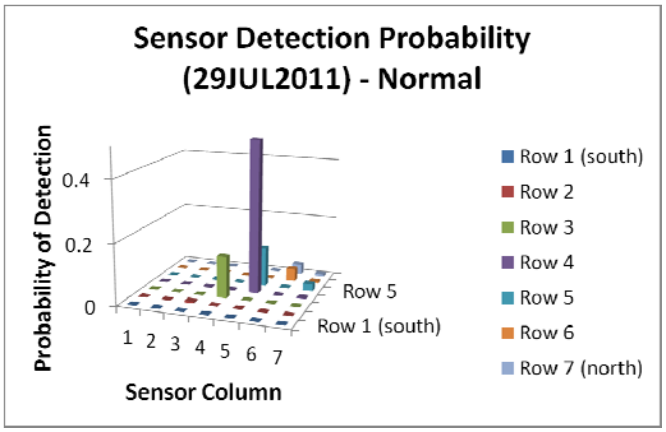

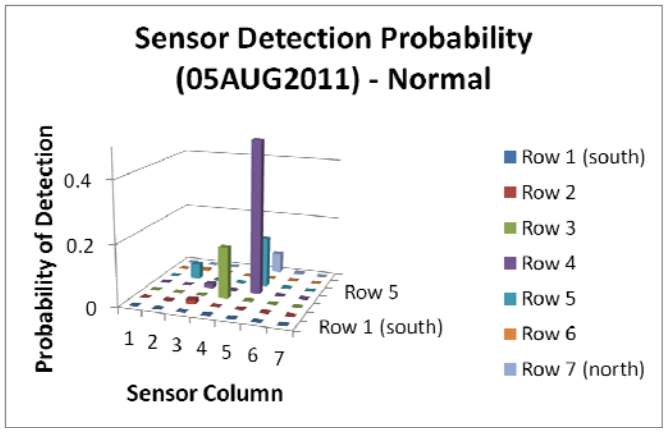

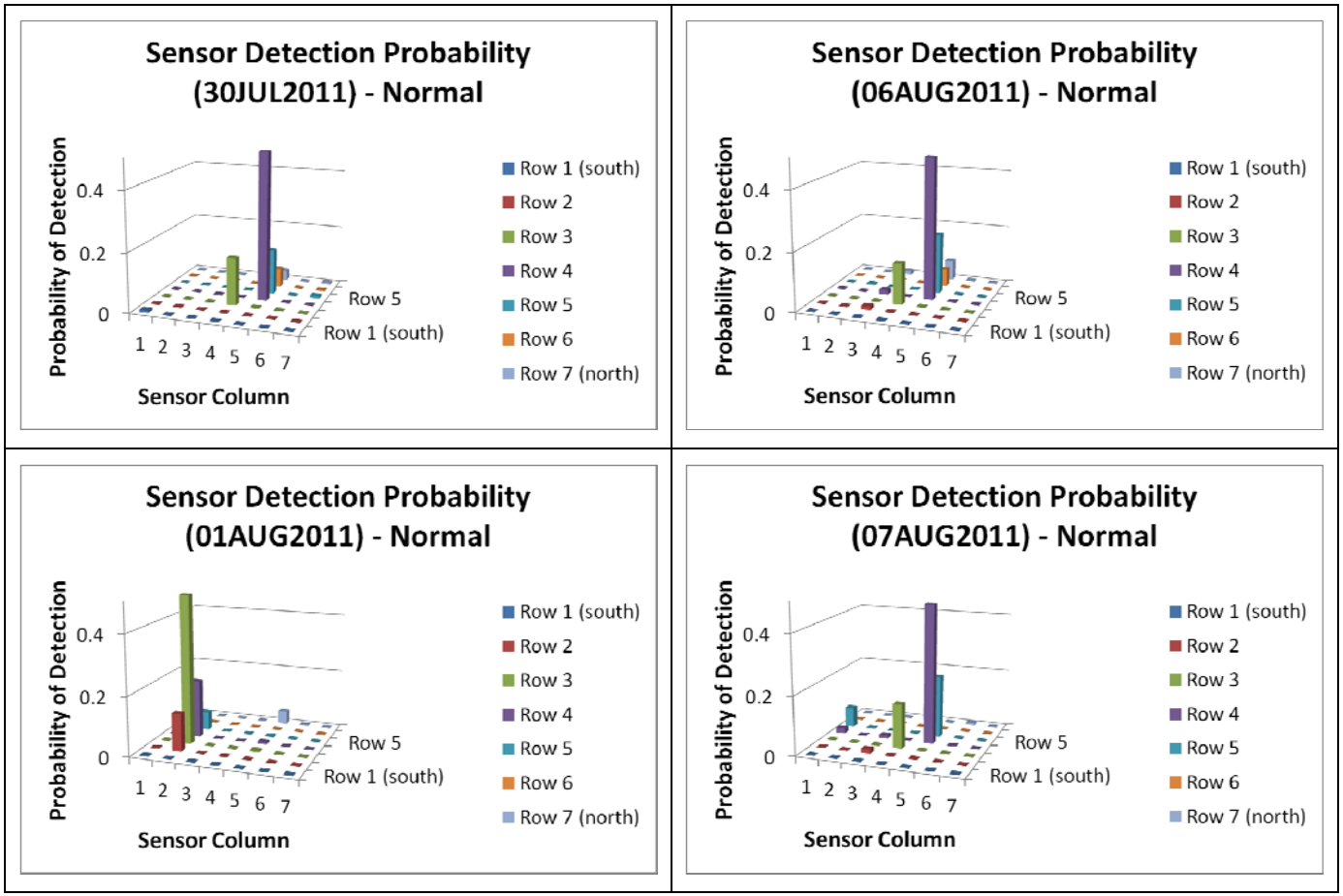
Sensor Detection Probability
(30JUL2011) - Normal
Probability of Detection
0.4
0.2
0
Row 5
Row 1 (south)
1 2 3 4 5 6 7
Sensor Column
Row 1 (south)
Row 2
Row 3
Row 4
Row 5
Row 6
Row 7 (north)
Sensor Detection Probability
(06AUG2011) - Normal
Probability of Detection
0.4
0.2
0
Row 5
Row 1 (south)
1 2 3 4 5 6 7
Sensor Column
Row 1 (south)
Row 2
Row 3
Row 4
Row 5
Row 6
Row 7 (north)
Sensor Detection Probability
(01AUG2011) - Normal
Probability of Detection
0.4
0.2
0
Row 5
Row 1 (south)
1 2 3 4 5 6 7
Sensor Column
Row 1 (south)
Row 2
Row 3
Row 4
Row 5
Row 6
Row 7 (north)
Sensor Detection Probability
(07AUG2011) - Normal
Probability of Detection
0.4
0.2
0
Row 5
Row 1 (south)
1 2 3 4 5 6 7
Sensor Column
Row 1 (south)
Row 2
Row 3
Row 4
Row 5
Row 6
Row 7 (north)

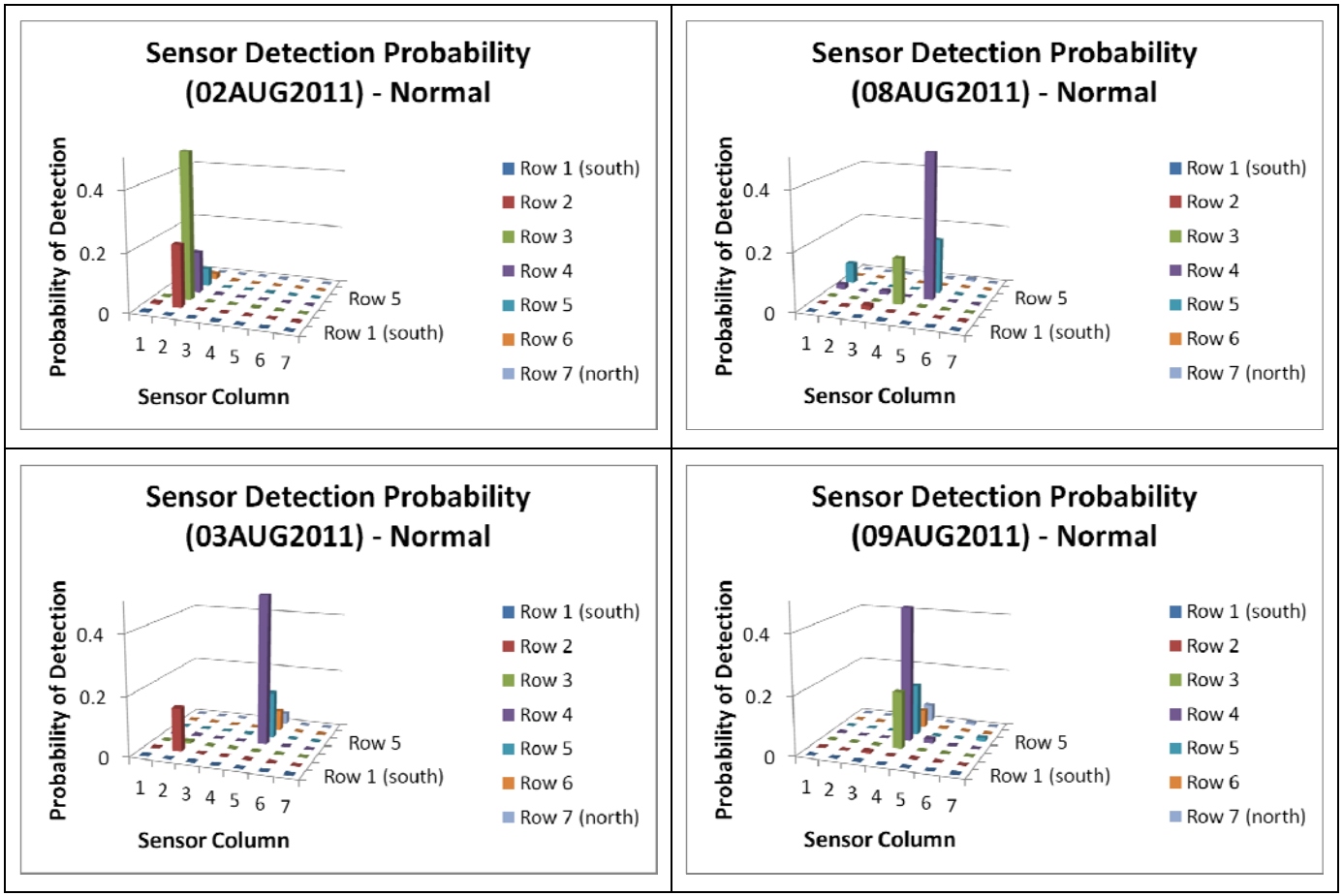
Sensor Detection Probability
(02AUG2011) - Normal
Probability of Detection
0.4
0.2
0
Row 5
Row 1 (south)
1 2 3 4 5 6 7
Sensor Column
Row 1 (south)
Row 2
Row 3
Row 4
Row 5
Row 6
Row 7 (north)
Sensor Detection Probability
(08AUG2011) - Normal
Probability of Detection
0.4
0.2
0
Row 5
Row 1 (south)
1 2 3 4 5 6 7
Sensor Column
Row 1 (south)
Row 2
Row 3
Row 4
Row 5
Row 6
Row 7 (north)
Sensor Detection Probability
(03AUG2011) - Normal
Probability of Detection
0.4
0.2
0
Row 5
Row 1 (south)
1 2 3 4 5 6 7
Sensor Column
Row 1 (south)
Row 2
Row 3
Row 4
Row 5
Row 6
Row 7 (north)
Sensor Detection Probability
(09AUG2011) - Normal
Probability of Detection
0.4
0.2
0
Row 5
Row 1 (south)
1 2 3 4 5 6 7
Sensor Column
Row 1 (south)
Row 2
Row 3
Row 4
Row 5
Row 6
Row 7 (north)

APPENDIX B

Uniform Distribution

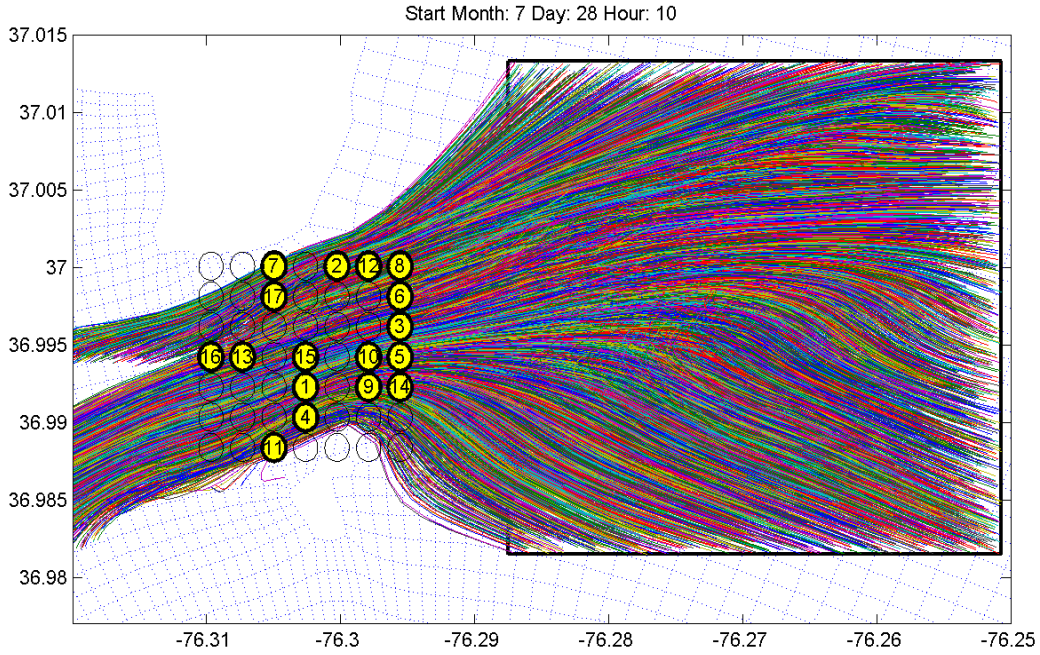

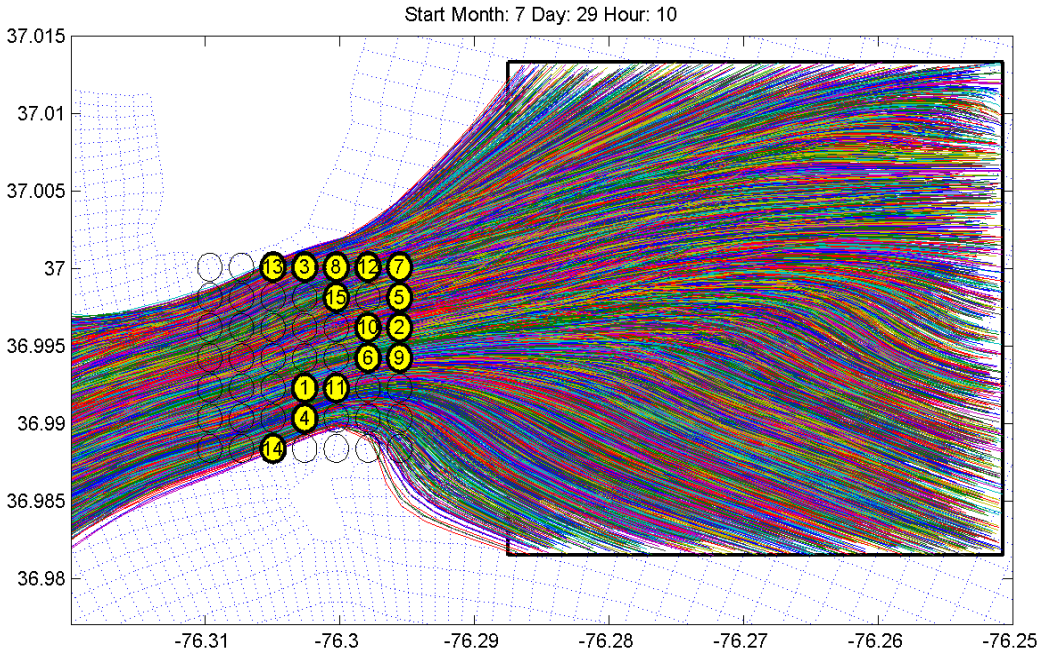

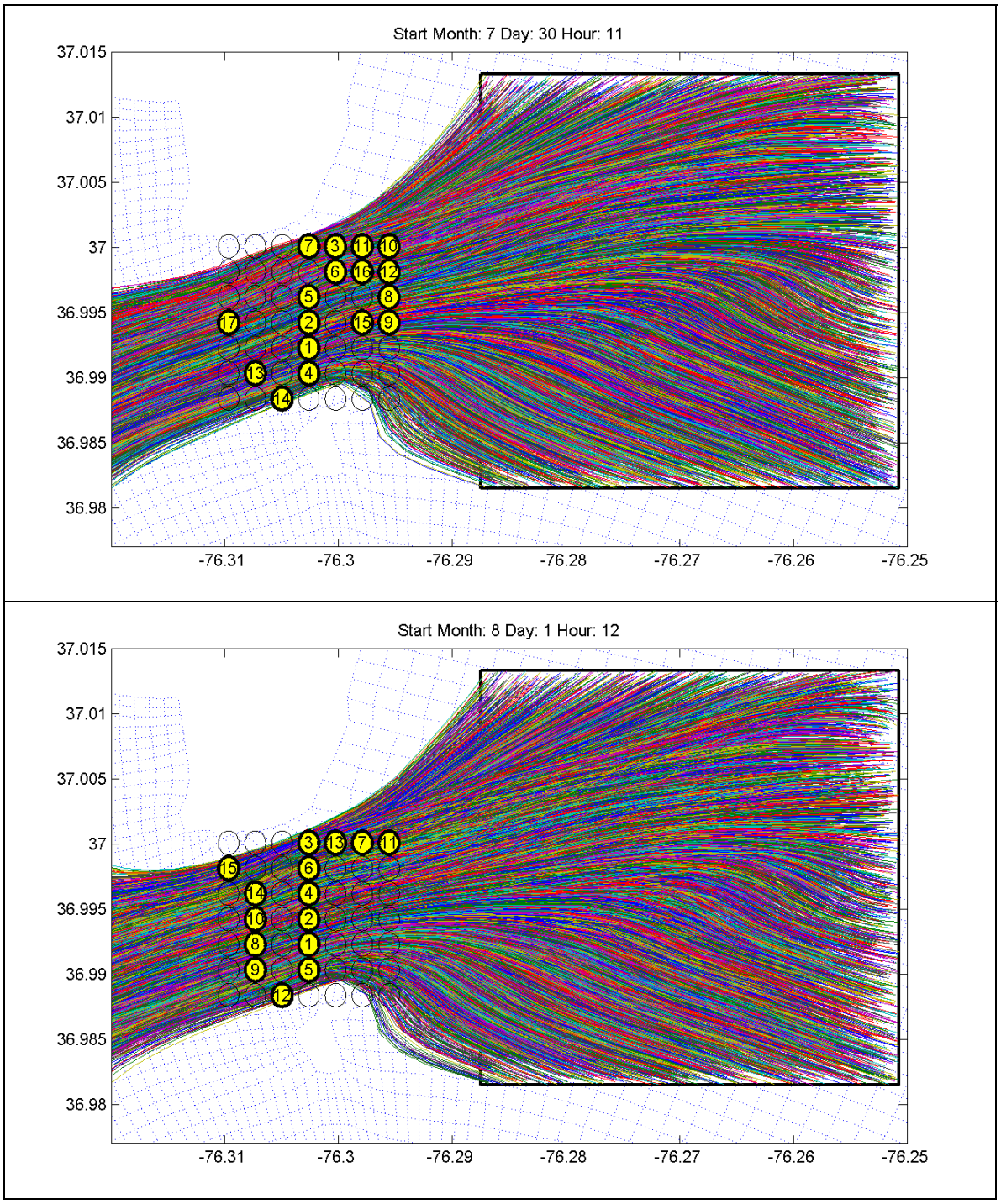
Start Month: 7 Day: 30 Hour: 11
37.015
37.01
37.005
37
36.995
36.99
36.985
36.98
-76.31
-76.3
-76.29
-76.28
-76.27
-76.26
-76.25
7
3
11
10
6
16
12
5
8
17
2
15
9
1
13
4
14
Start Month: 8 Day: 1 Hour: 12
37.015
37.01
37.005
37
36.995
36.99
36.985
36.98
-76.31
-76.3
-76.29
-76.28
-76.27
-76.26
-76.25
3
13
7
11
15
6
14
4
10
2
8
1
9
5
12

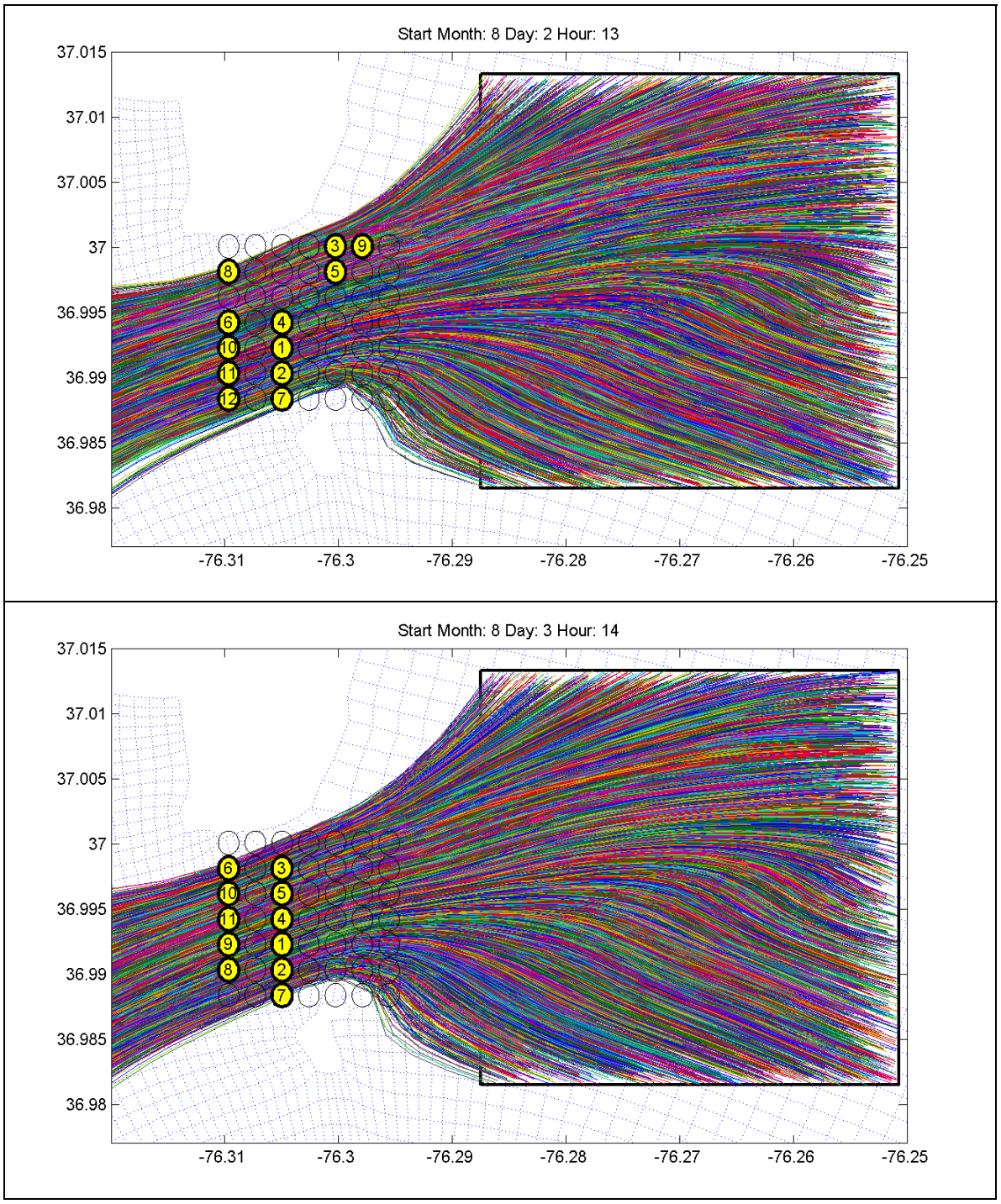
Start Month: 8 Day: 2 Hour: 13
37.015
37.01
37.005
37
36.995
36.99
36.985
36.98
-76.31
-76.3
-76.29
-76.28
-76.27
-76.26
-76.25
3
9
8
5
6
4
10
1
11
2
12
7
Start Month: 8 Day: 3 Hour: 14
37.015
37.01
37.005
37
36.995
36.99
36.985
36.98
-76.31
-76.3
-76.29
-76.28
-76.27
-76.26
-76.25
6
3
10
5
11
4
9
1
8
2
7

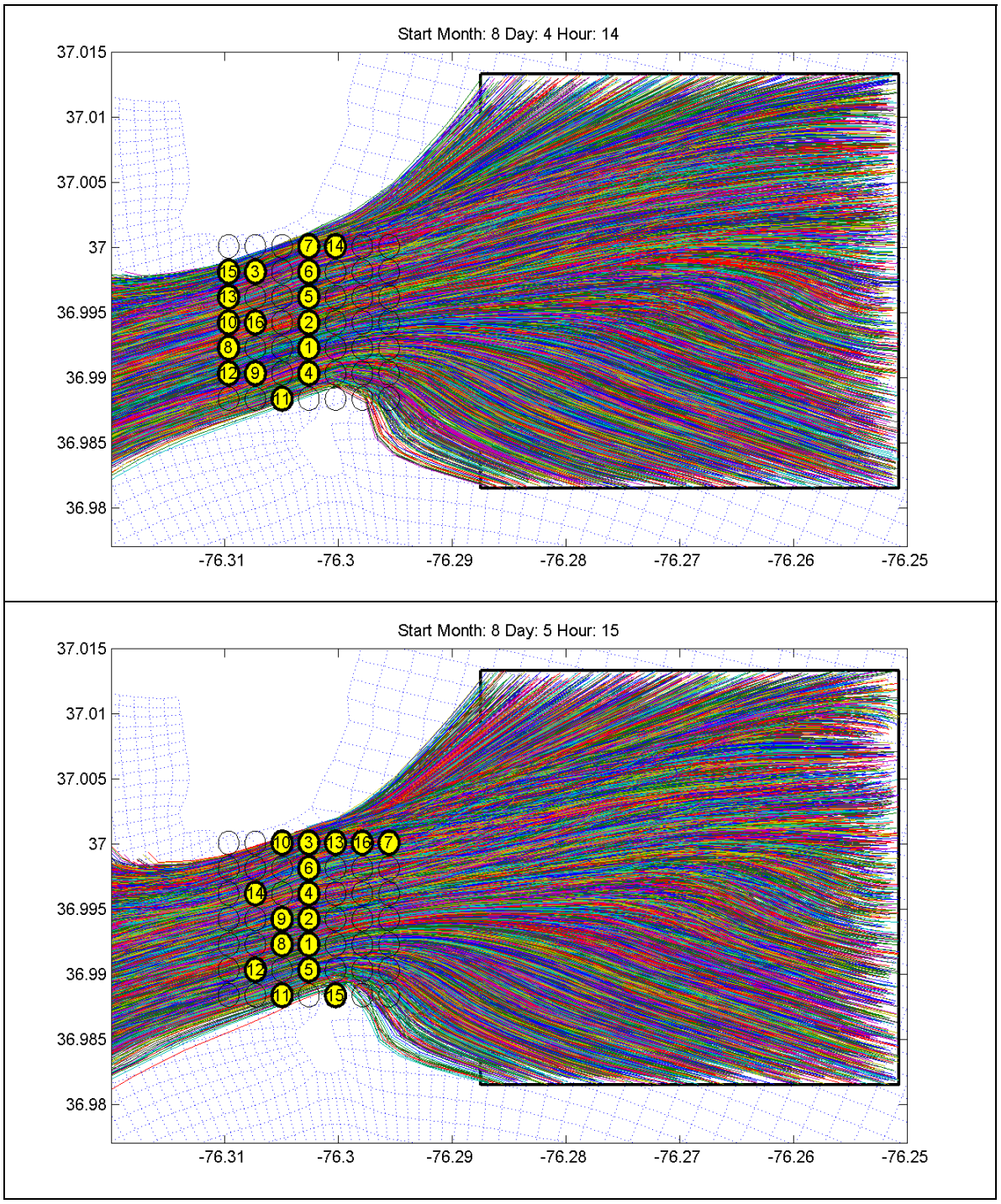
Start Month: 8 Day: 4 Hour: 14
37.015
37.01
37.005
37
36.995
36.99
36.985
36.98
-76.31
-76.3
-76.29
-76.28
-76.27
-76.26
-76.25
7
14
15
3
6
13
5
10
16
2
8
1
12
9
4
11
Start Month: 8 Day: 5 Hour: 15
37.015
37.01
37.005
37
36.995
36.99
36.985
36.98
-76.31
-76.3
-76.29
-76.28
-76.27
-76.26
-76.25
10
3
13
16
7
6
14
4
9
2
8
1
12
5
11
15

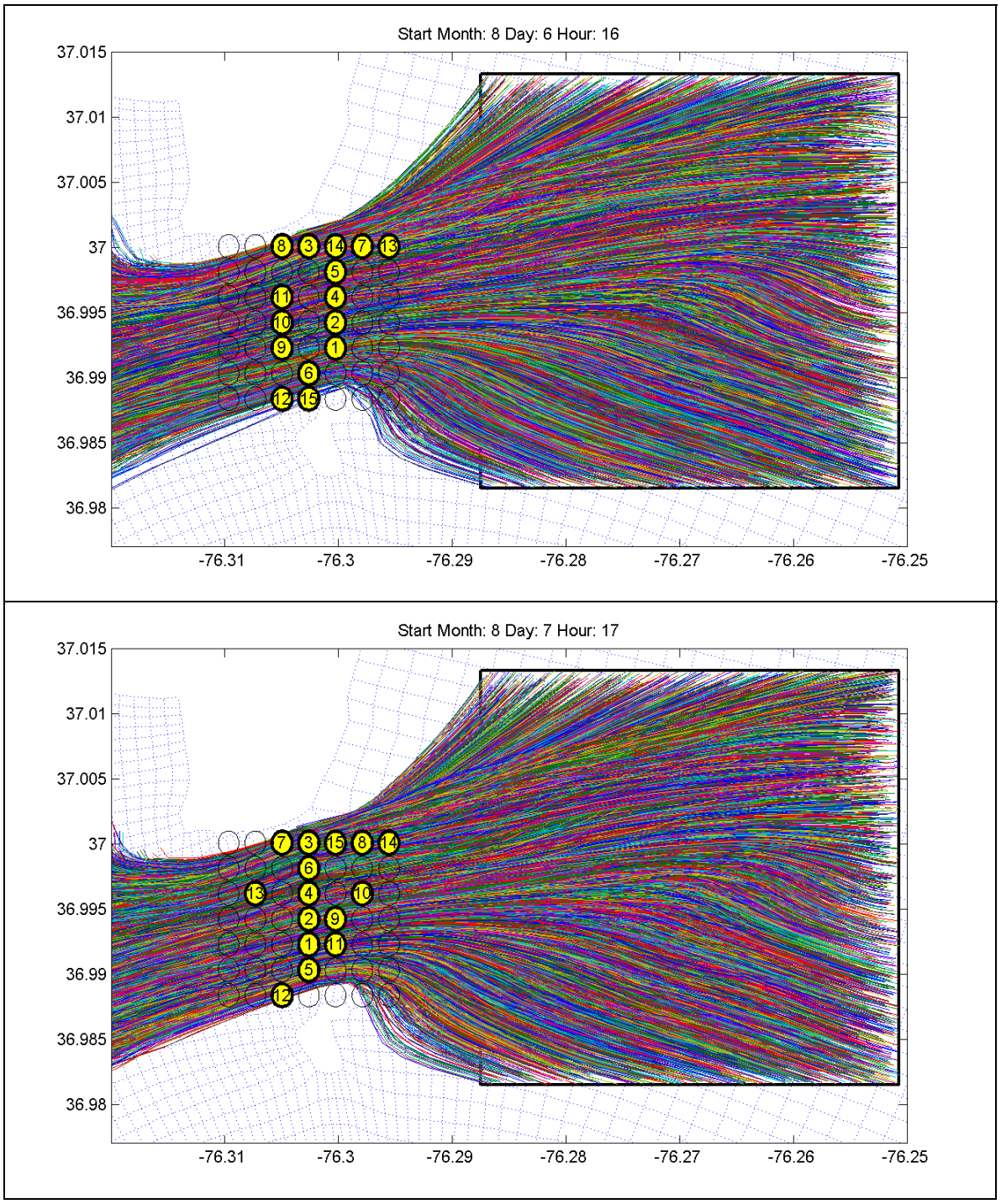
Start Month: 8 Day: 6 Hour: 16
37.015
37.01
37.005
37
36.995
36.99
36.985
36.98
-76.31
-76.3
-76.29
-76.28
-76.27
-76.26
-76.25
8
3
14
7
13
5
11
4
10
2
9
1
6
12
15
Start Month: 8 Day: 7 Hour: 17
37.015
37.01
37.005
37
36.995
36.99
36.985
36.98
-76.31
-76.3
-76.29
-76.28
-76.27
-76.26
-76.25
7
3
15
8
14
6
13
4
10
2
9
1
11
5
12

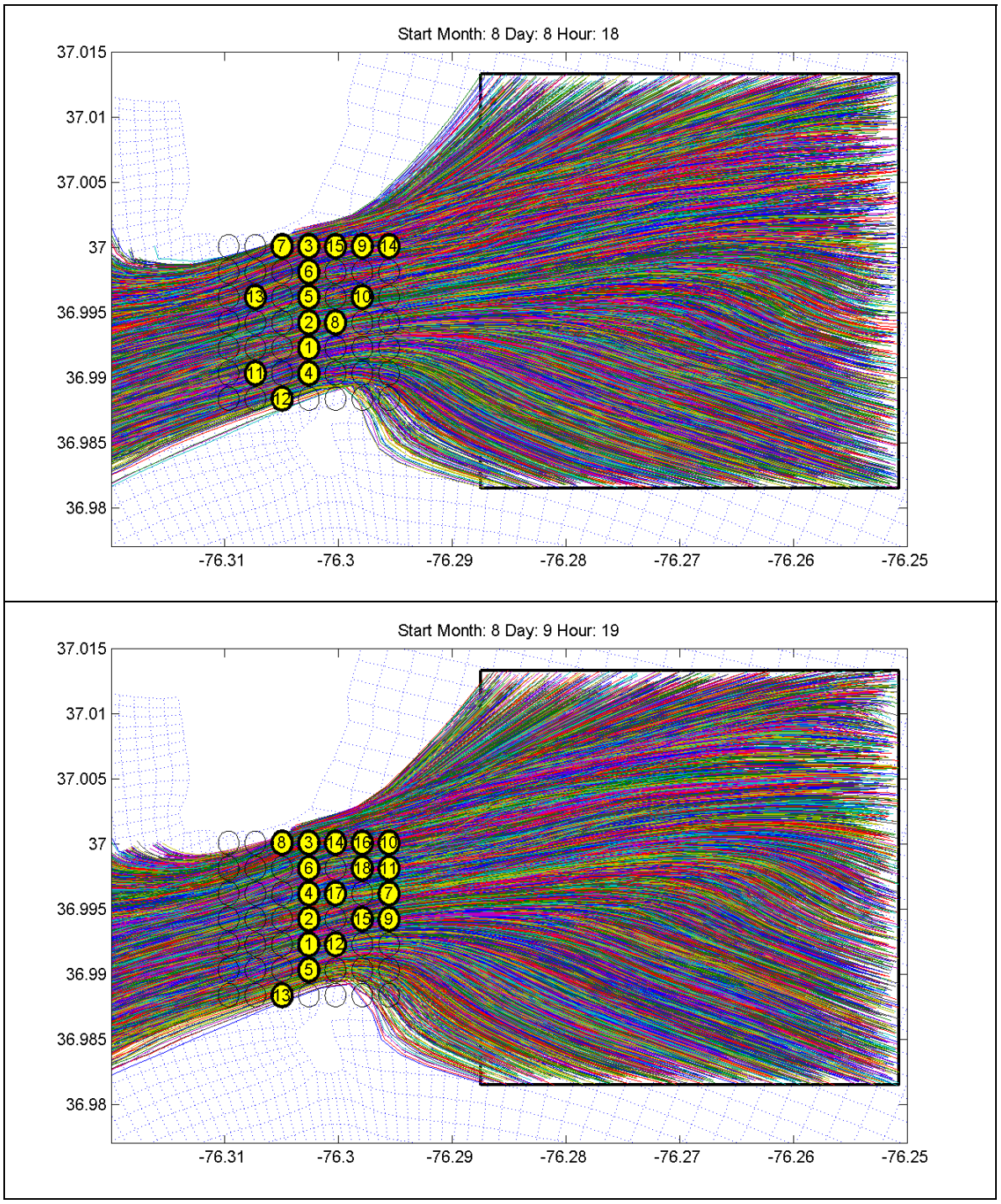
Start Month: 8 Day: 8 Hour: 18
37.015
37.01
37.005
37
36.995
36.99
36.985
36.98
-76.31
-76.3
-76.29
-76.28
-76.27
-76.26
-76.25
7
3
15
9
14
6
13
5
10
2
8
1
11
4
12
Start Month: 8 Day: 9 Hour: 19
37.015
37.01
37.005
37
36.995
36.99
36.985
36.98
-76.31
-76.3
-76.29
-76.28
-76.27
-76.26
-76.25
8
3
14
16
10
6
18
11
4
17
7
2
15
9
1
12
5
13

Normal Distribution

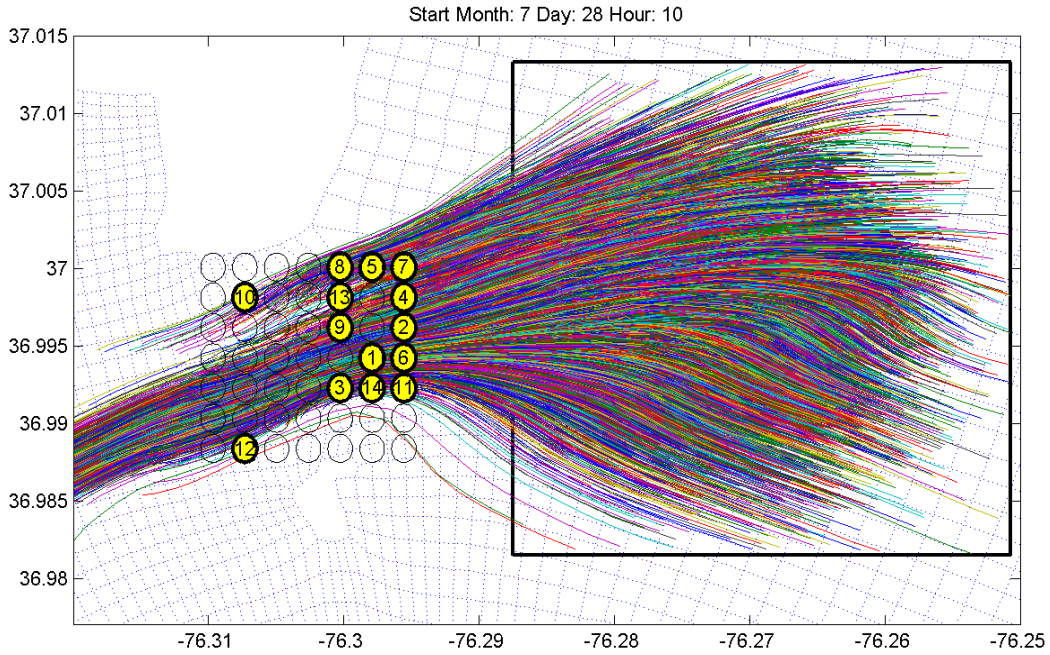

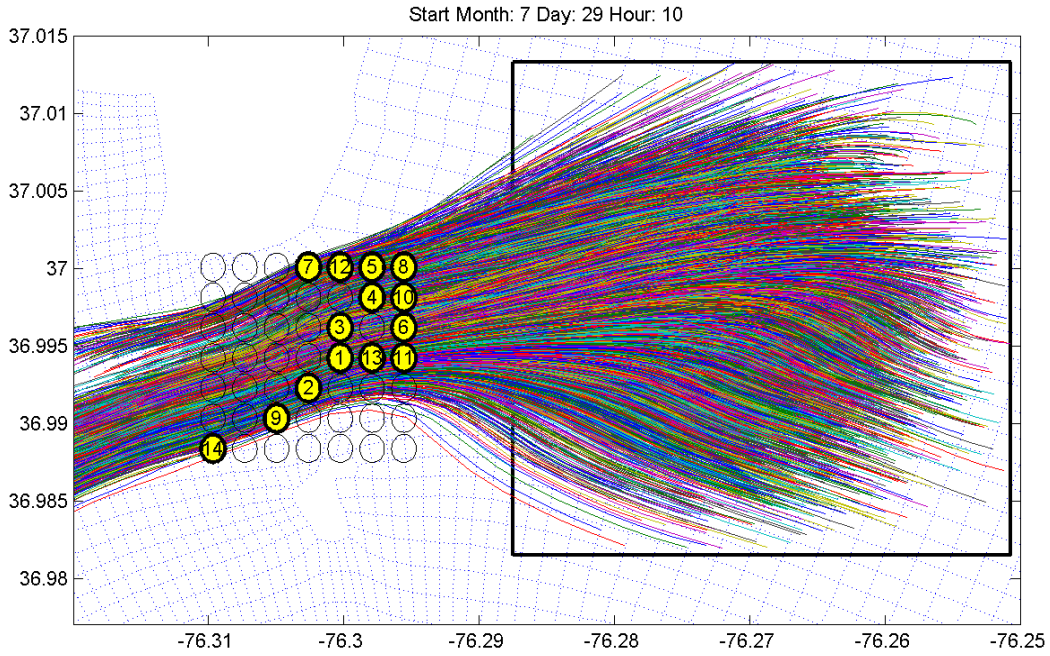

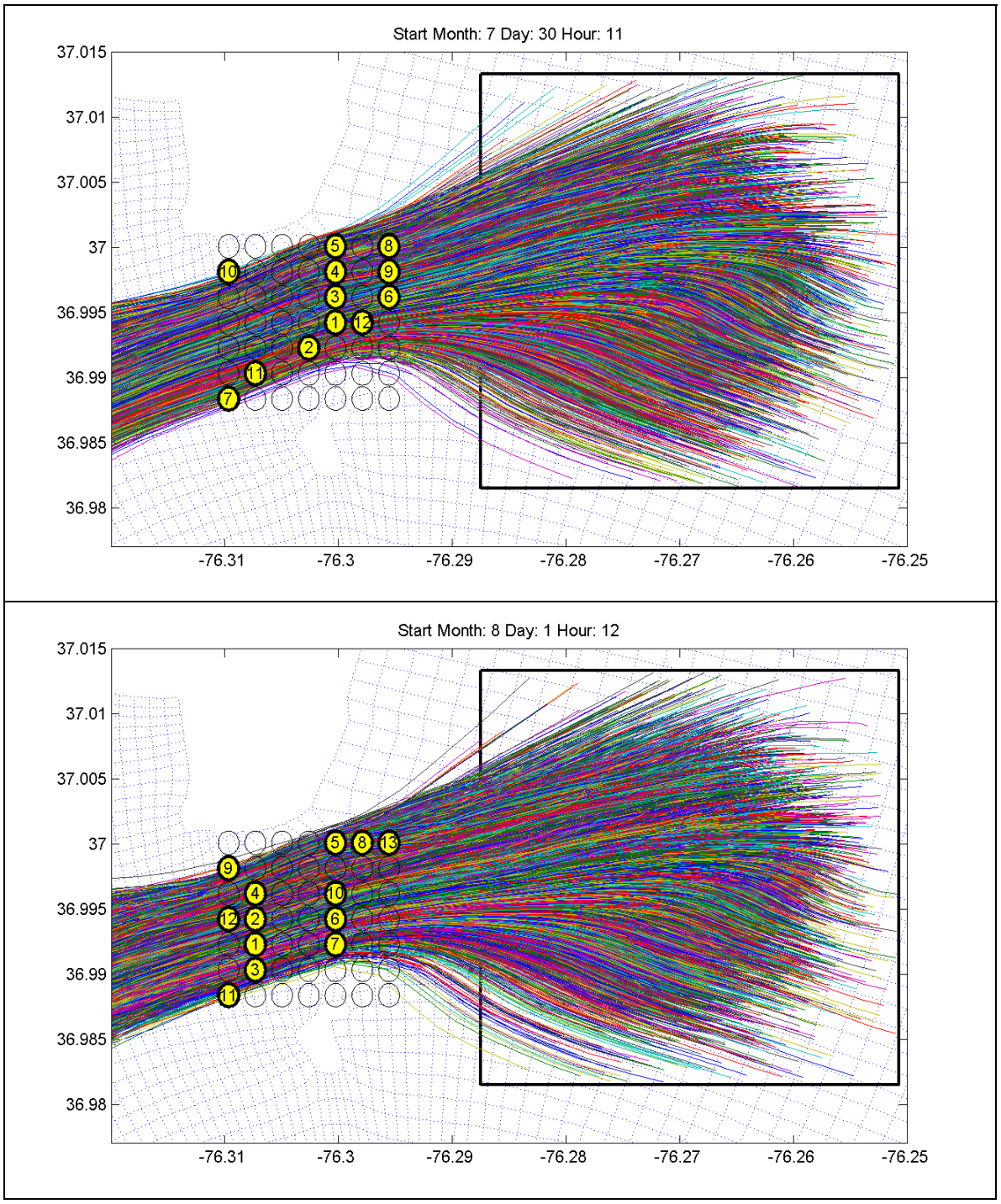
Start Month: 7 Day: 30 Hour: 11
37.015
37.01
37.005
37
36.995
36.99
36.985
36.98
-76.31
-76.3
-76.29
-76.28
-76.27
-76.26
-76.25
5
8
10
4
9
3
6
1
12
2
11
7
Start Month: 8 Day: 1 Hour: 12
37.015
37.01
37.005
37
36.995
36.99
36.985
36.98
-76.31
-76.3
-76.29
-76.28
-76.27
-76.26
-76.25
5
8
13
9
4
10
12
2
6
1
7
3
11

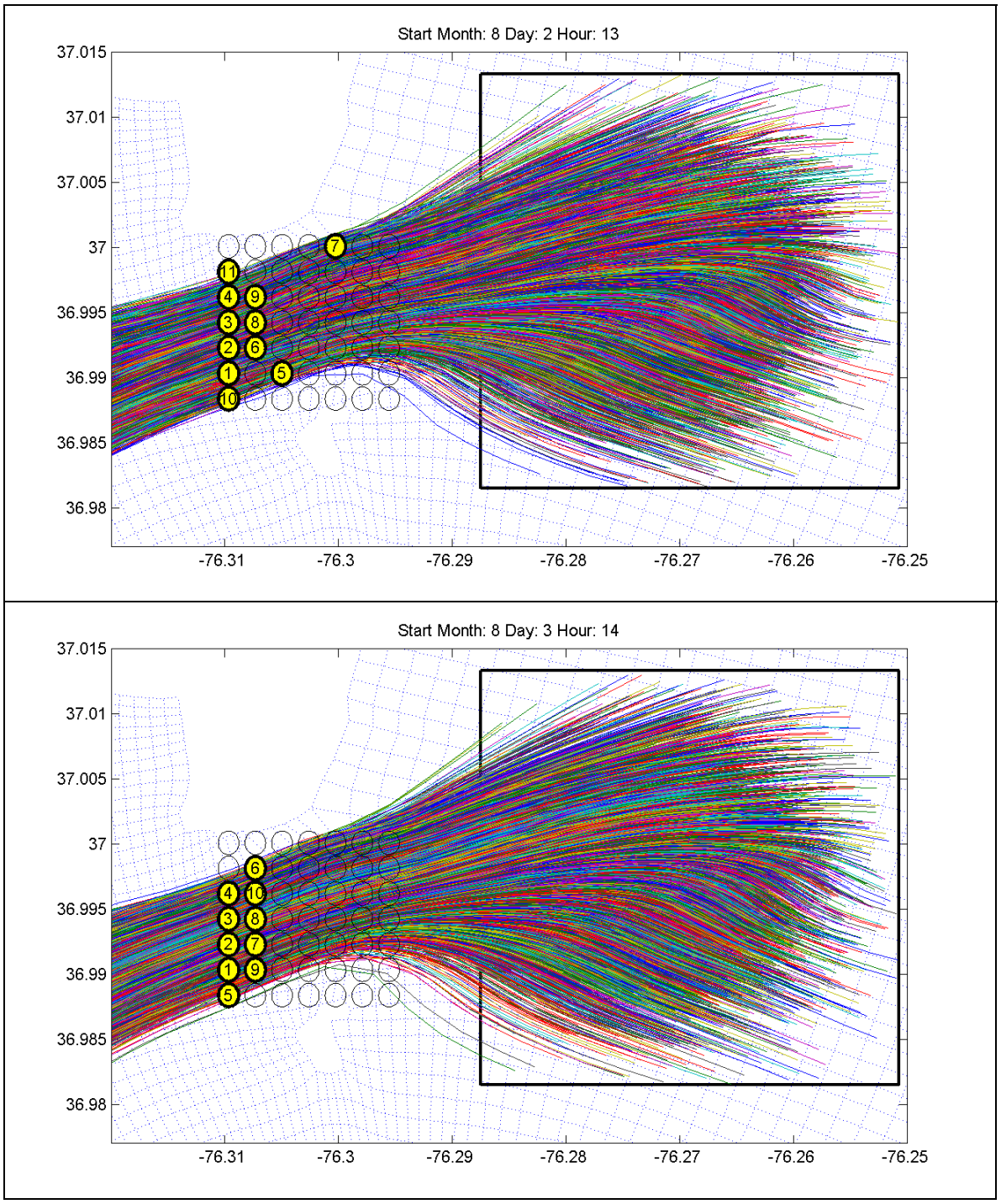
Start Month: 8 Day: 2 Hour: 13
37.015
37.01
37.005
37
36.995
36.99
36.985
36.98
-76.31
-76.3
-76.29
-76.28
-76.27
-76.26
-76.25
7
11
4
9
3
8
2
6
1
5
10
Start Month: 8 Day: 3 Hour: 14
37.015
37.01
37.005
37
36.995
36.99
36.985
36.98
-76.31
-76.3
-76.29
-76.28
-76.27
-76.26
-76.25
6
4
10
3
8
2
7
1
9
5

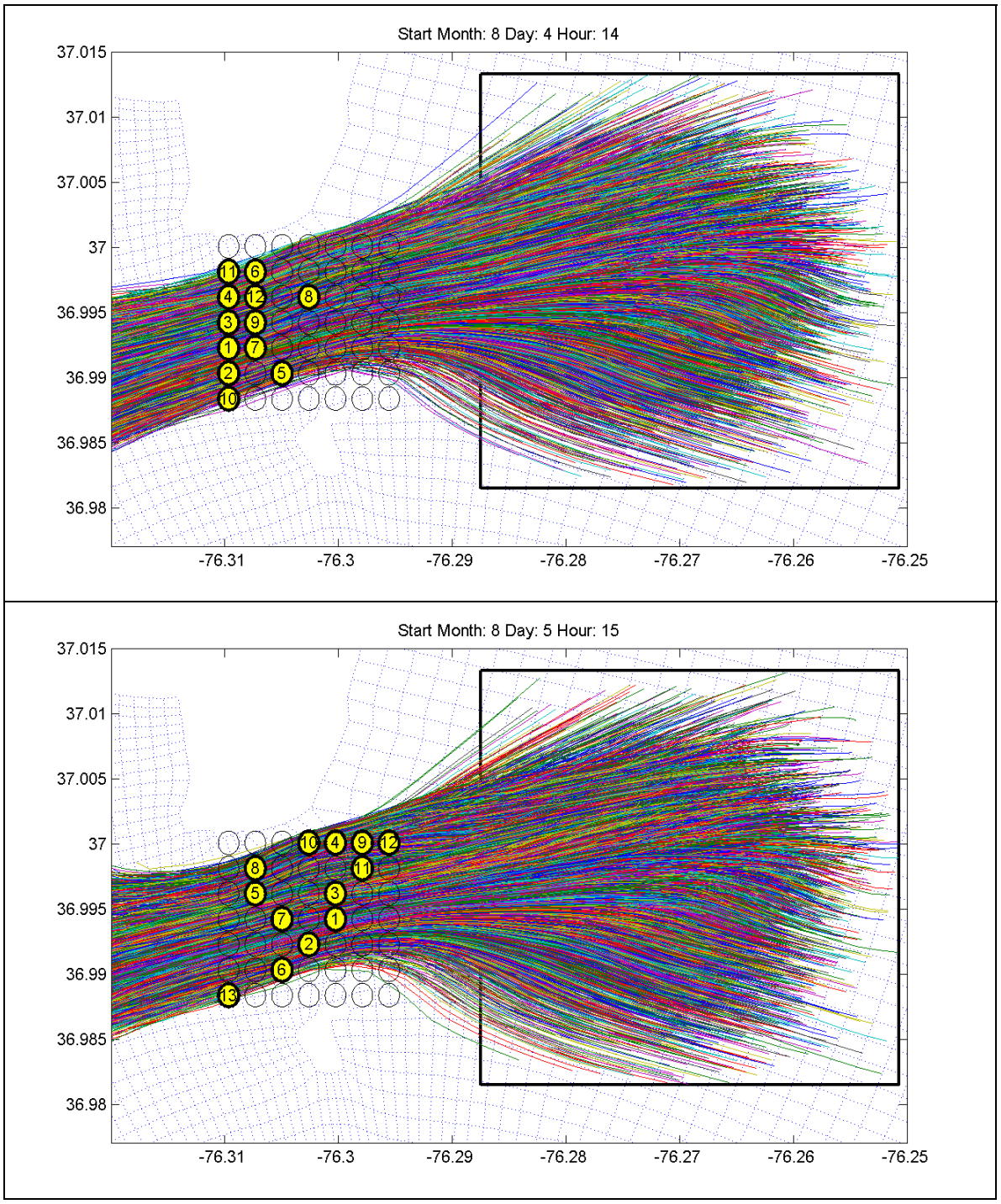
Start Month: 8 Day: 4 Hour: 14
37.015
37.01
37.005
37
36.995
36.99
36.985
36.98
-76.31
-76.3
-76.29
-76.28
-76.27
-76.26
-76.25
11
6
4
12
8
3
9
1
7
2
5
10
Start Month: 8 Day: 5 Hour: 15
37.015
37.01
37.005
37
36.995
36.99
36.985
36.98
-76.31
-76.3
-76.29
-76.28
-76.27
-76.26
-76.25
10
4
9
12
8
11
5
3
7
1
2
6
13

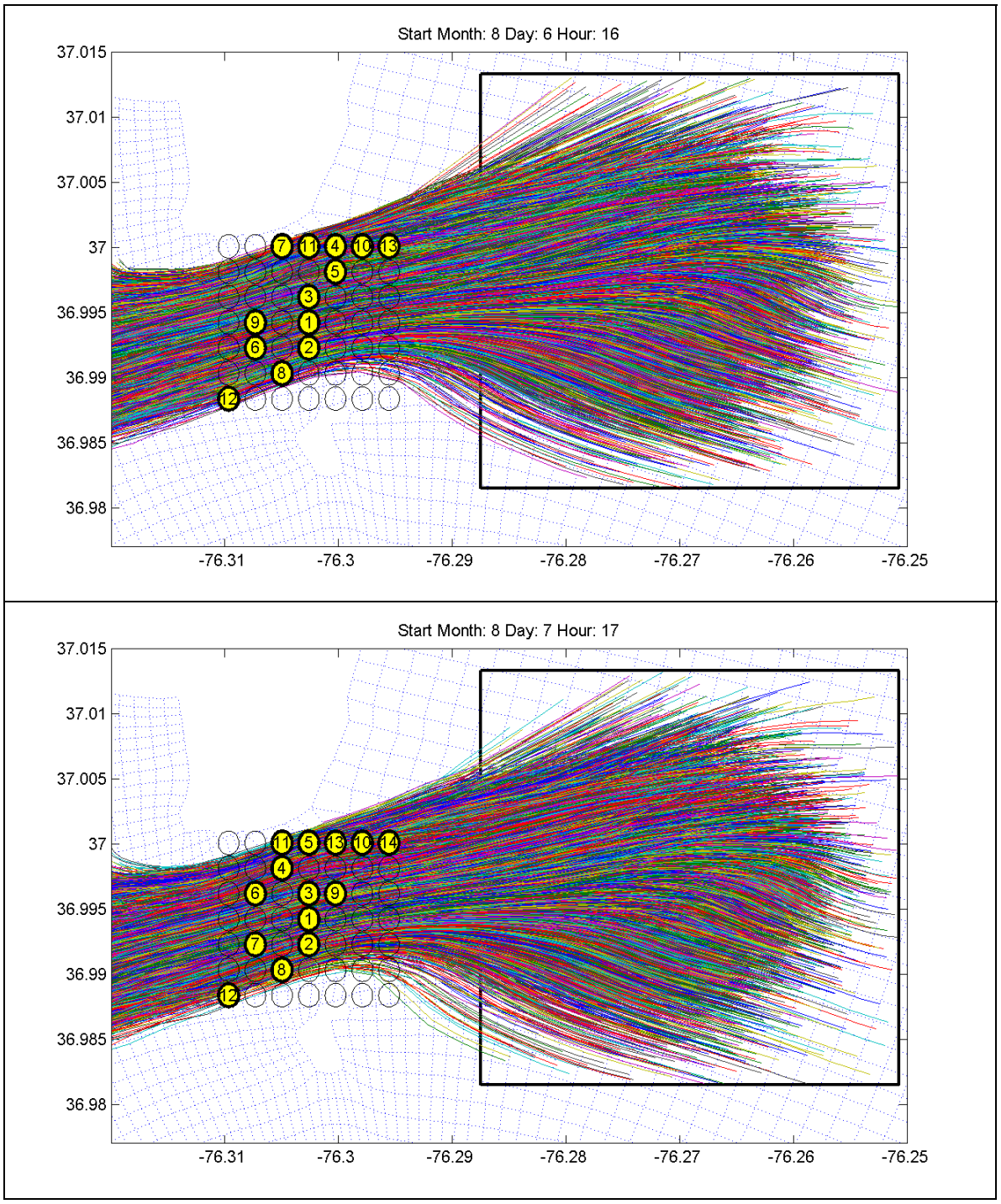
Start Month: 8 Day: 6 Hour: 16
37.015
37.01
37.005
37
36.995
36.99
36.985
36.98
-76.31
-76.3
-76.29
-76.28
-76.27
-76.26
-76.25
7
11
4
10
13
5
3
9
1
6
2
8
12
Start Month: 8 Day: 7 Hour: 17
37.015
37.01
37.005
37
36.995
36.99
36.985
36.98
-76.31
-76.3
-76.29
-76.28
-76.27
-76.26
-76.25
11
5
13
10
14
4
6
3
9
1
7
2
8
12

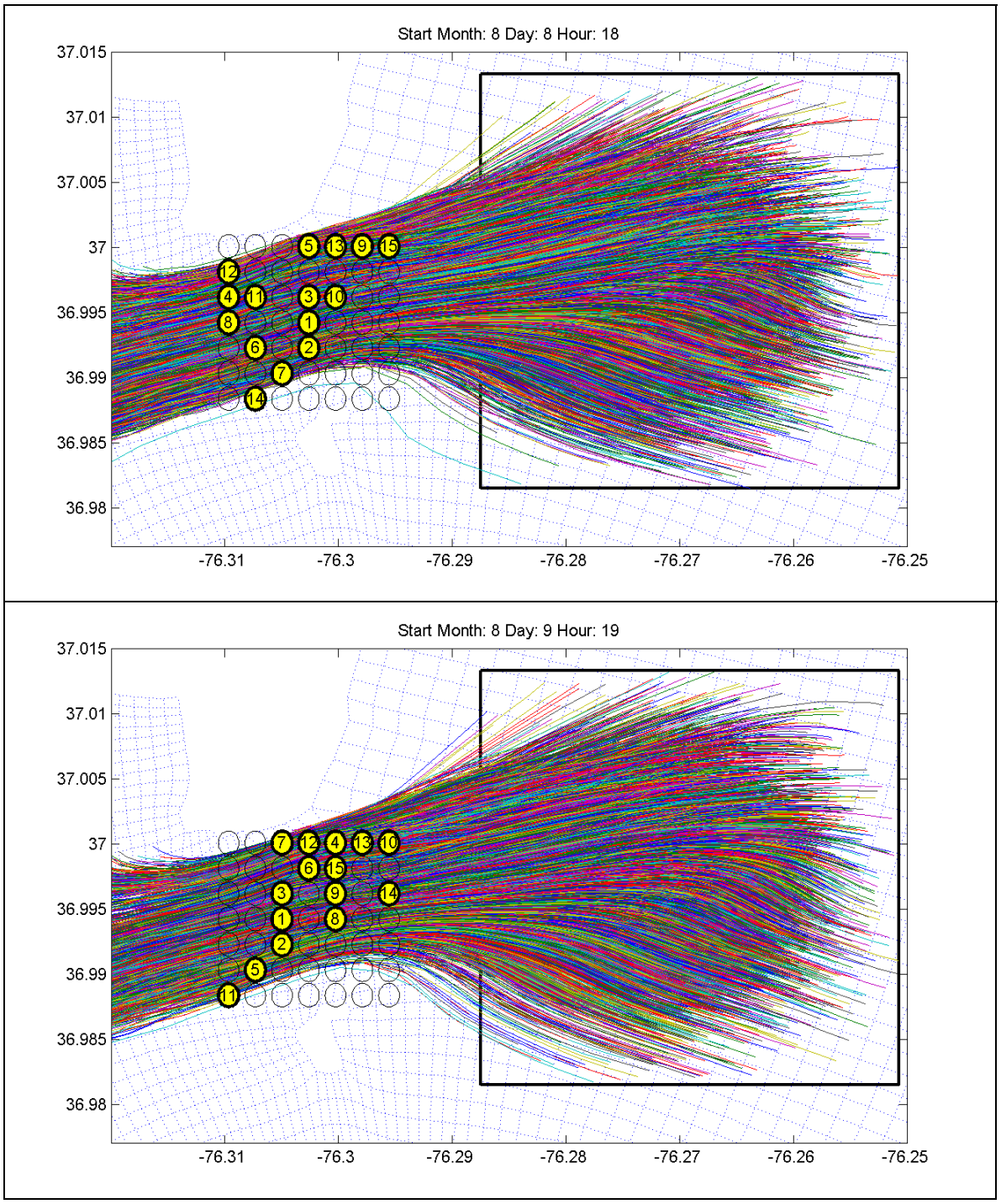
Start Month: 8 Day: 8 Hour: 18
37.015
37.01
37.005
37
36.995
36.99
36.985
36.98
-76.31
-76.3
-76.29
-76.28
-76.27
-76.26
-76.25
5
13
9
15
12
4
11
3
10
8
1
6
2
7
14
Start Month: 8 Day: 9 Hour: 19
37.015
37.01
37.005
37
36.995
36.99
36.985
36.98
-76.31
-76.3
-76.29
-76.28
-76.27
-76.26
-76.25
7
12
4
13
10
6
15
3
9
14
1
8
2
5
11

APPENDIX C

	Uniform Distribution																							
Pd	Days																							
Sensors	1U	7/28	2U	7/29	3U	7/30	4U	8/1	5U	8/2	6U	8/3	7U	8/4	8U	8/5	9U	8/6	10U	8/7	11U	8/8	12U	8/9
1	0.1854	24	0.2428	24	0.2775	24	0.2674	24	0.2933	17	0.3224	17	0.2614	24	0.2558	24	0.2319	31	0.234	24	0.2454	24	0.2316	24
2	0.2753	35	0.393	47	0.4771	25	0.4886	25	0.4985	16	0.5046	16	0.4724	25	0.4412	25	0.4315	32	0.4254	25	0.4435	25	0.4076	25
3	0.3622	47	0.5224	28	0.6322	35	0.6576	28	0.6855	35	0.6853	20	0.6614	13	0.6137	28	0.6117	28	0.5904	28	0.609	28	0.5312	28
4	0.4283	23	0.6062	23	0.7266	23	0.766	26	0.8521	18	0.8615	18	0.7896	23	0.7304	26	0.7457	33	0.7058	26	0.7201	23	0.6483	26
5	0.4664	46	0.6766	48	0.8154	26	0.8696	23	0.936	34	0.9388	19	0.8876	26	0.8431	23	0.8153	34	0.8167	23	0.8223	26	0.7365	23
6	0.4995	48	0.7335	39	0.8603	34	0.9462	27	0.9606	4	0.9864	6	0.9497	27	0.91	27	0.8819	23	0.8869	27	0.8957	27	0.7959	27
7	0.5245	21	0.7737	49	0.8881	28	0.9562	42	0.979	15	0.9982	15	0.9784	28	0.9216	49	0.9089	42	0.9069	21	0.9136	21	0.8175	47
8	0.5466	49	0.7817	35	0.9088	47	0.962	10	0.9938	6	0.9986	2	0.9832	3	0.928	17	0.9244	21	0.9162	42	0.9221	32	0.8388	21
9	0.5538	38	0.7879	46	0.9277	46	0.9654	9	0.9964	42	0.999	3	0.9873	9	0.934	18	0.9329	17	0.9244	32	0.9304	42	0.859	46
10	0.5582	39	0.7914	40	0.9372	49	0.9688	11	0.9982	3	0.9994	5	0.9913	4	0.939	21	0.9408	18	0.9318	40	0.9372	40	0.873	49
11	0.5607	15	0.7937	31	0.9395	42	0.9714	49	0.9999	2	0.9996	4	0.9953	15	0.9425	15	0.945	19	0.9381	31	0.9427	9	0.8782	48
12	0.563	42	0.7955	42	0.9418	48	0.9736	15	1	1			0.9963	2	0.9458	9	0.9485	15	0.9424	15	0.9471	15	0.883	31
13	0.5645	11	0.7972	21	0.944	9	0.9758	35					0.9971	5	0.9483	35	0.9499	49	0.9441	12	0.9494	12	0.8852	15
14	0.5656	45	0.7985	15	0.9461	15	0.9767	12					0.9977	35	0.9499	12	0.9507	35	0.9447	49	0.9509	49	0.8865	35
15	0.5658	25	0.7993	34	0.9468	39	0.9771	6					0.9978	6	0.9502	29	0.9508	22	0.9452	35	0.9513	35	0.8872	39
16	0.5659	4			0.9471	41							0.9979	11	0.9504	42							0.8878	42
17	0.566	20			0.9472	4																	0.8883	33
18																							0.8884	41

	Normal Distribution																							
Pd	Days																							
Sensors	1N	7/28	2N	7/29	3N	7/30	4N	8/1	5N	8/2	6N	8/3	7N	8/4	8N	8/5	9N	8/6	10N	8/7	11N	8/8	12N	8/9
1	0.4229	39	0.5512	32	0.5639	32	0.5503	10	0.5529	10	0.5797	32	0.5431	10	0.5048	32	0.4805	32	0.4697	32	0.4963	32	0.4539	25
2	0.5714	47	0.6874	24	0.7248	24	0.745	11	0.765	9	0.7352	33	0.7185	11	0.6748	24	0.6853	33	0.6797	33	0.6831	33	0.6456	24
3	0.6052	31	0.8167	33	0.8754	33	0.872	9	0.9071	11	0.8807	9	0.8838	9	0.837	33	0.8257	24	0.8298	24	0.8419	24	0.8172	26
4	0.6329	48	0.857	41	0.938	34	0.9355	12	0.9683	12	0.9495	34	0.9441	5	0.9028	35	0.8926	35	0.8975	5	0.9105	5	0.8773	27
5	0.65	42	0.8907	42	0.9713	35	0.9795	35	0.9884	13	0.9862	35	0.9677	19	0.9526	12	0.9513	34	0.9461	28	0.9479	28	0.9331	28
6	0.6612	46	0.9131	47	0.9796	47	0.9865	32	0.9943	2	0.9934	10	0.9837	13	0.966	18	0.9666	18	0.9631	4	0.9656	4	0.949	32
7	0.6686	49	0.9222	28	0.9871	1	0.9906	31	0.9976	1	0.9964	11	0.9921	2	0.979	16	0.9787	21	0.9774	16	0.9796	16	0.9612	47
8	0.6735	35	0.9293	49	0.9925	49	0.9932	42	0.9995	3	0.998	1	0.997	3	0.9854	13	0.9896	16	0.9873	18	0.9903	18	0.9695	42
9	0.675	33	0.9349	16	0.9951	48	0.9951	6	0.9999	35	0.9989	2	0.9996	1	0.9884	42	0.9932	12	0.9943	42	0.996	42	0.9764	16
10	0.6756	13	0.9404	48	0.9959	6	0.9965	33	1	4	0.9998	5	1	6	0.99	28	0.9947	42	0.9962	12	0.9975	12	0.9797	34
11	0.6761	45	0.9424	46	0.996	9	0.9977	1							0.9913	41	0.9953	4	0.9967	21	0.998	6	0.9815	21
12	0.6764	8	0.9429	35	0.9961	39	0.9981	4							0.9916	49	0.9956	28	0.9971	1	0.9984	35	0.9825	49
13	0.6765	34	0.9431	39			0.9983	49							0.9917	1	0.9958	1	0.9974	35	0.9985	8	0.9832	35
14	0.6766	38	0.9432	1													0.9959	49	0.9976	49	0.9986	49	0.9833	1

THIS PAGE INTENTIONALLY LEFT BLANK

APPENDIX D

Uniform Distribution

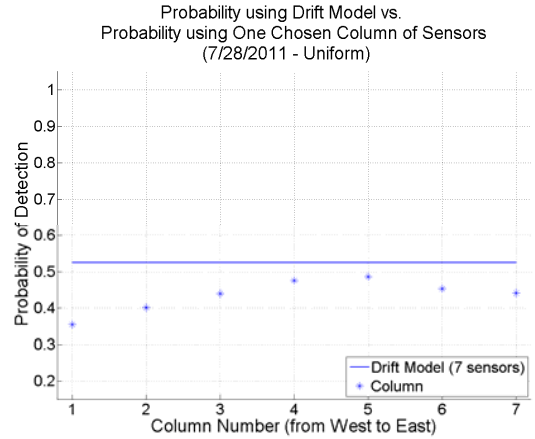

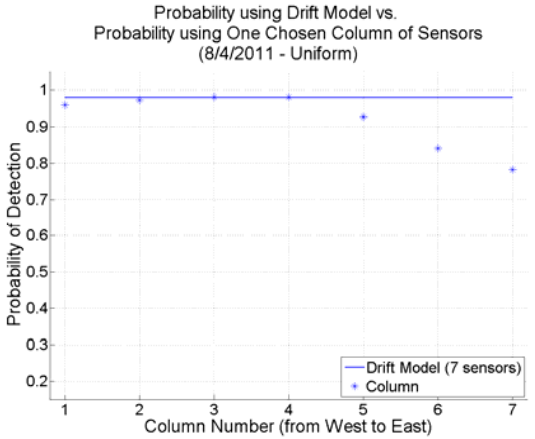

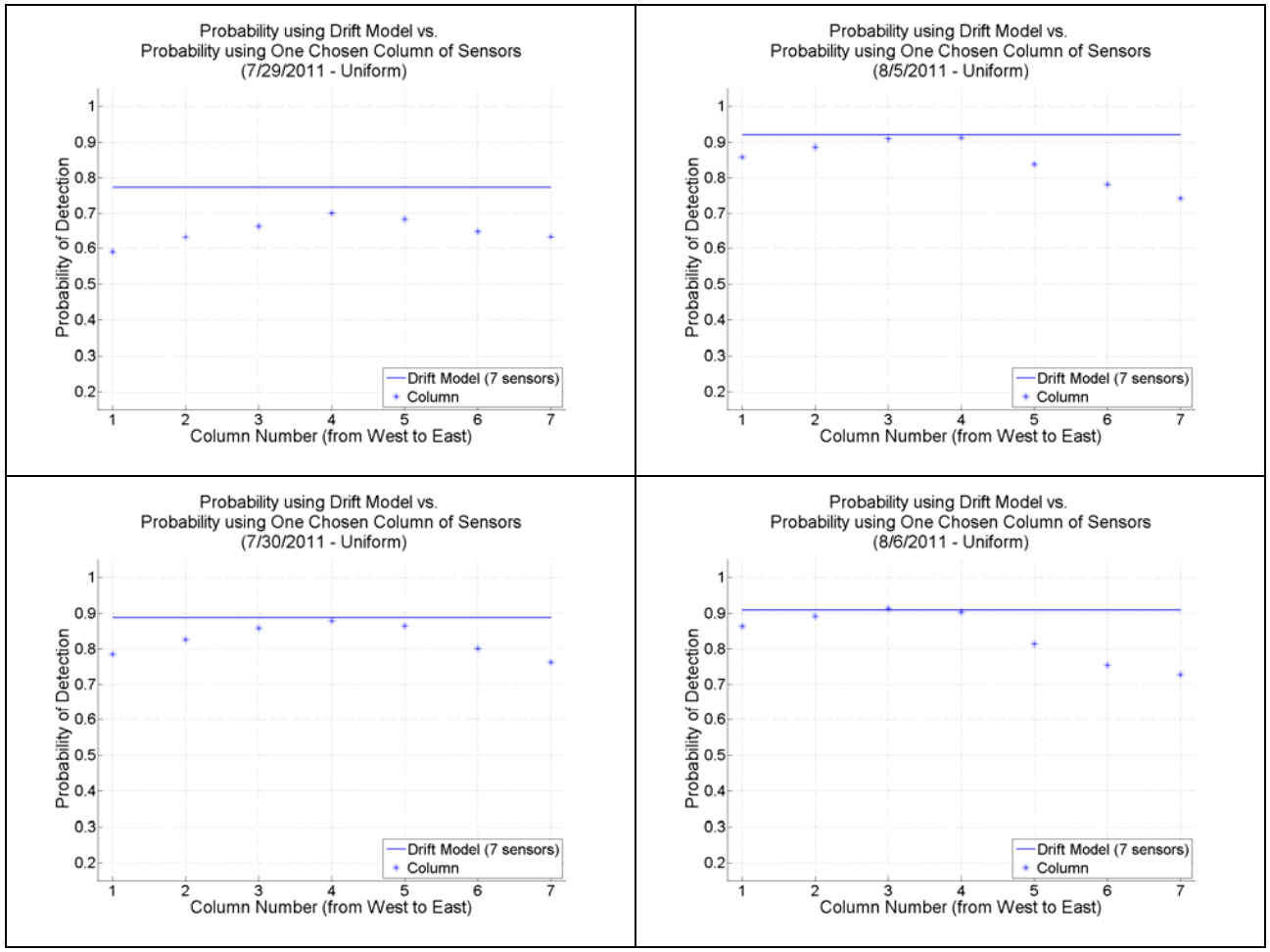
Probability using Drift Model vs.
Probability using One Chosen Column of Sensors
(7/29/2011 - Uniform)
Probability of Detection
Column Number (from West to East)
Drift Model (7 sensors)
Column
Probability using Drift Model vs.
Probability using One Chosen Column of Sensors
(8/5/2011 - Uniform)
Probability of Detection
Column Number (from West to East)
Drift Model (7 sensors)
Column
Probability using Drift Model vs.
Probability using One Chosen Column of Sensors
(7/30/2011 - Uniform)
Probability of Detection
Column Number (from West to East)
Drift Model (7 sensors)
Column
Probability using Drift Model vs.
Probability using One Chosen Column of Sensors
(8/6/2011 - Uniform)
Probability of Detection
Column Number (from West to East)
Drift Model (7 sensors)
Column

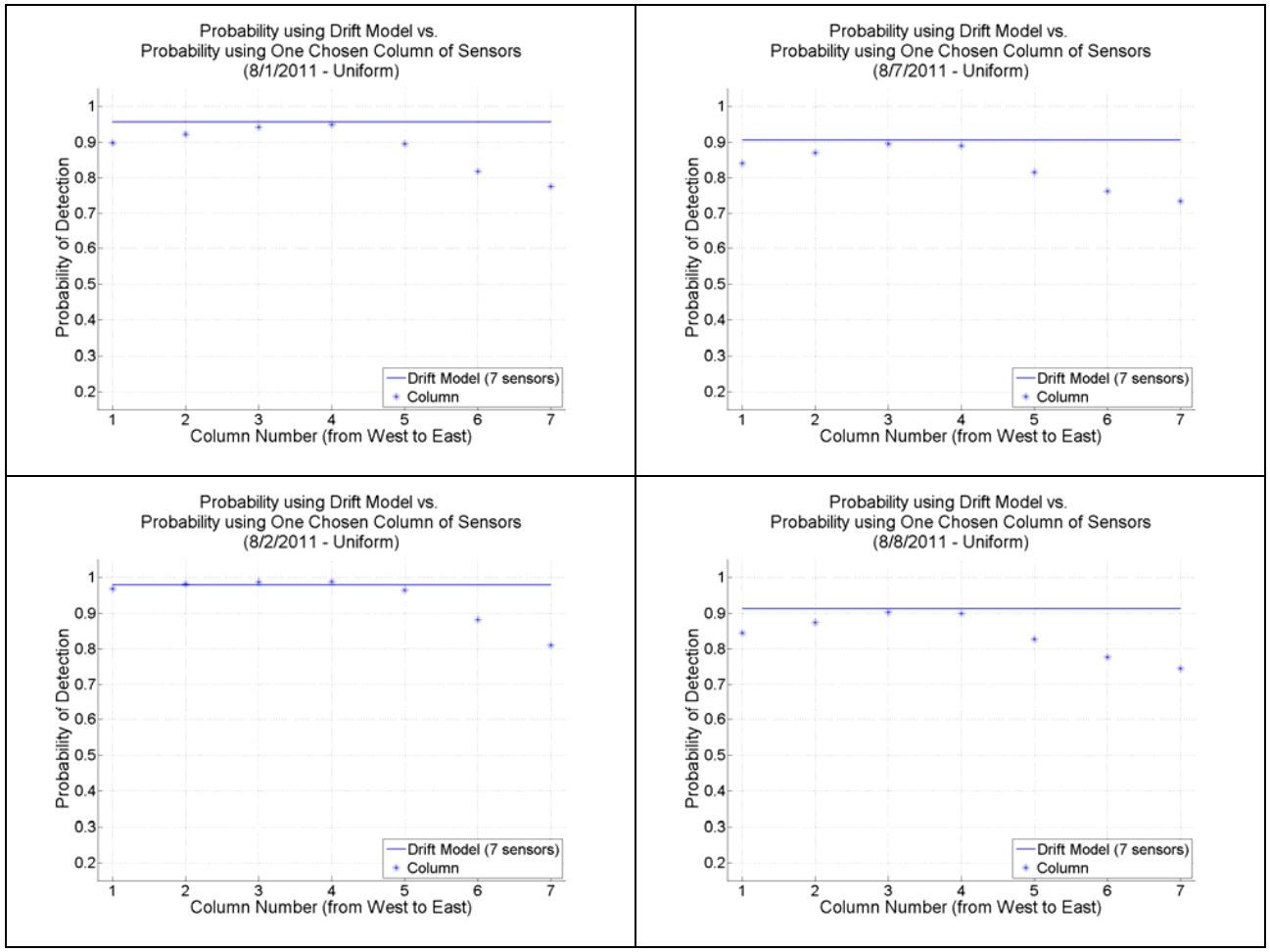
Probability using Drift Model vs.
Probability using One Chosen Column of Sensors
(8/1/2011 - Uniform)
Probability of Detection
Column Number (from West to East)
Drift Model (7 sensors)
Column
Probability using Drift Model vs.
Probability using One Chosen Column of Sensors
(8/7/2011 - Uniform)
Probability of Detection
Column Number (from West to East)
Drift Model (7 sensors)
Column
Probability using Drift Model vs.
Probability using One Chosen Column of Sensors
(8/2/2011 - Uniform)
Probability of Detection
Column Number (from West to East)
Drift Model (7 sensors)
Column
Probability using Drift Model vs.
Probability using One Chosen Column of Sensors
(8/8/2011 - Uniform)
Probability of Detection
Column Number (from West to East)
Drift Model (7 sensors)
Column

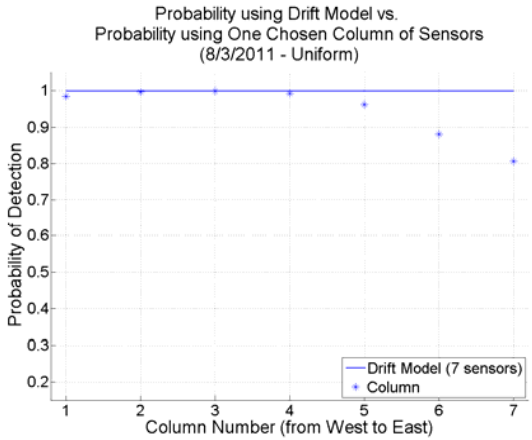

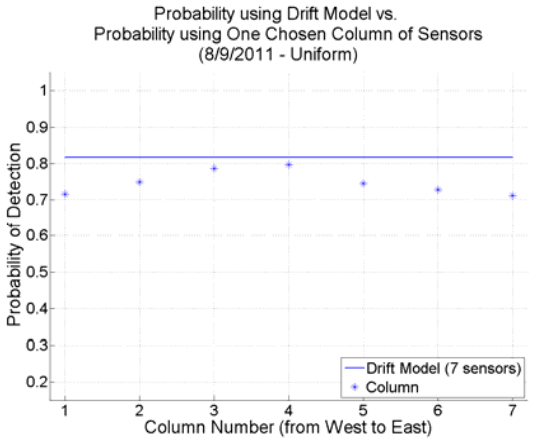

Normal Distribution

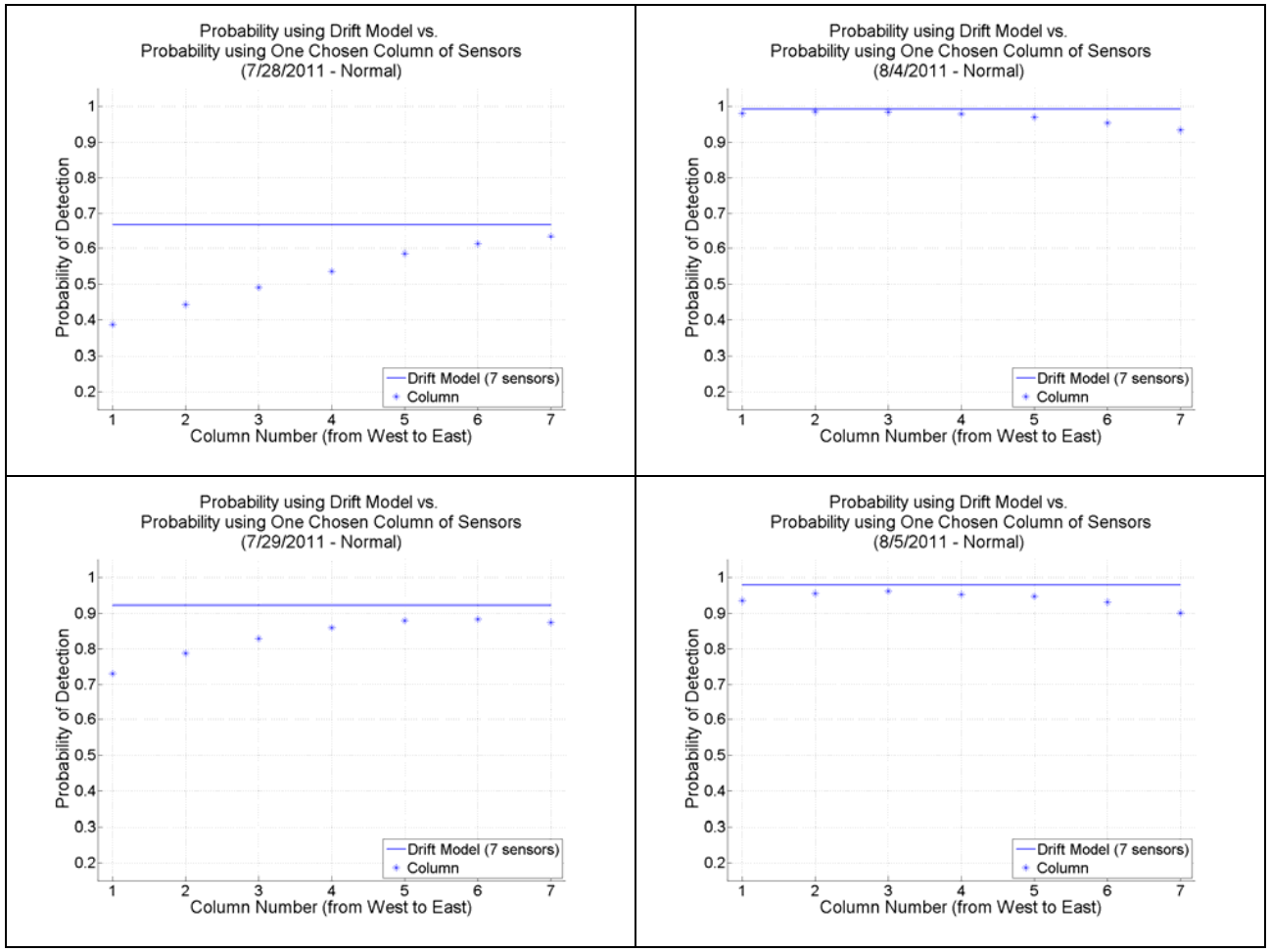
Probability using Drift Model vs.
Probability using One Chosen Column of Sensors
(7/28/2011 - Normal)
Probability of Detection
Column Number (from West to East)
Drift Model (7 sensors)
Column
Probability using Drift Model vs.
Probability using One Chosen Column of Sensors
(8/4/2011 - Normal)
Probability of Detection
Column Number (from West to East)
Drift Model (7 sensors)
Column
Probability using Drift Model vs.
Probability using One Chosen Column of Sensors
(7/29/2011 - Normal)
Probability of Detection
Column Number (from West to East)
Drift Model (7 sensors)
Column
Probability using Drift Model vs.
Probability using One Chosen Column of Sensors
(8/5/2011 - Normal)
Probability of Detection
Column Number (from West to East)
Drift Model (7 sensors)
Column

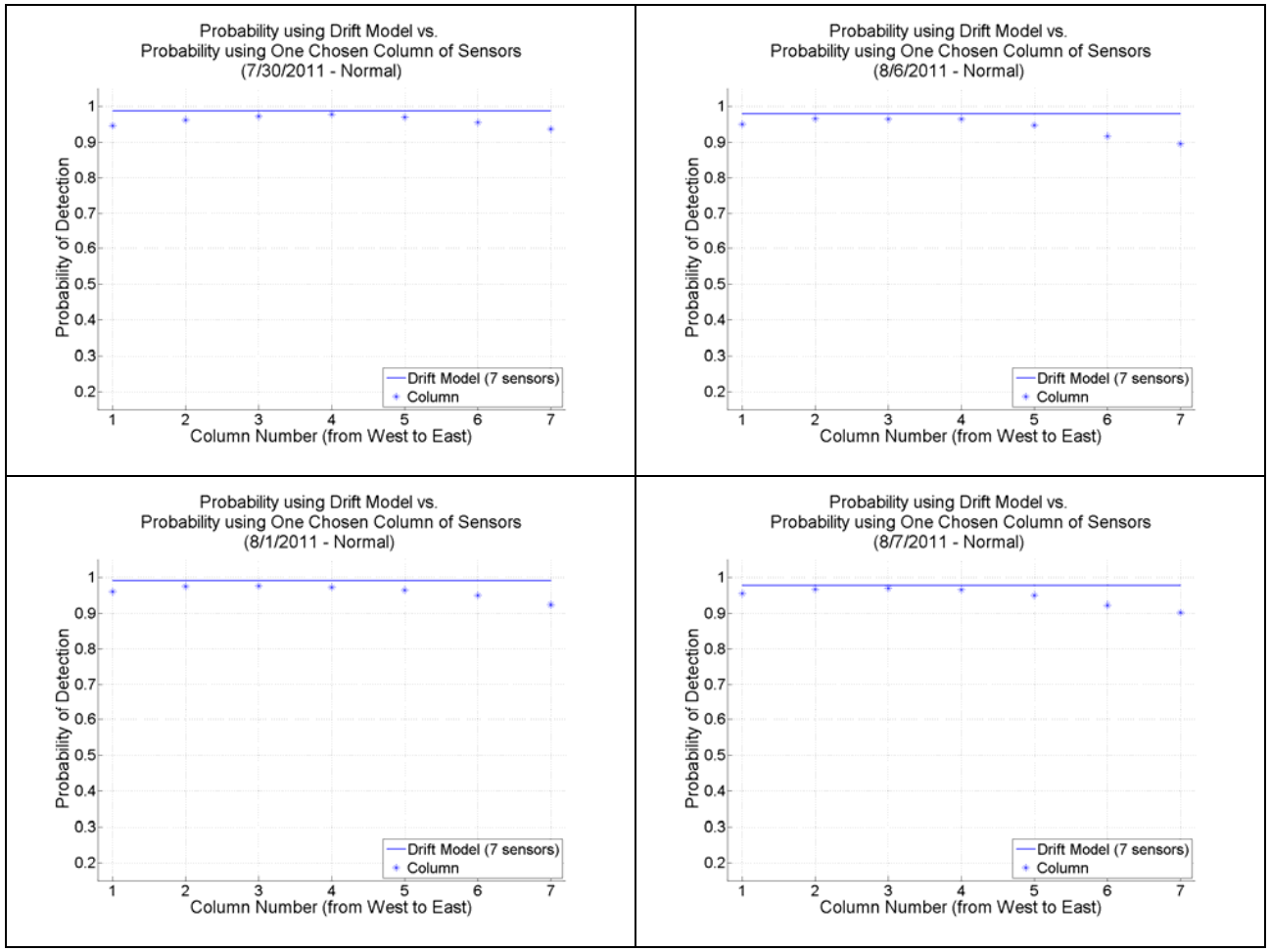
Probability using Drift Model vs.
Probability using One Chosen Column of Sensors
(7/30/2011 - Normal)
Probability of Detection
Column Number (from West to East)
Drift Model (7 sensors)
Column
Probability using Drift Model vs.
Probability using One Chosen Column of Sensors
(8/6/2011 - Normal)
Probability of Detection
Column Number (from West to East)
Drift Model (7 sensors)
Column
Probability using Drift Model vs.
Probability using One Chosen Column of Sensors
(8/1/2011 - Normal)
Probability of Detection
Column Number (from West to East)
Drift Model (7 sensors)
Column
Probability using Drift Model vs.
Probability using One Chosen Column of Sensors
(8/7/2011 - Normal)
Probability of Detection
Column Number (from West to East)
Drift Model (7 sensors)
Column

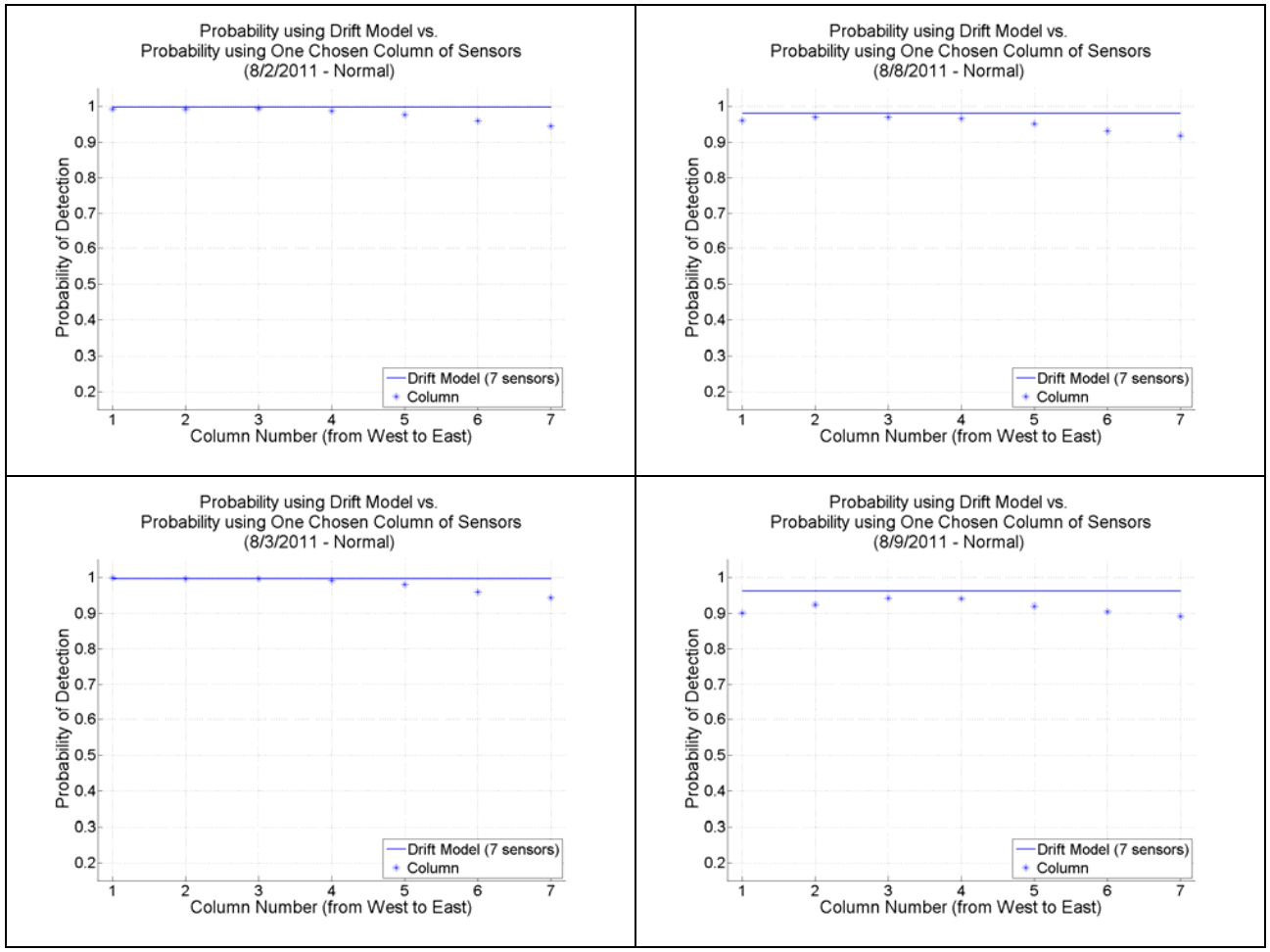
Probability using Drift Model vs.
Probability using One Chosen Column of Sensors
(8/2/2011 - Normal)
Probability of Detection
Column Number (from West to East)
Drift Model (7 sensors)
Column
Probability using Drift Model vs.
Probability using One Chosen Column of Sensors
(8/8/2011 - Normal)
Probability of Detection
Column Number (from West to East)
Drift Model (7 sensors)
Column
Probability using Drift Model vs.
Probability using One Chosen Column of Sensors
(8/3/2011 - Normal)
Probability of Detection
Column Number (from West to East)
Drift Model (7 sensors)
Column
Probability using Drift Model vs.
Probability using One Chosen Column of Sensors
(8/9/2011 - Normal)
Probability of Detection
Column Number (from West to East)
Drift Model (7 sensors)
Column

THIS PAGE INTENTIONALLY LEFT BLANK

INITIAL DISTRIBUTION LIST

1. Defense Technical Information Center
   Ft. Belvoir, VA

2. Dudley Knox Library
   Naval Postgraduate School
   Monterey, CA

3. RADM Jonathan White, USN
   Oceanographer and Navigator of the Navy
   Washington, DC

4. RADM Brian Brown
   Commander, Naval Meteorology and Oceanography Command
   Stennis Space Center, MS

5. Mr. Robert Winokur
   Technical Director
   Oceanographer & Navigator of the Navy
   Washington DC

6. Dr. William H. Burnett
   Technical Director
   Commander, Naval Meteorology and Oceanography Command
   Stennis Space Center, MS

7. Captain Paul Oosterling
   Commander, Naval Oceanographic Office
   Stennis Space Center, MS

8. Mr. Thomas Cuff
   Technical Director
   Naval Oceanographic Office
   Stennis Space Center, MS

9. Dr. Richard Jeffries
   Commander, Naval Meteorology and Oceanography Command
   Stennis Space Center, MS

10. NOMWC RBC
    Naval Oceanography Mine Warfare Center
    Stennis Space Center, MS

11. NOAC RBC
Naval Oceanography Anit-submarine Warfare Center
Stennis Space Center, MS

12. Professor Mary L. Batteen
Naval Postgraduate School
Monterey, CA

13. Professor Jeffrey Paduan
Naval Postgraduate School
Monterey, CA

14. Professor Peter Chu
Naval Postgraduate School
Monterey, CA

15. Dr. Thomas Wettergren
Naval Undersea Warfare Center
Newport, RI

16. Ronald E. Betsch
MIW Program Manager
Stennis Space Center, MS

17. Dr. James Rigney
Naval Oceanographic Office
Stennis Space Center, MS

18. Richard D. Williams, Rear Admiral (ret.)
Naval Postgraduate School
Monterey, CA

19. Kevin Oakes
Naval Surface Warfare Center
Panama City, FL

20. John E. Joseph
Naval Postgraduate School
Monterey, CA

21. Chris Miller
Naval Postgraduate School
Monterey, CA

22. Dennis Krynen
Naval Oceanographic Office
Stennis Space Center, MS

23. Wade Sigstedt
Naval Oceanographic Office
Stennis Space Center, MS

24. William Teague
Naval Research Laboratory
Stennis Space Center, MS

25. Nicole Lassiter
Naval Surface Warfare Center
Panama City, FL

26. Joseph Rice
Naval Postgraduate School
Monterey, CA

27. Captain Van Gurley
Commander, Naval Oceanography Operations Command
Stennis Space Center, MS